4
Deep inelastic scattering

The original, and still the most powerful, test of perturbative QCD is the breaking of Bjorken scaling in deep inelastic lepton-hadron scattering (DIS). Nowadays, deep inelastic structure function analyses not only provide some of the most precise tests of the theory but also determine the momentum distributions of partons in hadrons, for use as input in predicting cross sections in high-energy hadron collisions. In this chapter we begin by discussing deep inelastic scattering and the 'naive' parton model. We then show how QCD modifies the simple Bjorken scaling property of the parton model, and discuss how these scaling violations can be calculated in perturbation theory. We compare the theoretical predictions with experimental data, and consider the behaviour of the parton distributions in various kinematic limits.

4.1 Deep inelastic scattering and the parton model

We begin with an overview of how deep inelastic lepton-hadron scattering has a natural interpretation in terms of the parton picture of quarks and gluons in hadrons. In this section our derivation of the parton model will be rather heuristic. In the following section we will present a more rigorous derivation.

Consider the scattering of a high-energy charged lepton off a hadron target. If we label the incoming and outgoing lepton four-momenta by k^μ and k'^μ respectively, the momentum of the target hadron (assumed hereafter to be a proton) by p^μ and the momentum transfer by $q^\mu = k^\mu - k'^\mu$, then the standard deep inelastic variables are defined by:

$$Q^2 = -q^2$$

Downloaded from https://www.cambridge.org/core. UNIVERSIDAD AUTONOMA METROPOLITANA, on 15 Nov 2026 at 15:53:11, subject to the Cambridge Core terms of use, available at https://www.cambridge.org/core/terms. https://doi.org/10.1017/CBO9780511628788.005

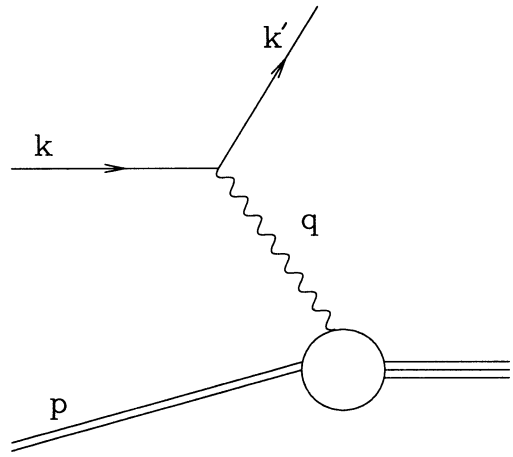


Fig. 4.1. Deep inelastic charged lepton-proton scattering.

$$\begin{aligned} M^2 &= p^2 \\ \nu &= p\cdot q = M(E'-E) \\ x &= \frac{Q^2}{2\nu} = \frac{Q^2}{2M(E-E')} \\ y &= \frac{q\cdot p}{k\cdot p} = 1 - E'/E\ , \end{aligned} \tag{4.1}$$

where the energy variables refer to the target rest frame and M is the proton mass. If the lepton is an electron or muon, then the scattering is mediated by the exchange of a virtual photon, Fig. 4.1.

Structure functions $F_i(x,Q^2)$ — which parametrize the structure of the target as 'seen' by the virtual photon — are defined in terms of the lepton scattering cross sections. For charged lepton scattering, $lp \to lX$,[1]

$$\begin{aligned} \frac{d^2\sigma^{em}}{dxdy} &= \frac{8\pi\alpha^2 ME}{Q^4}\Big[\Big(\frac{1+(1-y)^2}{2}\Big)2xF_1^{em} \\ &\quad +(1-y)(F_2^{em}-2xF_1^{em}) - (M/2E)xyF_2^{em}\Big]\ , \end{aligned} \tag{4.2}$$

and for neutrino (antineutrino) scattering, $\nu p \to lX$,

$$\begin{aligned} \frac{d^2\sigma^{\nu(\bar\nu)}}{dxdy} &= \frac{G_F^2 ME}{\pi}\Big[(1-y-\frac{M}{2E}xy)F_2^{\nu(\bar\nu)} \\ &\quad +y^2xF_1^{\nu(\bar\nu)} + (-)\ y(1-\tfrac{1}{2}y)xF_3^{\nu(\bar\nu)}\Big]\ . \end{aligned} \tag{4.3}$$

[1] This expression is strictly valid only for $Q^2 \ll M_Z^2$, see below.

Downloaded from https://www.cambridge.org/core. UNIVERSIDAD AUTONOMA METROPOLITANA, on 15 Nov 2026 at 15:53:11, subject to the Cambridge Core terms of use, available at https://www.cambridge.org/core/terms. https://doi.org/10.1017/CBO9780511628788.005

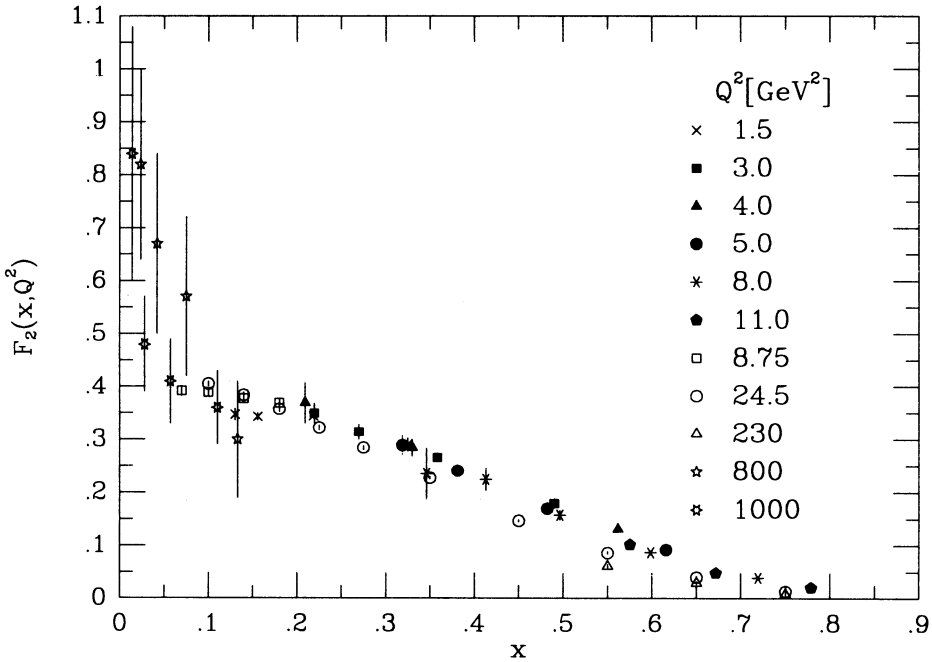


Fig. 4.2. The F_2 structure function from the SLAC-MIT, BCDMS, H1 and ZEUS collaborations.

We will explain the structure of these equations in the next section. The *Bjorken limit* is defined as $Q^2, \nu \to \infty$ with x fixed. In this limit the structure functions are observed to obey an approximate *scaling* law [1,2], *i.e.* they depend only on the dimensionless variable x:

$$F_i(x, Q^2) \longrightarrow F_i(x) \; . \tag{4.4}$$

This is illustrated in Fig. 4.2, where data on the electromagnetic structure function F_2, measured with a proton target, are displayed. The data span two decades of experiments, from the original SLAC-MIT measurements [3] to the high precision fixed-target measurements from the BCDMS collaboration [4] and the recent high-energy electron-proton collider measurements from the H1 [5] and ZEUS [6] experiments at HERA. Only a representative sample of data points is shown. Note that even though the Q^2 values vary by three orders of magnitude, to a good approximation the data lie on a universal curve.

Bjorken scaling implies that the virtual photon scatters off *pointlike constituents*, since otherwise the dimensionless structure functions would depend on the ratio Q/Q_0, with $1/Q_0$ some length scale characterizing the size of the constituents. The parton model picture of deep inelastic scattering is most easily formulated in the 'infinite momentum frame' in

Downloaded from https://www.cambridge.org/core. UNIVERSIDAD AUTONOMA METROPOLITANA, on 15 Nov 2026 at 15:53:11, subject to the Cambridge Core terms of use, available at https://www.cambridge.org/core/terms. https://doi.org/10.1017/CBO9780511628788.005

which the proton is moving very fast, $p^\mu \approx (P, 0, 0, P)$ with $P \gg M$. In this frame, we can consider a simple model where the photon scatters off a pointlike quark constituent which is moving parallel with the proton and carrying a fraction ξ of its momentum, *i.e.* $p_q^\mu = \xi p^\mu$. Neglecting the proton mass M, we can rewrite Eq. (4.2) as

$$\frac{d^2\sigma}{dxdQ^2} = \frac{4\pi\alpha^2}{Q^4}\left[[1+(1-y)^2]F_1 + \frac{(1-y)}{x}(F_2 - 2xF_1)\right] . \tag{4.5}$$

Now the spin-averaged matrix element squared for massless $e^-q \to e^-q$ scattering can be obtained from the corresponding matrix element for $e^+e^- \to q\bar{q}$ considered in Chapter 3. The two amplitudes are related by crossing symmetry, which requires that the amplitude for a process with a particle of momentum k in the initial state is equal to the amplitude for the process with an antiparticle of momentum $-k$ in the final state. Thus the amplitudes for the two processes

$$e^-(k) + q(p_q) \to e^-(k') + q(p_q') \tag{4.6}$$
$$e^+(-k') + e^-(k) \to \bar{q}(-p_q) + q(p_q') \tag{4.7}$$

are equal. In terms of the usual Mandelstam variables $\hat{s} = (k+p_q)^2$, $\hat{t} = (k-k')^2$ and $\hat{u} = (p_q - k')^2$, the matrix element squared for amplitude (4.6) is

$$\overline{\sum}|\mathcal{M}|^2 = 2e_q^2 e^4 \frac{\hat{s}^2 + \hat{u}^2}{\hat{t}^2} . \tag{4.8}$$

The notation $\overline{\sum}$ denotes the average (sum) over initial (final) colours and spins. Using Eq. (4.1) we can substitute for the deep inelastic variables: $\hat{t} = -Q^2$, $\hat{u} = \hat{s}(y-1)$ and $\hat{s} = \xi Q^2/xy$. Using the standard result for the cross section for massless $2 \to 2$ scattering,

$$\frac{d\hat{\sigma}}{d\hat{t}} = \frac{1}{16\pi\hat{s}^2}\overline{\sum}|\mathcal{M}|^2 , \tag{4.9}$$

and substituting for the kinematic variables in the matrix element squared, gives

$$\frac{d\hat{\sigma}}{dQ^2} = \frac{2\pi\alpha^2 e_q^2}{Q^4}[1+(1-y)^2] . \tag{4.10}$$

The mass-shell constraint for the outgoing quark,

$$p_q'^2 = (p_q+q)^2 = q^2 + 2p_q\cdot q = -2p\cdot q(x-\xi) = 0 , \tag{4.11}$$

implies $x = \xi$. By writing $\int_0^1 dx\delta(x-\xi) = 1$, we obtain the double differential cross section for the quark scattering process:

$$\frac{d^2\hat{\sigma}}{dxdQ^2} = \frac{4\pi\alpha^2}{Q^4}[1+(1-y)^2]\,\frac{1}{2}e_q^2\delta(x-\xi) . \tag{4.12}$$

Downloaded from https://www.cambridge.org/core. UNIVERSIDAD AUTONOMA METROPOLITANA, on 15 Nov 2026 at 15:53:11, subject to the Cambridge Core terms of use, available at https://www.cambridge.org/core/terms. https://doi.org/10.1017/CBO9780511628788.005

By comparing Eqs. (4.5) and (4.12) we see that the structure functions in this simple model are:

$$\hat{F}_2 = xe_q^2\delta(x-\xi) = 2x\hat{F}_1 \,. \tag{4.13}$$

This result suggests that the structure function $F_2(x)$ 'probes' a quark constituent with momentum fraction $\xi = x$. From Fig. 4.2, the measured structure function is evidently a *distribution* in x rather than a delta function, which indicates that the quark constituents carry a range of momentum fractions.

The above ideas are incorporated in what is now known as the 'naive parton model' [2]:

— $q(\xi)d\xi$ represents the probability that a quark q carries momentum fraction between ξ and $\xi + d\xi$, where $0 \leq \xi \leq 1$,

— the virtual photon scatters incoherently off the quark constituents.

Thus the proton structure functions are obtained by weighting the quark structure functions with the probability distribution $q(\xi)$,

$$\begin{aligned} F_2(x) = 2xF_1(x) &= \sum_{q,\bar{q}} \int_0^1 d\xi\, q(\xi)\, xe_q^2\delta(x-\xi) \\ &= \sum_{q,\bar{q}} e_q^2\, xq(x) \,. \end{aligned} \tag{4.14}$$

In particular, for the scattering of a charged lepton off a proton target by virtual photon exchange, $lp \to lX$, with four quark flavours,

$$\begin{aligned} F_2^{em}(x) &= x\Big[\frac{4}{9}\left(u(x)+\bar{u}(x)+c(x)+\bar{c}(x)\right) \\ &\quad + \frac{1}{9}\left(d(x)+\bar{d}(x)+s(x)+\bar{s}(x)\right)\Big] \,. \end{aligned} \tag{4.15}$$

For neutrino scattering, $\nu p \to lX$, the virtual W^+ probe measures the quark distributions weighted by the corresponding *weak* charge:

$$F_2^{\nu}(x) = 2x\left[d(x)+s(x)+\bar{u}(x)+\bar{c}(x)\right] \,. \tag{4.16}$$

A list of the most commonly encountered parton-model deep inelastic structure functions for scattering off an unpolarized proton target is given below:

$$\begin{aligned} F_2^{\nu} &= 2x[d+s+\bar{u}+\bar{c}] \\ xF_3^{\nu} &= 2x[d+s-\bar{u}-\bar{c}] \\ F_2^{\bar{\nu}} &= 2x[u+c+\bar{d}+\bar{s}] \\ xF_3^{\bar{\nu}} &= 2x[u+c-\bar{d}-\bar{s}] \\ F_2^{em} &= x\left[\frac{4}{9}(u+\bar{u}+c+\bar{c})+\frac{1}{9}(d+\bar{d}+s+\bar{s})\right] \end{aligned}$$

Downloaded from https://www.cambridge.org/core. UNIVERSIDAD AUTONOMA METROPOLITANA, on 15 Nov 2026 at 15:53:11, subject to the Cambridge Core terms of use, available at https://www.cambridge.org/core/terms. https://doi.org/10.1017/CBO9780511628788.005

$$2xF_1 \;=\; F_2\,. \tag{4.17}$$

This last result (the *Callan-Gross relation*) is a direct consequence of the spin-$\frac{1}{2}$ property of the quarks. To understand this, we note that the two terms in the square brackets on the right-hand side of Eq. (4.5) correspond to the absorption of transversely (F_1) and longitudinally ($F_2 - 2xF_1$) polarized virtual photons. In fact the combination

$$F_L(x,Q^2) = \left(1+\frac{4M^2x^2}{Q^2}\right)F_2(x,Q^2) - 2xF_1(x,Q^2) \overset{Q^2\to\infty}{\longrightarrow} F_2 - 2xF_1\,, \tag{4.18}$$

called the *longitudinal structure function*, is sometimes used instead of F_1 or F_2. The Callan-Gross relation follows from the fact that a spin-$\frac{1}{2}$ quark cannot absorb a longitudinally polarized vector boson. In contrast, spin-0 (scalar) quarks cannot absorb transversely polarized vector bosons and so would have $F_1 = 0$, *i.e.* $F_L = F_2$, in the Bjorken limit. Structure function measurements show that $F_L \ll F_2$, confirming the spin-$\frac{1}{2}$ property of quarks. Note that in the QCD-improved parton model F_L is only non-zero at leading order in perturbation theory, *i.e.* $F_L = O(\alpha_S)$, see Section 4.3.1.

At very high energies, in particular for $Q^2 \sim M_Z^2$, the contribution to $ep \to eX$ scattering from Z exchange cannot be ignored. The calculation of the Z-exchange and the $Z-\gamma$ interference contributions proceeds in a similar way to the corresponding calculation of high-energy e^+e^- annihilation discussed in Chapter 3. The generalization of Eq. (4.5) which incorporates the complete *neutral current* (γ and Z) exchange for $e^-p \to e^-X$ scattering is

$$\frac{d^2\sigma_{NC}}{dxdQ^2} = \frac{4\pi\alpha^2}{xQ^4}\left[xy^2F_1^{NC} + (1-y)F_2^{NC} + y\left(1-\tfrac{1}{2}y\right)F_3^{NC}(x,Q^2)\right]\,, \tag{4.19}$$

where

$$\begin{aligned} F_2^{NC}(x) = 2xF_1^{NC}(x) &= \sum_q x[q(x)+\bar{q}(x)]\,C_q(Q^2) \\ xF_3^{NC}(x) &= \sum_q x[q(x)-\bar{q}(x)]\,D_q(Q^2)\,, \end{aligned} \tag{4.20}$$

with

$$\begin{aligned} C_q(Q^2) &= e_q^2 - 2e_qV_eV_qP_Z + (V_e^2+A_e^2)(V_q^2+A_q^2)P_Z^2 \\ D_q(Q^2) &= -2e_qA_eA_qP_Z + 4V_eA_eV_qA_qP_Z^2 \\ P_Z &= \frac{Q^2}{Q^2+M_Z^2}\,. \end{aligned} \tag{4.21}$$

Note the appearance of an additional parity-violating structure function F_3. The vector and axial couplings of the fermions to the Z boson are

Downloaded from https://www.cambridge.org/core. UNIVERSIDAD AUTONOMA METROPOLITANA, on 15 Nov 2026 at 15:53:11, subject to the Cambridge Core terms of use, available at https://www.cambridge.org/core/terms. https://doi.org/10.1017/CBO9780511628788.005

defined in Chapter 8, Table 8.3. The *charged-current* (W-exchange) contribution, $e^- p \to \nu_e X$ also becomes significant at high Q^2. The corresponding parton-distribution decomposition of the cross section is

$$\frac{d^2\sigma_{CC}}{dx dQ^2} = \frac{(1-\lambda_e)\pi\alpha^2}{8\sin^4\theta_W (Q^2+M_W^2)^2} \times \sum_{i,j} \left[|V_{u_i d_j}|^2 u_i(x) + (1-y)^2 |V_{u_j d_i}|^2 d_i(x)\right] , \quad (4.22)$$

where λ_e is the helicity of the electron, u_i and d_i refer to up- and down-type quarks respectively, and the $V_{u_i d_j}$ are the elements of the CKM matrix, which describes the couplings of the quarks to the charged weak current (see Chapter 8).

The above relations can in principle be inverted to give the individual quark distribution functions in terms of the measured structure functions. From such an analysis, the following picture emerges. The proton consists of three *valence* quarks (uud) which carry its electric charge and baryon quantum numbers, and an infinite *sea* of light $q\bar{q}$ pairs. When probed at momentum scale Q, the sea contains all quark flavours with mass $m_q \ll Q$. Thus at a scale of $O(1\text{ GeV})$, and assuming the sea to be symmetric in the quark flavours, we would have

$$\begin{aligned} u(x) &= u_V(x) + S(x) \\ d(x) &= d_V(x) + S(x) \\ S(x) &= \bar{u}(x) = \bar{d}(x) = s(x) = \bar{s}(x) , \end{aligned} \quad (4.23)$$

with the sum rules

$$\int_0^1 dx\, u_V(x) = 2 , \qquad \int_0^1 dx\, d_V(x) = 1 ,$$
$$\sum_q \int_0^1 dx\, x[q(x)+\bar{q}(x)] = \int_0^1 dx\, x[u_V(x)+d_V(x)+6S(x)] \approx 0.5 . \quad (4.24)$$

The last of these is an experimental result. It indicates that the quarks only carry about 50% of the proton's momentum. The rest is attributed to *gluon* constituents. Although the electroweak-neutral gluons are not directly measured in deep inelastic lepton hadron scattering, their presence is evident in other high-energy processes such as large transverse momentum jet, prompt photon and heavy quark production (see Chapters 7 and 10). Fig. 4.3 shows a typical set of quark and gluon distributions [7] extracted from fits to deep inelastic data, when probed at a momentum scale $\mu^2 = 10\text{ GeV}^2$. Notice the differences compared to the naive expectations of Eq. (4.23). The sea is *not* SU(3) flavour symmetric, rather the strange quark distribution is roughly a factor of two smaller than the average of

Downloaded from https://www.cambridge.org/core. UNIVERSIDAD AUTONOMA METROPOLITANA, on 15 Nov 2026 at 15:53:11, subject to the Cambridge Core terms of use, available at https://www.cambridge.org/core/terms. https://doi.org/10.1017/CBO9780511628788.005

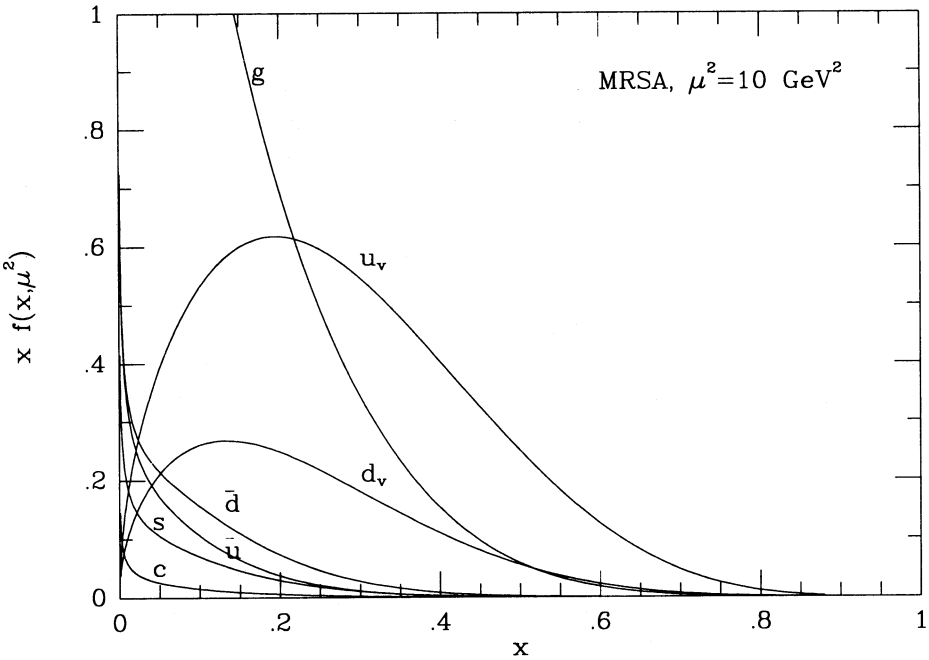


Fig. 4.3. Quark and gluon distribution functions at $\mu^2 = 10\ \mathrm{GeV}^2$, from ref. [7].

the light quark distributions, and there is an asymmetry between the $\bar{u}$ and $\bar{d}$ quarks in the sea. Neither of these features is quantitatively understood at present. Notice also that at this scale a small charm quark component is observed, consistent with the expectation that the virtual photon should be able to resolve $c\bar{c}$ pairs in the quark sea when $Q^2 \gtrsim m_c^2$.

Closer examination of Fig. 4.2 reveals a systematic deviation from exact Bjorken scaling: the structure function decreases with increasing Q^2 at large x and has the opposite behaviour at small x. In Section 4.3 we will show that these scaling violations arise naturally in perturbative QCD. First, however, we give a more rigorous formulation of the parton model.

4.2 The parton model from field theory

The 'naive' parton model introduced in the previous section existed before the invention of QCD. It has a special status as a model because much of the motivation comes from field theory, with additional assumptions added from the phenomenology of hadronic interactions.

The basic assumption of the naive parton model is that the interactions of hadrons are due to the interactions of partons; in certain types of reactions the structure of the hadrons may be described by an instantaneous

Downloaded from https://www.cambridge.org/core. UNIVERSIDAD AUTONOMA METROPOLITANA, on 15 Nov 2026 at 15:53:11, subject to the Cambridge Core terms of use, available at https://www.cambridge.org/core/terms. https://doi.org/10.1017/CBO9780511628788.005

distribution of partons. A necessary condition for such a picture to make sense is that changes in the number and momenta of the partons should be negligible during the time which they are probed. An analogy with diffraction studies of a crystal may be useful. An X-ray diffracted by a crystal reveals its detailed structure, because the atoms in the crystal lattice can be considered to be at rest during the transit time of the X-ray across the crystal. In hadronic systems we ensure that the transit time across the target is less than the timescale of internal motion by moving to an infinite momentum frame.

Although the simplest description makes use of the infinite momentum frame, the model can be formulated covariantly. To see how this is achieved, we return to the basic deep inelastic scattering diagram, Fig. 4.1. The amplitude for this process is[2]

$$\mathcal{A} = e\bar{u}(k')\gamma^{\alpha}u(k)\,\frac{1}{q^2}\,\left\langle X\left|j_{\alpha}(0)\right|P\right\rangle\ , \tag{4.25}$$

where j_α is the electromagnetic current. The key point is that the cross section, which is proportional to the amplitude squared, can be factored into a leptonic and a hadronic piece,

$$\frac{d^2\sigma}{dxdy} \propto L_{\alpha\beta}\,W^{\alpha\beta}\ . \tag{4.26}$$

The structure of the leptonic tensor, assuming photon exchange only, is completely determined by QED:

$$L_{\alpha\beta} = e^2\mathrm{Tr}[\not{k}'\gamma_\alpha\not{k}\gamma_\beta] = 4e^2\left(k_\alpha k'_\beta + k_\beta k'_\alpha - g_{\alpha\beta}\,k\cdot k'\right)\ . \tag{4.27}$$

In contrast, the hadronic tensor contains all the information about the interaction of the electromagnetic current j_α with the target proton P:

$$\begin{aligned} W_{\alpha\beta}(p,q) &= \frac{1}{4\pi}\sum_X \left\langle P\left|j^{\dagger}_{\beta}(0)\right|X\right\rangle\left\langle X\left|j_{\alpha}(0)\right|P\right\rangle(2\pi)^4\delta^4(q+p-p_X) \\ &= \frac{1}{4\pi}\int d^4z\ e^{iq\cdot z}\left\langle P\left|j^{\dagger}_{\beta}(z)j_{\alpha}(0)\right|P\right\rangle \\ &= \frac{1}{4\pi}\int d^4z\ e^{iq\cdot z}\left\langle P\left|\left[j^{\dagger}_{\beta}(z),j_{\alpha}(0)\right]\right|P\right\rangle\ . \end{aligned} \tag{4.28}$$

In deriving this result we have used the completeness of the final states X and introduced an integral representation for the four-dimensional delta function. Energy-momentum conservation implies that the second term in the current commutator gives no contribution. Because the electro-

[2] In what follows we omit spin labels and sums.

Downloaded from https://www.cambridge.org/core. UNIVERSIDAD AUTONOMA METROPOLITANA, on 15 Nov 2026 at 15:53:11, subject to the Cambridge Core terms of use, available at https://www.cambridge.org/core/terms. https://doi.org/10.1017/CBO9780511628788.005

magnetic current is conserved, $q \cdot W = 0$, we may write

$$W^{\alpha\beta}(p,q) = \left(g^{\alpha\beta} - \frac{q^\alpha q^\beta}{q^2}\right) W_1(x,Q^2) + \left(p^\alpha + \frac{1}{2x}q^\alpha\right)\left(p^\beta + \frac{1}{2x}q^\beta\right) W_2(x,Q^2) \tag{4.29}$$

where the information about the structure of the hadron as 'seen' by the virtual photon is contained in the two functions W_1 and W_2. The scattering cross section is then obtained by multiplying the leptonic and hadronic tensors and substituting into the right-hand side of Eq. (4.26). Comparing the resulting expression with that given in Eq. (4.2) allows us to relate the functions W_i to the electromagnetic structure functions defined in the previous section,

$$\begin{aligned} F_1(x,Q^2) &= W_1(x,Q^2) \\ F_2(x,Q^2) &= \nu W_2(x,Q^2). \end{aligned} \tag{4.30}$$

To analyse the hadronic tensor W it is convenient to introduce two light-like vectors p and n, with $n \cdot p = 1$ so that n has the dimensions of an inverse mass. Any four-vector can then be written in terms of p, n and a spacelike two-dimensional transverse vector:

$$k^\mu = ap^\mu + bn^\mu + k_T^\mu \,, \tag{4.31}$$

where

$$p^2 = n^2 = n \cdot k_T = p \cdot k_T = 0 \,. \tag{4.32}$$

In particular, we can identify p with the four-momentum of the target in the approximation in which we ignore its mass. The kinematic four-vectors for deep inelastic scattering can then be written as

$$\begin{aligned} P^\mu &= p^\mu + \frac{M^2}{2}n^\mu \\ q^\mu &= \nu n^\mu + q_T^\mu \,, \end{aligned} \tag{4.33}$$

where $q_T^2 = -q^2 = Q^2$. In the frame in which the struck proton is moving very fast along the positive z-axis, an explicit representation for the vectors p and n is[3]

$$\begin{aligned} p^\mu &= (P,0,0,P) \\ n^\mu &= (\frac{1}{2P},0,0,-\frac{1}{2P}) \,. \end{aligned} \tag{4.34}$$

For simplicity, in what follows we will ignore the mass M so that $p^\mu \equiv P^\mu$. Using the representation Eq. (4.33) the functions $W_{1,2}$ can be projected

[3] Our notation for four-vectors is (E, p_x, p_y, p_z).

Downloaded from https://www.cambridge.org/core. UNIVERSIDAD AUTONOMA METROPOLITANA, on 15 Nov 2026 at 15:53:11, subject to the Cambridge Core terms of use, available at https://www.cambridge.org/core/terms. https://doi.org/10.1017/CBO9780511628788.005

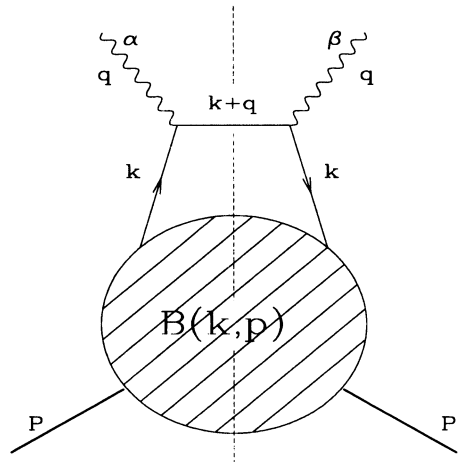


Fig. 4.4. Handbag diagram.

out of the hadronic tensor by

$$\begin{aligned} \nu n^\alpha n^\beta W_{\alpha\beta} &= \nu W_2 = F_2 \,, \\ \frac{4x^2}{\nu} p^\alpha p^\beta W_{\alpha\beta} &= \nu W_2 - 2xW_1 = F_L = F_2 - 2xF_1 \,. \end{aligned} \tag{4.35}$$

We next make the important assumption[4] that the photon scatters incoherently off the individual partons. The hadronic tensor W is then obtained from the simple 'handbag' diagram shown in Fig. 4.4:

$$W^{\alpha\beta}(p,q) = e_q^2 \int \frac{d^4k}{(2\pi)^4} \left[\gamma^\alpha (\not{k} + \not{q}) \gamma^\beta\right]_{ij} \left[B(k,p)\right]_{ji} \delta((k+q)^2) \,. \tag{4.36}$$

The quark four-momentum k can be decomposed in terms of p, n and a transverse vector k_T,

$$k^\mu = \xi p^\mu + \frac{k^2 + {k_T}^2}{2\xi} n^\mu + {k_T}^\mu \,. \tag{4.37}$$

The assumption of the parton model is that the structure of the amplitude $B(k,p)$ is such that it is strongly damped when the transverse momentum k_T^2 and the virtuality k^2 are large. Thus the integral in (4.36) is dominated by small values of these variables and the delta function may be simplified to give

$$\delta((k+q)^2) = \delta(k^2 + 2\xi\nu - 2q_T \cdot k_T + q^2) \approx \delta(2\xi\nu - Q^2) = \frac{1}{2\nu}\delta(\xi - x). \tag{4.38}$$

[4] This can be justified by considering the general behaviour of parton-proton scattering amplitudes.

Downloaded from https://www.cambridge.org/core. UNIVERSIDAD AUTONOMA METROPOLITANA, on 15 Nov 2026 at 15:53:11, subject to the Cambridge Core terms of use, available at https://www.cambridge.org/core/terms. https://doi.org/10.1017/CBO9780511628788.005

This gives

$$\begin{aligned} \nu W_2 \equiv F_2 &= \frac{e_q^2}{2}\int \frac{d^4k}{(2\pi)^4}\left[\not n(\not k+\not q)\not n\right]_{ij} B_{ji}(k,p)\delta(\xi-x) \\ &= e_q^2 x \int \frac{d^4k}{(2\pi)^4}\left[\not n\right]_{ij} B_{ji}(k,p)\delta(\xi-x) \\ &\equiv e_q^2 x q(x)\,, \end{aligned} \tag{4.39}$$

where the quark distribution is

$$q(x) = \int \frac{d^4k}{(2\pi)^4}\,\mathrm{Tr}[\,\not n\, B(k,p)\,]\,\delta(n\cdot k - x)\,. \tag{4.40}$$

We therefore see that the structure function *scales*, *i.e.* it depends only on the dimensionless variable x:

$$F_2(x,Q^2) \longrightarrow F_2(x)\,. \tag{4.41}$$

We can project out the longitudinal structure function in a similar way by multiplying the hadronic tensor $W_{\alpha\beta}$ by $p_\alpha p_\beta$. In this case we find $F_L = O(\nu^{-1})$ which vanishes in the Bjorken limit. We therefore derive the Callan-Gross relation $F_2 = 2xF_1$ characteristic of the spin-$\frac{1}{2}$ nature of the constituents.

It is also possible to give an operator representation for the quark distribution $q(x)$. In the light-cone gauge, $n\cdot\mathcal{A}=0$, the matrix element of the gauge-invariant operator product (2.67) of two quark fields separated by a light-like distance along the n^μ direction is independent of the gauge field $\mathcal{A}^\mu$. The quark distribution is given by the Fourier transform of this correlation function,

$$q(x) = \int \frac{d\lambda}{2\pi} e^{i\lambda x}\left\langle P\middle|\bar\psi(0)\not n\psi(\lambda n)\middle|P\right\rangle\,, \tag{4.42}$$

where ψ represents the quark field operator. Notice that the identification of $q(x)$ with a quark number density is only valid in the infinite momentum frame. To see this, we take the first moment of the quark distribution with respect to x to obtain

$$\int dx\; q(x) = \left\langle P\middle|\bar\psi(0)\not n\psi(0)\middle|P\right\rangle \approx \left\langle P\middle|\bar\psi^\dagger(0)\psi(0)\middle|P\right\rangle\,, \tag{4.43}$$

where the approximation is valid only in a fast moving frame in which

$$\bar\psi\gamma^0\psi \approx \bar\psi\gamma^3\psi\,. \tag{4.44}$$

How does a proton look in the infinite momentum frame? Because of the Lorentz contraction, the longitudinal size of the proton is contracted by a factor M/P with respect to its size in the rest frame. Partons with finite values of x and fixed transverse size are distributed on this disc, as shown

Downloaded from https://www.cambridge.org/core. UNIVERSIDAD AUTONOMA METROPOLITANA, on 15 Nov 2026 at 15:53:11, subject to the Cambridge Core terms of use, available at https://www.cambridge.org/core/terms. https://doi.org/10.1017/CBO9780511628788.005

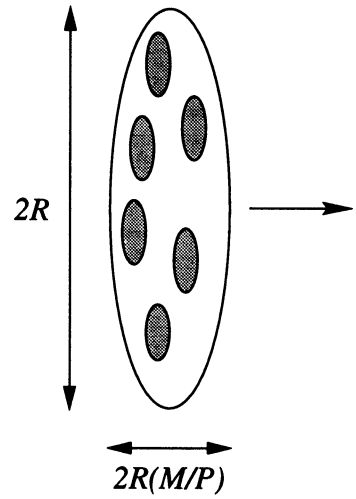


Fig. 4.5. The proton as viewed in the infinite momentum frame.

in Fig. 4.5, and the number of partons per unit of longitudinal phase space dx/x is rather small. Partons with very small values of x such that $x \sim 1\ \mathrm{GeV}/P$ are sometimes called 'wee' partons [2]. Because of their very small momentum they are not confined to the Lorentz contracted disc. Their spatial extent is rather determined by the uncertainty principle,

$$\Delta z \sim \frac{1}{xP} \,. \tag{4.45}$$

4.3 The parton model and QCD

In the 'naive' parton model the structure functions *scale*, *i.e.* $F(x, Q^2) \to F(x)$ in the asymptotic (Bjorken) limit: $Q^2 \to \infty$, x fixed. In QCD, this scaling is *broken* by logarithms of Q^2. The key point is that the parton's transverse momentum (in the frame defined in the previous section) is *not* in fact restricted to be small. As we shall see below, a quark can emit a gluon and acquire large transverse momentum k_T with probability proportional to $\alpha_S\ dk_T^2/k_T^2$ at large k_T. The integral extends up to the kinematic limit $k_T^2 \sim Q^2$, and gives rise to contributions proportional to $\alpha_S \log Q^2$ which break scaling. These logarithmic scaling violations are a particular property of renormalizable gauge theories with point-like fermion–vector boson interactions. In contrast, one could imagine a different theory in which the probability for a parton to acquire large k_T was proportional to $dk_T^2(m^2/k_T^4)$, with m some mass scale in the theory.

Downloaded from https://www.cambridge.org/core. UNIVERSIDAD AUTONOMA METROPOLITANA, on 15 Nov 2026 at 15:53:11, subject to the Cambridge Core terms of use, available at https://www.cambridge.org/core/terms. https://doi.org/10.1017/CBO9780511628788.005

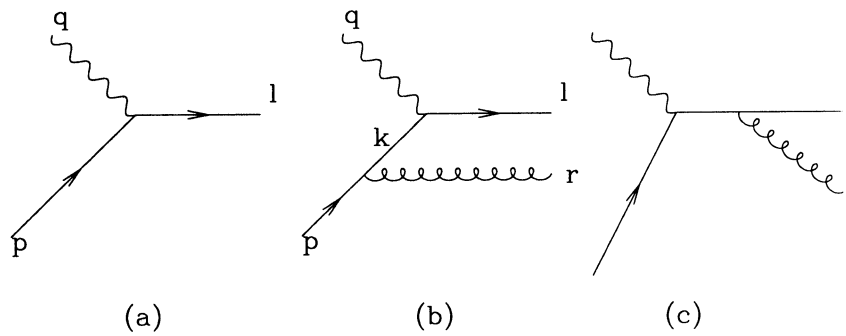


Fig. 4.6. Amplitudes for deep inelastic scattering off a quark.

In this case, the transverse momentum would be effectively cut off at $k_T^2 \sim m^2$, giving rise to Bjorken scaling for $Q^2 \gg m^2$.

In this section we will calculate the structure function of a quark which can emit a gluon, *i.e.* the $O(\alpha_S)$ correction to the parton model result $\hat{F}_2 = e_q^2 x\delta(x-\xi)$ obtained in Section 4.1.

4.3.1 *Contribution from one-gluon emission*

To establish the normalization we first calculate the scattering of a virtual photon off a free quark with momentum p (*i.e.* $\xi = 1$), represented by Fig. 4.6(a):

$$\gamma^*(q) + q(p) \to q(l) \,. \tag{4.46}$$

The four-momenta of the lines are shown in brackets. The invariant matrix element for this process is

$$\mathcal{M}_\alpha = -ie_q \bar{u}(l)\gamma^\alpha u(p) \,, \tag{4.47}$$

leading to a squared matrix element (summed and averaged over spins and colours and with the F_2 contribution projected out)

$$n^\alpha n^\beta \overline{\sum} |\mathcal{M}|^2_{\alpha\beta} = 4e_q^2 \,. \tag{4.48}$$

The one-dimensional phase space is

$$d\Phi_1 = 2\pi\delta((p+q)^2) \,. \tag{4.49}$$

Inserting the 'flux factor' of $1/4\pi$ from Eq. (4.28) we obtain

$$\hat{F}_2(x) = e_q^2\delta(1-x) \tag{4.50}$$

which is the naive parton model result with $\xi = 1$. The ' $\hat{}$ ' indicates that the structure function refers to a quark, rather than proton, target. We next investigate the more complicated parton process, Fig. 4.6(b,c),

Downloaded from https://www.cambridge.org/core. UNIVERSIDAD AUTONOMA METROPOLITANA, on 15 Nov 2026 at 15:53:11, subject to the Cambridge Core terms of use, available at https://www.cambridge.org/core/terms. https://doi.org/10.1017/CBO9780511628788.005

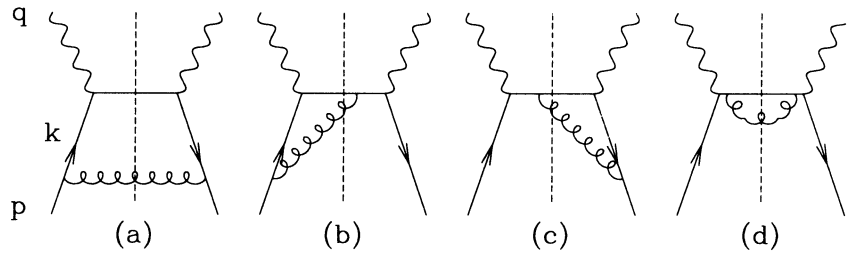


Fig. 4.7. Real gluon emission diagrams contributing to deep inelastic scattering.

in which the quark emits a gluon:

$$\gamma^*(q) + q(p) \to g(r) + q(l) \; . \tag{4.51}$$

The squares of the Feynman diagrams involving real radiation are shown in Fig. 4.7. We begin by considering the diagram of Fig. 4.7(a). Notice that this has the same topology as the hadron-quark amplitude of the previous section, where here the amplitude B in Fig. 4.4 is represented by single gluon exchange. The Lorentz invariant phase space for this contribution is

$$d\Phi_2 = \int \frac{d^4r}{(2\pi)^3} \frac{d^4l}{(2\pi)^3} \, \delta^+(r^2)\delta^+(l^2) \, (2\pi)^4 \delta^4(p+q-r-l) \; . \tag{4.52}$$

Introducing k^μ to denote the momentum of the struck parton line we obtain

$$d\Phi_2 = \frac{1}{4\pi^2} \int d^4k \; \delta^+((p-k)^2) \; \delta^+((k+q)^2) \; . \tag{4.53}$$

The four-vector k^μ can be written in terms of n, p and a transverse vector k_T^μ:

$$k^\mu = \xi p^\mu + \frac{k_T^2 - |k^2|}{2\xi} n^\mu + k_T^\mu \tag{4.54}$$

$$d^4k = \frac{d\xi}{2\xi} dk^2 d^2k_T \tag{4.55}$$

which gives

$$(p-k)^2 = (1-\xi)\frac{|k^2|}{\xi} - \frac{k_T^2}{\xi} \; , \tag{4.56}$$

$$(k+q)^2 = 2\xi\nu - Q^2 - |k^2| - 2q_T \cdot k_T \; . \tag{4.57}$$

In terms of the components of k^μ, the phase space becomes

$$d\Phi_2 = \frac{1}{16\nu\pi^2} \int d\xi dk^2 dk_T^2 d\theta \; \delta\left(k_T^2 - (1-\xi)\,|k^2|\right)$$

Downloaded from https://www.cambridge.org/core. UNIVERSIDAD AUTONOMA METROPOLITANA, on 15 Nov 2026 at 15:53:11, subject to the Cambridge Core terms of use, available at https://www.cambridge.org/core/terms. https://doi.org/10.1017/CBO9780511628788.005

$$\times \delta\left(\xi - x - \frac{|k^2| + 2q_T \cdot k_T}{2\nu}\right) \tag{4.58}$$

with $0 < \theta < \pi$. The corresponding matrix element is

$$\mathcal{M}^\alpha = -ige_q\, \bar{u}(l)\, \gamma^\alpha \frac{1}{\not{k}} \not{\varepsilon}\, t^A\, u(p) \tag{4.59}$$

where t^A is the SU(3) colour matrix introduced in Eq. (1.14). Squaring and averaging over colours and spins gives

$$\overline{\sum} |\mathcal{M}|^2_{\alpha\beta} = \tfrac{1}{2} e_q^2 g^2 \sum_{\text{pol}} C_F\, \text{Tr}[\gamma^\beta (\not{k} + \not{q}) \gamma^\alpha \not{k} \not{\varepsilon} \not{p} \not{\varepsilon}^* \not{k}] \frac{1}{k^4}\,, \tag{4.60}$$

where we have used the colour-matrix identity (1.17).

To perform the sum over the polarization of the real gluon we use the projector

$$\sum_{\text{pol}} \varepsilon_\mu(r) \varepsilon^*_\nu(r) = -g_{\mu\nu} + \frac{n_\mu r_\nu + n_\nu r_\mu}{n \cdot r}\,. \tag{4.61}$$

Thus in addition to the Lorentz condition $\varepsilon \cdot r = 0$, the gluon satisfies the (light-cone) gauge condition $\varepsilon \cdot n = 0$. This ensures that only two physical (*i.e.* transverse) polarizations propagate.

We can again project out the contribution to $\hat{F}_2$ by using the vector n as in Eq. (4.35). Using the kinematic relations implicit in the phase space terms we find

$$\frac{1}{4\pi} n^\alpha n^\beta \overline{\sum} |\mathcal{M}|^2_{\alpha\beta} = \frac{8e_q^2 \alpha_S}{|k^2|} \xi P(\xi)\,, \tag{4.62}$$

where the function $P(\xi)$ is known as the *splitting function*:

$$P(\xi) = C_F \frac{1 + \xi^2}{1 - \xi}\,. \tag{4.63}$$

Its form is specific to the qqg vertex of QCD. Note that the $1/k^4$ factor in Eq. (4.60) has been reduced to $1/k^2$ by terms in the numerator coming from the trace over the Dirac matrices. Putting everything together and performing the k_T^2 and θ integrations gives

$$\hat{F}_2 = e_q^2 \frac{\alpha_S}{2\pi^2} \int_0^{2\nu} \frac{d|k^2|}{|k^2|} \int_{\xi_-}^{\xi_+} d\xi\, \frac{\xi P(\xi)}{\sqrt{(\xi_+ - \xi)(\xi - \xi_-)}} \tag{4.64}$$

where

$$\xi_\pm(z, x) = x + z - 2zx \pm \sqrt{4x(1-x)z(1-z)}\,. \tag{4.65}$$

In order to simplify the notation we have introduced the variable $z = |k^2|/(2\nu)$. Requiring real roots for the quadratic gives the limits $0 < z < 1$.

Downloaded from https://www.cambridge.org/core. UNIVERSIDAD AUTONOMA METROPOLITANA, on 15 Nov 2026 at 15:53:11, subject to the Cambridge Core terms of use, available at https://www.cambridge.org/core/terms. https://doi.org/10.1017/CBO9780511628788.005

As anticipated at the start of this section, the transverse momentum (equivalently, the virtuality $|k^2|$) is *not* restricted to small values.[5] In addition, we see that the $|k^2|$ integral is logarithmically divergent at small $|k^2|$. The origin and treatment of this singularity will be discussed below, but in the meantime we can introduce a small cut-off κ^2 in the integral and calculate the coefficient of the resulting logarithm. Noting that $\xi_\pm \to x$ as $z \to 0$, and using the result

$$\int_{\xi_-}^{\xi_+} d\xi \frac{1}{\sqrt{(\xi_+ - \xi)(\xi - \xi_-)}} = \pi \tag{4.66}$$

we obtain

$$\hat{F}_2\Big|_{\text{div}} = e_q^2 \frac{\alpha_S}{2\pi}\, xP(x) \int_{\kappa^2}^{2\nu} \frac{d\,|k^2|}{|k^2|} = e_q^2 \frac{\alpha_S}{2\pi}\, xP(x)\, \ln\left(\frac{2\nu}{\kappa^2}\right) . \tag{4.67}$$

So far we have only considered the diagram of Fig. 4.7(a). In fact in the light-cone gauge (4.61) this is the only diagram which gives a logarithmic divergence — the other diagrams give finite corrections to the structure function. Consider for example Fig. 4.7(b). Instead of the $1/k^4$ present in Fig. 4.7(a), this diagram contains only one propagator which can diverge. The other propagator involves $1/(p+q)^2$. The numerator factors at the qqg vertex contribute another factor of $k_T \sim \sqrt{|k^2|}$, in the light-cone gauge, and so this diagram gives only a finite contribution to the structure function.

In summary, the four diagrams of Fig. 4.7, together with the leading-order diagram, give a structure function

$$\hat{F}_2(x, Q^2) = e_q^2 x \left[\delta(1-x) + \frac{\alpha_S}{2\pi}\left(P(x) \ln \frac{Q^2}{\kappa^2} + C(x)\right)\right] , \tag{4.68}$$

where P is given by Eq. (4.63) and C is a calculable function. Note that in deriving Eq. (4.68) we have used $\ln(2\nu) = \ln Q^2 - \ln x$ and absorbed the latter logarithm into the function $C(x)$.

Our calculation shows that *beyond leading order the structure function is Q^2 dependent*, with Bjorken scaling broken by logarithms of Q^2. The corresponding quark distribution function to this order in perturbation theory is

$$q(x, Q^2) = \delta(1-x) + \frac{\alpha_S}{2\pi}\left(P(x) \ln \frac{Q^2}{\kappa^2} + C(x)\right) . \tag{4.69}$$

This is not quite the complete answer for q. The full result requires the inclusion of virtual gluon radiation, specifically the inclusion of self-energy

[5] This is to be expected since there is no small scale in the calculation which could provide such a limit.

Downloaded from https://www.cambridge.org/core. UNIVERSIDAD AUTONOMA METROPOLITANA, on 15 Nov 2026 at 15:53:11, subject to the Cambridge Core terms of use, available at https://www.cambridge.org/core/terms. https://doi.org/10.1017/CBO9780511628788.005

insertions on the quark legs and the photon vertex correction. The calculation of these diagrams is straightforward using standard loop-integral methods.[6] The ultraviolet divergences which appear in individual loop diagrams cancel in the sum. In fact, a physical argument provides a useful short-cut to the answer [8]. First we note that because the delta function $\delta((p+q)^2)$ is common to all the virtual diagrams, their contribution to the structure function is proportional to $\delta(1-x)$. Thus, for example, the splitting function becomes

$$P(x) \longrightarrow P(x) + K\delta(1-x) \,. \tag{4.70}$$

Second, in order to conserve quark (*i.e.* baryon) number, the integral of the quark distribution cannot vary with Q^2. This implies that the function on the right-hand side of Eq. (4.70) must integrate to 0. This is achieved with

$$P(x) = C_F \left[\frac{1+x^2}{(1-x)_+} + \frac{3}{2}\delta(1-x) \right] \,, \tag{4.71}$$

where the 'plus' distribution is defined so that its integral with any sufficiently smooth distribution f is

$$\int_0^1 dx \frac{f(x)}{(1-x)_+} = \int_0^1 dx \frac{f(x)-f(1)}{1-x} \,, \tag{4.72}$$

and

$$\frac{1}{(1-x)_+} = \frac{1}{1-x} \quad \text{for } 0 \le x < 1 \,. \tag{4.73}$$

The one-gluon contribution to the longitudinal structure function can be calculated in a similar way. In this case, following Eq. (4.35), the projection of the matrix element in Eq. (4.62) is replaced by

$$\frac{x^2}{\pi\nu^2} p^\alpha p^\beta \overline{\sum} |\mathcal{M}|^2_{\alpha\beta} \,. \tag{4.74}$$

Once again the leading contribution comes from Fig. 4.7(a), since it is the only diagram to give non-zero transverse momentum to the struck quark. However in this case there is no logarithmic singularity: the integral over the quark virtuality is $\nu^{-1}\int^{2\nu} d|k^2| = O(1)$. The result is (*cf.* Eq. (4.68))

$$\hat{F}_L(x,Q^2) = e_q^2 x \left[0 + \frac{\alpha_S}{2\pi} C_F \, 2x \right] \,. \tag{4.75}$$

[6] In fact the treatment of these graphs in the light-cone gauge is somewhat delicate, and so in practice it is simpler to use a covariant gauge for these diagrams.

Downloaded from https://www.cambridge.org/core. UNIVERSIDAD AUTONOMA METROPOLITANA, on 15 Nov 2026 at 15:53:11, subject to the Cambridge Core terms of use, available at https://www.cambridge.org/core/terms. https://doi.org/10.1017/CBO9780511628788.005

4.3.2 Factorization

Our procedure for regulating the singularity at $|k^2| = 0$ by introducing a small cut-off κ^2 was completely *ad hoc*. One could in fact have performed a regularization in other ways. For example, dimensional regularization, which is a convenient method for handling *ultraviolet* divergences, can be used in the present context as well. The idea is to change the number of space-time dimensions from 4 to $n = 4 - 2\epsilon$, whereupon the divergent integral becomes $d|k^2|/|k^2|^{1+\epsilon}$. The result is then finite for any $\epsilon < 0$, and the analogue of Eq. (4.67) is

$$\hat{F}_2\Big|_{\text{div}} = e_q^2 \frac{\alpha_S}{2\pi} xP(x) \left(-\frac{1}{\epsilon}\right) . \tag{4.76}$$

How should we interpret the divergence in the structure function at $O(\alpha_S)$? Notice that the singularity arises when the gluon is emitted parallel to the quark ($k_T = 0$), and for this reason is often called a collinear divergence. This divergence is not subject to the theorems for cancellation of singularities discussed in Chapter 3, because the virtual photon *can* distinguish between a quark and a collinear quark-gluon pair carrying the same overall momentum. The key to understanding what is happening is to realize that the limit $k_T^2 \to 0$ corresponds to a long-range ('soft') part of the strong interaction which is not calculable in perturbation theory. In order to obtain a proton structure function we must convolute the quark structure function $\hat{F}_2$ of Eq. (4.68) with a 'bare' distribution q_0 of a quark in a proton and sum over quark flavours, as we did in Section 4.1 for the naive parton model. This gives

$$\begin{aligned} F_2(x,Q^2) &= x\sum_{q,\bar{q}} e_q^2 \left[q_0(x) + \frac{\alpha_S}{2\pi}\int_x^1 \frac{d\xi}{\xi}\, q_0(\xi) \right. \\ &\qquad \left. \left\{ P\left(\frac{x}{\xi}\right) \ln\frac{Q^2}{\kappa^2} + C\left(\frac{x}{\xi}\right)\right\} + \ldots \right] , \end{aligned} \tag{4.77}$$

where the ellipsis represents contributions from higher orders in perturbation theory.

Exactly as for the renormalization of the coupling constant, we can regard $q_0(x)$ as an unmeasurable, *bare* distribution. The collinear singularities are absorbed into this bare distribution at a 'factorization scale' μ, which plays a similar role to the renormalization scale. In other words, we define a 'renormalized' distribution $q(x,\mu^2)$ by

$$q(x,\mu^2) = q_0(x) + \frac{\alpha_S}{2\pi}\int_x^1 \frac{d\xi}{\xi}\, q_0(\xi) \left\{ P\left(\frac{x}{\xi}\right) \ln\frac{\mu^2}{\kappa^2} + C\left(\frac{x}{\xi}\right)\right\} + \ldots , \tag{4.78}$$

Downloaded from https://www.cambridge.org/core. UNIVERSIDAD AUTONOMA METROPOLITANA, on 15 Nov 2026 at 15:53:11, subject to the Cambridge Core terms of use, available at https://www.cambridge.org/core/terms. https://doi.org/10.1017/CBO9780511628788.005

in terms of which

$$F_2(x,Q^2) = x\sum_{q,\bar{q}} e_q^2 \int_x^1 \frac{d\xi}{\xi}\, q(\xi,\mu^2) \times \left\{\delta(1-\frac{x}{\xi}) + \frac{\alpha_S}{2\pi} P\left(\frac{x}{\xi}\right) \ln\frac{Q^2}{\mu^2} + \ldots\right\} . \quad (4.79)$$

The distribution $q(x,\mu^2)$ cannot be calculated from first principles in perturbation theory, since it receives contributions from the long-distance (non-perturbative) part of the strong interaction. It can of course be determined from structure function data at any particular scale, since $F_2(x,Q^2) = x\sum e_q^2 q(x,Q^2)$.

The ability to separate or factorize the long- and short-distance contributions to the structure function (or more generally, to any physical cross section involving large momentum transfers) in this way is a fundamental property of the theory. Although we have only demonstrated factorization to $O(\alpha_S)$, proofs to all orders in perturbation theory exist. A more complete discussion will be given in Chapter 7.

It is interesting to note that while factorization provides a prescription for dealing with the logarithmic singularities, there is an arbitrariness in how the *finite* (non-logarithmic) contributions are treated. In the example given above, all of the finite contribution C was absorbed into the quark distribution $q(x,\mu^2)$. We could, however, have factored out an arbitrary finite term, C' say, which would have left behind an additional finite contribution $C-C'$ in the expression for the structure function. How much finite contribution is factored out defines what is called the 'factorization scheme'. The example above, in which $F_2(x,Q^2) = x\sum_{q,\bar{q}} e_q^2 q(x,Q^2)$ with no finite $O(\alpha_S)$ corrections, is called the DIS (Deep Inelastic Scattering) scheme [9]. A more common choice in practice is the $\overline{\rm MS}$ scheme, in which in addition to the divergent piece only a ubiquitous $\ln(4\pi) - \gamma_E$ contribution is absorbed into the quark distribution. In this case one has

$$F_2(x,Q^2) = x\sum_{q,\bar{q}} e_q^2 \int_x^1 \frac{d\xi}{\xi}\, q(\xi,Q^2) \left\{\delta(1-\frac{x}{\xi}) + \frac{\alpha_S}{2\pi} C_{\overline{\rm MS}}\left(\frac{x}{\xi}\right) + \ldots\right\} . \quad (4.80)$$

It might at first sight appear that the arbitrariness in defining a factorization scheme removes any predictive power from the theory. This is not the case, since once a scheme has been fixed, say in deep inelastic scattering, it must be used in *all* other cross section calculations. For example, the higher-order corrections to the cross section for lepton pair production in hadron-hadron collisions will depend on the factorization scheme used to define the parton distributions (see Chapter 9).

In order to obtain a complete description of the deep inelastic structure functions in terms of parton distributions, there is one further contribu-

Downloaded from https://www.cambridge.org/core. UNIVERSIDAD AUTONOMA METROPOLITANA, on 15 Nov 2026 at 15:53:11, subject to the Cambridge Core terms of use, available at https://www.cambridge.org/core/terms. https://doi.org/10.1017/CBO9780511628788.005

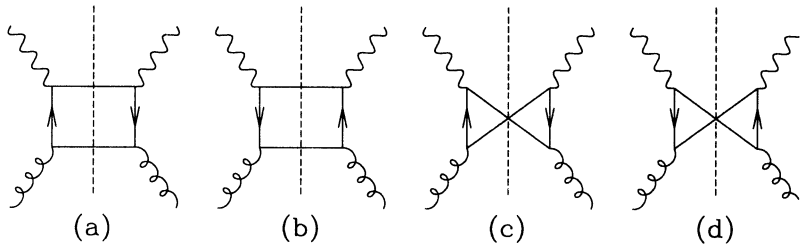


Fig. 4.8. Deep inelastic scattering with initial gluons.

tion that we must include, the $O(\alpha_S)$ contribution from the $\gamma^* g \to q\bar{q}$ process shown in Fig. 4.8. The calculation of this contribution, which we denote by $\hat{F}_2^g$, proceeds in the same way as the $\gamma^* q \to qg$ calculation described in Section 4.3.1. The result is

$$\hat{F}_2^g(x,Q^2) = x \sum_{q,\bar{q}} e_q^2 \frac{\alpha_S}{2\pi} \left(P_{qg}(x) \ln \frac{Q^2}{\kappa^2} + C_g(x) \right) . \tag{4.81}$$

Note the similarity between this result and that for the quark contribution, Eq. (4.68). There is again a logarithmic singularity from vanishing quark virtuality, $|k^2| \to 0$. The splitting function coefficient is now

$$P_{qg}(x) = T_R[x^2 + (1-x)^2] . \tag{4.82}$$

The colour factor $T_R = \frac{1}{2}$ is obtained from Eq. (1.16). The sum in Eq. (4.81) is over the n_f massless quark and antiquark flavours which contribute, *i.e.* the quark contributions from Figs. 4.8(a,c) and the identical antiquark contributions from Figs. 4.8(b,d).

To obtain the physical structure function, the contribution (4.81) must be folded with a bare gluon distribution $g_0(x)$ and added to the result obtained in Eq. (4.77). Exactly as for the $O(\alpha_S)$ quark contribution, the logarithmic singularity in (4.81) can then be absorbed into the bare quark distribution at the factorization scale μ, so that Eq. (4.78) becomes

$$\begin{aligned} q(x,\mu^2) \;=\; & q_0(x) + \frac{\alpha_S}{2\pi} \int_x^1 \frac{d\xi}{\xi} q_0(\xi) \left\{ P_{qq}\left(\frac{x}{\xi}\right) \ln \frac{\mu^2}{\kappa^2} + C_q\left(\frac{x}{\xi}\right) \right\} + \\ & + \frac{\alpha_S}{2\pi} \int_x^1 \frac{d\xi}{\xi} g_0(\xi) \left\{ P_{qg}\left(\frac{x}{\xi}\right) \ln \frac{\mu^2}{\kappa^2} + C_g\left(\frac{x}{\xi}\right) \right\} + \ldots . \end{aligned} \tag{4.83}$$

By absorbing *all* the gluon contribution into the quark distribution — the DIS factorization scheme — we still have $F_2(x,Q^2) = x \sum_{q,\bar{q}} e_q^2 q(x,Q^2)$. In the $\overline{\text{MS}}$ scheme, only the divergent part is absorbed into the renormalized

Downloaded from https://www.cambridge.org/core. UNIVERSIDAD AUTONOMA METROPOLITANA, on 15 Nov 2026 at 15:53:11, subject to the Cambridge Core terms of use, available at https://www.cambridge.org/core/terms. https://doi.org/10.1017/CBO9780511628788.005

quark distribution, so that

$$F_2(x,Q^2) = x\sum_{q,\bar{q}} e_q^2 \int_x^1 \frac{d\xi}{\xi}\, q(\xi,Q^2)\left\{\delta(1-\frac{x}{\xi}) + \frac{\alpha_S}{2\pi}C_q^{\overline{\rm MS}}\left(\frac{x}{\xi}\right)+\ldots\right\}$$
$$+x\sum_{q,\bar{q}} e_q^2 \int_x^1 \frac{d\xi}{\xi}\, g(\xi,Q^2)\left\{\frac{\alpha_S}{2\pi}C_g^{\overline{\rm MS}}\left(\frac{x}{\xi}\right)+\ldots\right\}. \quad (4.84)$$

The functions $C_q(x)$ and $C_g(x)$ are called *coefficient functions*. They depend on the factorization and renormalization schemes, and also on the structure function under consideration (*i.e.* they are different in general for F_1, F_2 and F_3). In the DIS scheme these functions for F_2 are zero at all non-leading orders in perturbation theory. The $\overline{\rm MS}$ $O(\alpha_S)$ coefficient functions for F_2 are [10]

$$C_q^{\overline{\rm MS}}(z) = C_F\left[2\left(\frac{\ln(1-z)}{1-z}\right)_+ - \frac{3}{2}\left(\frac{1}{1-z}\right)_+ - (1+z)\ln(1-z)\right.$$
$$\left. -\frac{1+z^2}{1-z}\ln z + 3 + 2z - \left(\frac{\pi^2}{3}+\frac{9}{2}\right)\delta(1-z)\right],$$
$$C_g^{\overline{\rm MS}}(z) = T_R\left[\left((1-z)^2+z^2\right)\ln\left(\frac{1-z}{z}\right) - 8z^2 + 8z - 1\right]. \quad (4.85)$$

For the longitudinal structure function, the leading-order coefficient functions are scheme independent:

$$F_L(x,Q^2) = x\sum_{q,\bar{q}} e_q^2 \int_x^1 \frac{d\xi}{\xi}\, q(\xi,Q^2)\left\{\frac{\alpha_S}{2\pi}\left[2C_F\frac{x}{\xi}\right]+\ldots\right\}$$
$$+x\sum_{q,\bar{q}} e_q^2 \int_x^1 \frac{d\xi}{\xi}\, g(\xi,Q^2)\left\{\frac{\alpha_S}{2\pi}\left[4T_R\frac{x}{\xi}\left(1-\frac{x}{\xi}\right)\right]+\ldots\right\}. \quad (4.86)$$

We have already stated that the first-principles calculation of the parton distributions is beyond the scope of perturbation theory. Attempts to use non-perturbative methods, for example numerical calculations based on lattice gauge theory, have been so far been unable to achieve a level of precision necessary to make a meaningful comparison with the experimental measurements, see for example ref. [11]. However what *can* be calculated perturbatively is how they depend on the factorization scale μ^2. To see how this is achieved, we simply have to notice that the right-hand side of Eq. (4.79) must be independent of μ^2. Taking the derivative $\partial/\partial\ln\mu^2$ of both sides will give us a differential equation for the μ^2 dependence of $q(x,\mu^2)$, and hence for the Q^2 dependence (scaling violations) of the deep inelastic structure function.

Downloaded from https://www.cambridge.org/core. UNIVERSIDAD AUTONOMA METROPOLITANA, on 15 Nov 2026 at 15:53:11, subject to the Cambridge Core terms of use, available at https://www.cambridge.org/core/terms. https://doi.org/10.1017/CBO9780511628788.005

4.3.3 Scaling violations and the GLAP equation

If we define $t = \mu^2$ and take the $\ln t$ partial derivative of Eq. (4.79) we obtain

$$t\frac{\partial}{\partial t}q(x,t) = \frac{\alpha_S(t)}{2\pi}\int_x^1 \frac{d\xi}{\xi} P\left(\frac{x}{\xi}\right) q(\xi,t)\,. \tag{4.87}$$

This equation — known as the (Dokshitzer)-Gribov-Lipatov-Altarelli-Parisi (GLAP) equation [12] — is the analogue of the β function equation describing the variation of $\alpha_S(t)$ with t and is one of the most important equations of perturbative QCD.

The above derivation is not completely rigorous, for example we have introduced t as the argument of the running coupling, but a more exact treatment based on the operator product expansion and the renormalization group equation [13,14] confirms Eq. (4.87) and extends the result to higher orders in perturbation theory. The full prediction of the theory is

$$t\frac{\partial}{\partial t}q(x,t) = \frac{\alpha_S(t)}{2\pi}\int_x^1 \frac{d\xi}{\xi} P_{qq}\left(\frac{x}{\xi},\alpha_S(t)\right) q(\xi,t). \tag{4.88}$$

The function P_{qq} has a perturbative expansion in the running coupling,

$$P_{qq}(z,\alpha_S) = P_{qq}^{(0)}(z) + \frac{\alpha_S}{2\pi}P_{qq}^{(1)}(z) + \ldots\,. \tag{4.89}$$

Retaining only the first term in this expansion gives precisely the result of Eq. (4.87), with $P \equiv P_{qq}^{(0)}$.

In fact the above equation is strictly only correct for 'non-singlet' distributions, defined as differences between quark distributions, *e.g.* $q_{\rm NS} = q_i - q_j$. More generally, the GLAP equation is a $(2n_f+1)$–dimensional matrix equation in the space of quarks, antiquarks and gluons,

$$t\frac{\partial}{\partial t}\begin{pmatrix} q_i(x,t) \\ g(x,t)\end{pmatrix} = \frac{\alpha_S(t)}{2\pi}\sum_{q_j,\bar{q}_j}\int_x^1\frac{d\xi}{\xi} \times \begin{pmatrix} P_{q_iq_j}\left(\frac{x}{\xi},\alpha_S(t)\right) & P_{q_ig}\left(\frac{x}{\xi},\alpha_S(t)\right) \\ P_{gq_j}\left(\frac{x}{\xi},\alpha_S(t)\right) & P_{gg}\left(\frac{x}{\xi},\alpha_S(t)\right)\end{pmatrix}\begin{pmatrix} q_j(\xi,t) \\ g(\xi,t)\end{pmatrix}, \tag{4.90}$$

where each splitting function (or 'evolution kernel') is again calculable as a power series in α_S,

$$\begin{aligned} P_{q_iq_j}(z,\alpha_S) &= \delta_{ij}P_{qq}^{(0)}(z) + \frac{\alpha_S}{2\pi}P_{q_iq_j}^{(1)}(z) + \ldots \\ P_{qg}(z,\alpha_S) &= P_{qg}^{(0)}(z) + \frac{\alpha_S}{2\pi}P_{qg}^{(1)}(z) + \ldots \\ P_{gq}(z,\alpha_S) &= P_{gq}^{(0)}(z) + \frac{\alpha_S}{2\pi}P_{gq}^{(1)}(z) + \ldots \end{aligned}$$

Downloaded from https://www.cambridge.org/core. UNIVERSIDAD AUTONOMA METROPOLITANA, on 15 Nov 2026 at 15:53:11, subject to the Cambridge Core terms of use, available at https://www.cambridge.org/core/terms. https://doi.org/10.1017/CBO9780511628788.005

$$P_{gg}(z,\alpha_S) = P_{gg}^{(0)}(z) + \frac{\alpha_S}{2\pi}P_{gg}^{(1)}(z) + \ldots . \tag{4.91}$$

Note that because of charge conjugation invariance and SU(n_f) flavour symmetry we have

$$\begin{aligned} P_{q_iq_j} &= P_{\bar{q}_i\bar{q}_j} \\ P_{q_i\bar{q}_j} &= P_{\bar{q}_iq_j} \\ P_{q_ig} &= P_{\bar{q}_ig} \equiv P_{qg} \\ P_{gq_i} &= P_{g\bar{q}_i} \equiv P_{gq} , \end{aligned} \tag{4.92}$$

i.e. the splitting functions P_{qg} and P_{gq} are independent of the quark flavour and the same for quarks and antiquarks. The leading-order $P_{q_iq_j}$ splitting function is zero unless $q_i = q_j$. This allows the matrix equation to be considerably simplified at this order (see below).

The leading-order GLAP splitting functions $P_{ab}^{(0)}(x)$ have an attractive physical interpretation as the probabilities of finding a parton of type a in a parton of type b with a fraction x of the longitudinal momentum of the parent parton and a transverse momentum squared much less than μ^2 [8]. The interpretation as probabilities implies that the splitting functions are positive definite for $x < 1$, and satisfy the sum rules

$$\begin{aligned} \int_0^1 dx P_{qq}^{(0)}(x) &= 0 \\ \int_0^1 dx\, x\left[P_{qq}^{(0)}(x) + P_{gq}^{(0)}(x)\right] &= 0 \\ \int_0^1 dx\, x\left[2n_f P_{qg}^{(0)}(x) + P_{gg}^{(0)}(x)\right] &= 0 , \end{aligned} \tag{4.93}$$

which correspond to quark number conservation and momentum conservation in the splittings of quarks and gluons respectively.

Both the leading-order [8] and $O(\alpha_S)$ [15,16,17] contributions to the GLAP splitting functions have been calculated. The leading-order contributions are

$$\begin{aligned} P_{qq}^{(0)}(x) &= C_F\left[\frac{1+x^2}{(1-x)_+} + \frac{3}{2}\delta(1-x)\right] , \\ P_{qg}^{(0)}(x) &= T_R\left[x^2 + (1-x)^2\right], \quad T_R = \frac{1}{2} , \\ P_{gq}^{(0)}(x) &= C_F\left[\frac{1+(1-x)^2}{x}\right] , \\ P_{gg}^{(0)}(x) &= 2C_A\left[\frac{x}{(1-x)_+} + \frac{1-x}{x} + x(1-x)\right] \\ &\quad + \delta(1-x)\frac{(11C_A - 4n_fT_R)}{6} , \end{aligned} \tag{4.94}$$

Downloaded from https://www.cambridge.org/core. UNIVERSIDAD AUTONOMA METROPOLITANA, on 15 Nov 2026 at 15:53:11, subject to the Cambridge Core terms of use, available at https://www.cambridge.org/core/terms. https://doi.org/10.1017/CBO9780511628788.005

where the 'plus prescription' on the singular parts of the functions has been defined in Eq. (4.72). Beyond leading order, the flavour structure of the $P_{q_iq_j}$ function is non-trivial. Using SU(n_f) flavour symmetry, we can write this in terms of flavour singlet (S) and non-singlet (V) quantities:

$$\begin{aligned} P_{q_iq_k} &= \delta_{ik}P^V_{qq} + P^S_{qq} \\ P_{q_i\bar{q}_k} &= \delta_{ik}P^V_{q\bar{q}} + P^S_{q\bar{q}} \\ P^{\pm} &= P^V_{qq} \pm P^V_{q\bar{q}} \,. \end{aligned} \tag{4.95}$$

At next-to-leading order, the functions P^S_{qq} and $P^S_{q\bar{q}}$ are non-zero, but we have the additional relation

$$P^S_{qq} = P^S_{q\bar{q}}. \tag{4.96}$$

which simplifies the treatment of the non-singlet pieces.

An efficient method for calculating the evolution of the individual quark distributions is to introduce a sequence of non-singlet combinations:

$$\begin{aligned} V_i &= q_i^- \\ T_3 &= u^+ - d^+ \\ T_8 &= u^+ + d^+ - 2s^+ \\ T_{15} &= u^+ + d^+ + s^+ - 3c^+ \\ T_{24} &= u^+ + d^+ + s^+ + c^+ - 4b^+ \\ T_{35} &= u^+ + d^+ + s^+ + c^+ + b^+ - 5t^+ \end{aligned} \tag{4.97}$$

where

$$q_i^{\pm} = q_i \pm \bar{q}_i \tag{4.98}$$

and u, d, s, c, b, t are the distributions of the various flavours of quarks. It is then straightforward to show that (at next-to-leading order) the combinations V_i and T_j evolve according to Eq. (4.88) with $P^{(1)}_{qq} \equiv P^-$ and $P^{(1)}_{qq} \equiv P^+$ respectively.

The one remaining combination of quark distributions is the *singlet* distribution,

$$\Sigma(x,t) = \sum_i q_i^+(x,t) \equiv \sum_i [q_i(x,t) + \bar{q}_i(x,t)] \tag{4.99}$$

whose evolution is coupled with that of the gluon distribution:

$$\begin{aligned} t\frac{\partial}{\partial t}\begin{pmatrix} \Sigma(x,t) \\ g(x,t) \end{pmatrix} &= \frac{\alpha_S(t)}{2\pi}\int_x^1 \frac{d\xi}{\xi} \\ &\times \begin{pmatrix} P_{qq}\left(\frac{x}{\xi},\alpha_S(t)\right) & 2n_f P_{qg}\left(\frac{x}{\xi},\alpha_S(t)\right) \\ P_{gq}\left(\frac{x}{\xi},\alpha_S(t)\right) & P_{gg}\left(\frac{x}{\xi},\alpha_S(t)\right) \end{pmatrix} \begin{pmatrix} \Sigma(\xi,t) \\ g(\xi,t) \end{pmatrix}, \end{aligned} \tag{4.100}$$

Downloaded from https://www.cambridge.org/core. UNIVERSIDAD AUTONOMA METROPOLITANA, on 15 Nov 2026 at 15:53:11, subject to the Cambridge Core terms of use, available at https://www.cambridge.org/core/terms. https://doi.org/10.1017/CBO9780511628788.005

where now

$$P_{qq} = P^+ + n_f(P^S_{qq} + P^S_{q\bar{q}}) \,. \tag{4.101}$$

Knowing the 6 V_i combinations, the 5 T_j combinations and Σ one can solve for each of the 12 individual quark and antiquark distributions.

For completeness, we give here the full set of next-to-leading-order splitting functions in the $\overline{\text{MS}}$ factorization/renormalization scheme. We first introduce the notation

$$T_f = T_R n_f = \frac{1}{2} n_f \tag{4.102}$$

$$p_{qq}(x) = \frac{2}{1-x} - 1 - x \tag{4.103}$$

$$p_{qg}(x) = x^2 + (1-x)^2 \tag{4.104}$$

$$p_{gq}(x) = \frac{1+(1-x)^2}{x} \tag{4.105}$$

$$p_{gg}(x) = \frac{1}{1-x} + \frac{1}{x} - 2 + x(1-x) \,. \tag{4.106}$$

Then for $x \neq 1$, the non-singlet functions are [15]

$$\begin{aligned} P^{V(1)}_{qq} = {} & C_F^2 \left\{ -\left[2\ln x \ln(1-x) + \frac{3}{2}\ln x \right] p_{qq}(x) \right. \\ & \left. - \left(\frac{3}{2} + \frac{7}{2}x \right) \ln x - \frac{1}{2}(1+x)\ln^2 x - 5(1-x) \right\} \\ & + C_F C_A \left\{ \left[\frac{1}{2}\ln^2 x + \frac{11}{6}\ln x + \frac{67}{18} - \frac{\pi^2}{6} \right] p_{qq}(x) \right. \\ & \left. + (1+x)\ln x + \frac{20}{3}(1-x) \right\} \\ & + C_F T_f \left\{ -\left[\frac{2}{3}\ln x + \frac{10}{9} \right] p_{qq}(x) - \frac{4}{3}(1-x) \right\} \,, \end{aligned} \tag{4.107}$$

$$\begin{aligned} P^{V(1)}_{q\bar{q}} = {} & C_F \left(C_F - \frac{C_A}{2} \right) \left\{ 2p_{qq}(-x) S_2(x) \right. \\ & \left. + 2(1+x)\ln x + 4(1-x) \right\} \,, \end{aligned} \tag{4.108}$$

and for the singlet functions [16],

$$\begin{aligned} P^{(1)}_{qq} = {} & C_F^2 \left\{ -1 + x + \left(\frac{1}{2} - \frac{3}{2}x \right) \ln x - \frac{1}{2}(1+x)\ln^2 x \right. \\ & \left. - \left[\frac{3}{2}\ln x + 2\ln x \ln(1-x) \right] p_{qq}(x) + 2p_{qq}(-x) S_2(x) \right\} \\ & + C_F C_A \left\{ \frac{14}{3}(1-x) + \left[\frac{11}{6}\ln x + \frac{1}{2}\ln^2 x + \frac{67}{18} - \frac{\pi^2}{6} \right] p_{qq}(x) \right. \end{aligned}$$

Downloaded from https://www.cambridge.org/core. UNIVERSIDAD AUTONOMA METROPOLITANA, on 15 Nov 2026 at 15:53:11, subject to the Cambridge Core terms of use, available at https://www.cambridge.org/core/terms. https://doi.org/10.1017/CBO9780511628788.005

$$
\begin{aligned}
&-p_{qq}(-x)S_2(x)\Big\}\\
&+C_F T_f\left\{-\frac{16}{3}+\frac{40}{3}x+\left(10x+\frac{16}{3}x^2+2\right)\ln x\right.\\
&\left.-\frac{112}{9}x^2+\frac{40}{9x}-2(1+x)\ln^2 x-\left[\frac{10}{9}+\frac{2}{3}\ln x\right]p_{qq}(x)\right\} \qquad (4.109)
\end{aligned}
$$

$$
\begin{aligned}
P_{qg}^{(1)} \;=\;& C_F T_f\left\{4-9x-(1-4x)\ln x-(1-2x)\ln^2 x+4\ln(1-x)\right.\\
&\left.+\left[2\ln^2\left(\frac{1-x}{x}\right)-4\ln\left(\frac{1-x}{x}\right)-\frac{2}{3}\pi^2+10\right]p_{qg}(x)\right\}\\
&+C_A T_f\left\{\frac{182}{9}+\frac{14}{9}x+\frac{40}{9x}+\left(\frac{136}{3}x-\frac{38}{3}\right)\ln x\right.\\
&-4\ln(1-x)-(2+8x)\ln^2 x+2p_{qg}(-x)S_2(x)\\
&\left.+\left[-\ln^2 x+\frac{44}{3}\ln x-2\ln^2(1-x)+4\ln(1-x)\right.\right.\\
&\left.\left.+\frac{\pi^2}{3}-\frac{218}{9}\right]p_{qg}(x)\right\} \qquad (4.110)
\end{aligned}
$$

$$
\begin{aligned}
P_{gq}^{(1)} \;=\;& C_F^2\left\{-\frac{5}{2}-\frac{7x}{2}+\left(2+\frac{7}{2}x\right)\ln x-\left(1-\frac{1}{2}x\right)\ln^2 x\right.\\
&\left.-2x\ln(1-x)-\left[3\ln(1-x)+\ln^2(1-x)\right]p_{gq}(x)\right\}\\
&+C_F C_A\left\{\frac{28}{9}+\frac{65}{18}x+\frac{44}{9}x^2-\left(12+5x+\frac{8}{3}x^2\right)\ln x\right.\\
&+(4+x)\ln^2 x+2x\ln(1-x)+S_2(x)p_{gq}(-x)\\
&+\left[\frac{1}{2}-2\ln x\ln(1-x)+\frac{1}{2}\ln^2 x+\frac{11}{3}\ln(1-x)\right.\\
&\left.\left.+\ln^2(1-x)-\frac{\pi^2}{6}\right]p_{gq}(x)\right\}\\
&+C_F T_f\left\{-\frac{4}{3}x-\left[\frac{20}{9}+\frac{4}{3}\ln(1-x)\right]p_{gq}(x)\right\} \qquad (4.111)
\end{aligned}
$$

$$
\begin{aligned}
P_{gg}^{(1)} \;=\;& C_F T_f\left\{-16+8x+\frac{20}{3}x^2+\frac{4}{3x}\right.\\
&\left.-(6+10x)\ln x-(2+2x)\ln^2 x\right\}\\
&+C_A T_f\left\{2-2x+\frac{26}{9}\left(x^2-\frac{1}{x}\right)-\frac{4}{3}(1+x)\ln x-\frac{20}{9}p_{gg}(x)\right\}\\
&+C_A^2\left\{\frac{27}{2}(1-x)+\frac{67}{9}\left(x^2-\frac{1}{x}\right)-\left(\frac{25}{3}-\frac{11}{3}x+\frac{44}{3}x^2\right)\ln x\right.
\end{aligned}
$$

Downloaded from https://www.cambridge.org/core. UNIVERSIDAD AUTONOMA METROPOLITANA, on 15 Nov 2026 at 15:53:11, subject to the Cambridge Core terms of use, available at https://www.cambridge.org/core/terms. https://doi.org/10.1017/CBO9780511628788.005

$$+4(1+x)\ln^2 x + 2p_{gg}(-x)S_2(x) + \left[\frac{67}{9} - 4\ln x \ln(1-x) + \ln^2 x - \frac{\pi^2}{3}\right] p_{gg}(x)\Big\} \,. \tag{4.112}$$

The function $S_2(x)$ is defined by

$$S_2(x) = \int_{\frac{x}{1+x}}^{\frac{1}{1+x}} \frac{dz}{z} \ln\left(\frac{1-z}{z}\right) \,. \tag{4.113}$$

In terms of the dilogarithm function defined in Eq. (3.36), we have

$$S_2(x) = -2\mathrm{Li}_2(-x) + \frac{1}{2}\ln^2 x - 2\ln x \ln(1+x) - \frac{\pi^2}{6} \,. \tag{4.114}$$

The above results for the $P^{(1)}$ functions in Eqs. (4.107,4.109,4.112) can be extended to all values of x by using sum rules to fix the endpoint ($x = 1$) contributions: *i.e.* from the conservation of fermion number,

$$\int_0^1 dx \left(P_{qq}(x) - P_{q\bar{q}}(x)\right) \equiv \int_0^1 dx\, P^-(x) = 0 \,, \tag{4.115}$$

and momentum fraction,

$$\int_0^1 dx\, x\Big(P_{qq}(x) + P_{gq}(x)\Big) = 0 \,, \tag{4.116}$$

$$\int_0^1 dx\, x\Big(P_{qg}(x) + P_{gg}(x)\Big) = 0 \,. \tag{4.117}$$

These results for the integral of the splitting functions are satisfied if one makes the substitution

$$\frac{1}{1-x} \longrightarrow \frac{1}{(1-x)_+} \tag{4.118}$$

in Eqs. (4.103,4.106), and adds the following endpoint contributions to Eqs. (4.107), (4.109) and (4.112):

$$\delta P_{qq}^{V(1)} = \delta P_{qq}^{(1)} = \left[C_F^2\left\{\frac{3}{8} - \frac{\pi^2}{2} + 6\zeta(3)\right\} + C_F C_A\left\{\frac{17}{24} + \frac{11\pi^2}{18} - 3\zeta(3)\right\} - C_F T_f\left\{\frac{1}{6} + \frac{2\pi^2}{9}\right\}\right]\delta(1-x) \,, \tag{4.119}$$

$$\delta P_{gg}^{(1)} = \left[C_A^2\left\{\frac{8}{3} + 3\zeta(3)\right\} - C_F T_f - \frac{4}{3}C_A T_f\right]\delta(1-x) \,. \tag{4.120}$$

The values of the Riemann zeta functions are given in Eq. (3.19).

Downloaded from https://www.cambridge.org/core. UNIVERSIDAD AUTONOMA METROPOLITANA, on 15 Nov 2026 at 15:53:11, subject to the Cambridge Core terms of use, available at https://www.cambridge.org/core/terms. https://doi.org/10.1017/CBO9780511628788.005

In the small-x limit (see Section 4.6), Eq. (4.113) for S_2 gives

$$S_2 = \frac{1}{2}\ln^2 x - \frac{\pi^2}{6} + O(x) \,. \tag{4.121}$$

The small-x limit of the leading- and next-to-leading-order splitting functions for the evolution of the singlet quark and gluon distributions according to Eq. (4.100) is then

$$\begin{aligned} P_{qq} &\to \frac{\alpha_S}{2\pi}\frac{40C_F T_f}{9x} \\ P_{qg} &\to \frac{\alpha_S}{2\pi}\frac{40C_A T_f}{9x} \\ P_{gq} &\to \frac{2C_F}{x} + \frac{\alpha_S}{2\pi}\frac{9C_F C_A - 40C_F T_f}{x} \\ P_{gg} &\to \frac{2C_A}{x} + \frac{\alpha_S}{2\pi}\frac{12C_F T_f - 46C_A T_f}{9x} \,. \end{aligned} \tag{4.122}$$

The large-x limit is dominated by the diagonal terms of the splitting function matrix:

$$\begin{aligned} P_{qq} &\to \frac{2C_F}{(1-x)_+}\left(1 + \frac{\alpha_S}{2\pi}\kappa\right) \\ P_{gg} &\to \frac{2C_A}{(1-x)_+}\left(1 + \frac{\alpha_S}{2\pi}\kappa\right) \,, \end{aligned} \tag{4.123}$$

where

$$\kappa = C_A\left(\frac{67}{18} - \frac{\pi^2}{6}\right) - T_f\frac{10}{9} \,. \tag{4.124}$$

An alternative formulation of the evolution equations is in terms of the *moments* (Mellin transforms) of the parton distributions:

$$f(j,t) = \int_0^1 dx\; x^{j-1}\, f(x,t) \,, \quad f = q_i, g \,. \tag{4.125}$$

In terms of these moments, the t dependence of a non-singlet quark distribution function is given by

$$t\frac{\partial}{\partial t} q_{\rm NS}(j,t) = \frac{\alpha_S(t)}{2\pi}\,\gamma_{qq}\left(j, \alpha_S(t)\right) q_{\rm NS}\left(j,t\right) \,, \tag{4.126}$$

where the 'anomalous dimension' γ_{qq} is given by

$$\gamma_{qq}(j,\alpha_S) = \int_0^1 dx\; x^{j-1} P_{qq}(x,\alpha_S) \,. \tag{4.127}$$

Similar equations hold for the evolution of the singlet quark and gluon

Downloaded from https://www.cambridge.org/core. UNIVERSIDAD AUTONOMA METROPOLITANA, on 15 Nov 2026 at 15:53:11, subject to the Cambridge Core terms of use, available at https://www.cambridge.org/core/terms. https://doi.org/10.1017/CBO9780511628788.005

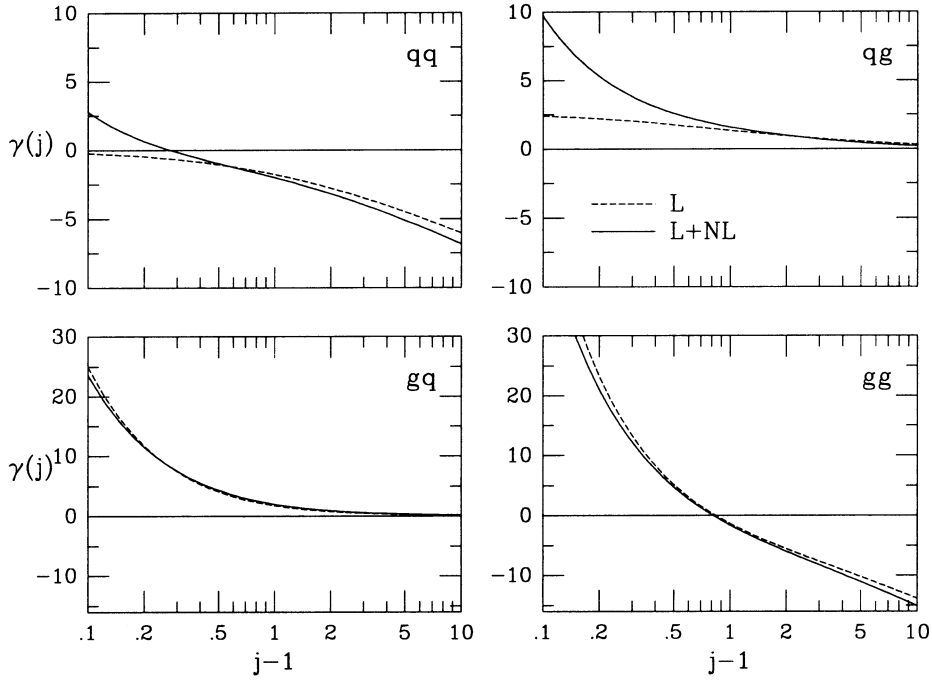


Fig. 4.9. The leading-order and next-to-leading-order singlet anomalous dimensions of Eq. (4.128) in the $\overline{\rm MS}$ scheme as a function of the moment number j, with $n_f = 4$ and $\alpha_S/(2\pi) = 1/30$.

distributions:

$$t\frac{\partial}{\partial t}\begin{pmatrix}\Sigma(j,t)\\ g(j,t)\end{pmatrix} = \frac{\alpha_S(t)}{2\pi}\begin{pmatrix}\gamma_{qq}(j,\alpha_S(t)) & 2n_f\gamma_{qg}(j,\alpha_S(t))\\ \gamma_{gq}(j,\alpha_S(t)) & \gamma_{gg}(j,\alpha_S(t))\end{pmatrix}\begin{pmatrix}\Sigma(j,t)\\ g(j,t)\end{pmatrix} \tag{4.128}$$

where $\Sigma(j,t)$ and $g(j,t)$ are the moments of the singlet quark and gluon distributions respectively. Notice that by taking moments we have reduced the convolution integral on the right-hand side of the evolution equations to a simple product. In the next section we shall see how this enables us to solve the equations analytically.

The complete set of leading-order anomalous dimensions is

$$\begin{aligned}
\gamma_{qq}^{(0)}(j) &= C_F\left[-\frac{1}{2}+\frac{1}{j(j+1)}-2\sum_{k=2}^{j}\frac{1}{k}\right],\\
\gamma_{qg}^{(0)}(j) &= T_R\left[\frac{(2+j+j^2)}{j(j+1)(j+2)}\right],\\
\gamma_{gq}^{(0)}(j) &= C_F\left[\frac{(2+j+j^2)}{j(j^2-1)}\right],
\end{aligned}$$

Downloaded from https://www.cambridge.org/core. UNIVERSIDAD AUTONOMA METROPOLITANA, on 15 Nov 2026 at 15:53:11, subject to the Cambridge Core terms of use, available at https://www.cambridge.org/core/terms. https://doi.org/10.1017/CBO9780511628788.005

$$\gamma_{gg}^{(0)}(j) = 2C_A\left[-\frac{1}{12}+\frac{1}{j(j-1)}+\frac{1}{(j+1)(j+2)}-\sum_{k=2}^{j}\frac{1}{k}\right]-\frac{2}{3}n_f T_R\,. \tag{4.129}$$

The dependence of the leading- and next-to-leading-order anomalous dimensions of Eq. (4.128) on the moment number j is illustrated in Fig. 4.9. Using the results

$$\begin{aligned}\int_0^1 dx\, x^{j-1}\,\frac{1}{x} &= \frac{1}{j-1}\\ \int_0^1 dx\, x^{j-1}\,\frac{1}{(1-x)_+} &= -\int_0^1 dx\,\frac{x^{j-1}-1}{(x-1)} \sim -\ln j\,, \quad \text{for } j\to\infty\,,\end{aligned} \tag{4.130}$$

we see that all the anomalous dimensions have poles at $j = 1$, and that the diagonal anomalous dimensions grow as $\ln j$ at large j. Notice from Fig. 4.9 that fixed-order perturbation theory appears to break down as $j \to 1$. This has important implications for the small-x behaviour of structure functions, and will be discussed in more detail in Section 4.6.

4.3.4 Solution of the leading-order GLAP equations

The solution of the GLAP equation is simplest for (flavour) non-singlet combinations of quark distributions, *e.g.* $V = q_i - q_j$. In such combinations the mixing with the flavour singlet gluon distribution drops out and we have simply

$$t\frac{\partial}{\partial t}V(x,t) = \frac{\alpha_S(t)}{2\pi}\left[P_{qq}(\xi)\otimes V(z,t)\right]\,, \tag{4.131}$$

where we have introduced $\otimes$ as a shorthand notation for the convolution integral of Eq. (4.88). In terms of moments, this equation becomes

$$t\frac{\partial}{\partial t}V(j,t) = \frac{\alpha_S(t)}{2\pi}\gamma_{qq}^{(0)}(j)\,V(j,t)\,, \tag{4.132}$$

with $\gamma_{qq}^{(0)}(j)$ given in Eq. (4.129). Inserting the lowest-order form (2.43) for the running coupling, we obtain the solution for the moments of the non-singlet distribution,

$$V(j,t) = V(j,t_0)\left(\frac{\alpha_S(t_0)}{\alpha_S(t)}\right)^{d_{qq}(j)}\,,\quad d_{qq}(j) = \frac{\gamma_{qq}^{(0)}(j)}{2\pi b} \tag{4.133}$$

where $b = (33-2n_f)/12\pi$. Finally, the distribution in x space can be obtained using the inverse Mellin transform integral,

$$V(x,t) = \frac{1}{2\pi i}\int_C dj\; x^{-j}\,V(j,t)\,, \tag{4.134}$$

Downloaded from https://www.cambridge.org/core. UNIVERSIDAD AUTONOMA METROPOLITANA, on 15 Nov 2026 at 15:53:11, subject to the Cambridge Core terms of use, available at https://www.cambridge.org/core/terms. https://doi.org/10.1017/CBO9780511628788.005

where the integration contour in the complex j plane is parallel to the imaginary axis and to the right of all singularities of the integrand. Except in very special cases, the inverse transformation can only be performed by numerical integration.

It is straightforward to show that $d_{qq}(1) = 0$ and that $d_{qq}(j) < 0$ for $j \geq 2$. This in turn implies that as μ^2 increases the non-singlet distribution function *decreases* at large x and *increases* at small x. Physically, this can be understood as an increase in the phase space for gluon emission by the quarks as μ^2 increases, with a corresponding reduction in quark momentum. The trend is clearly visible in the data. Fig. 4.10 shows data on the structure function $F_2^{\mu p}$ from the BCDMS [4] and NMC [18] collaborations. The slope $\partial F_2/\partial \ln Q^2$ is negative at large x and positive at small x respectively. In the limits $x \to 0$ and $x \to 1$ it is in fact possible to derive analytic approximations to the solution of the evolution equation. The small-x behaviour is determined by the rightmost singularities of the anomalous dimensions $\gamma_{ab}(j)$ on the positive real axis, and will be discussed in detail in Section 4.6. The large-x behaviour, on the other hand, is controlled by the form of the anomalous dimensions at large, real j. In particular, suppose that we look for a large-x solution of the form $V(x,t) \sim (1-x)^{a(t)}$. The large-j moments of such a solution are $V(j,t) \sim j^{-a(t)}$. From Eq. (4.129) we have also that

$$\gamma_{qq}(j) \sim -2C_F \ln j, \qquad j \gg 1\,, \tag{4.135}$$

so that the large-j limit of the right-hand side of the solution (4.133) is

$$j^{-a(t_0)} \left(\frac{\alpha_S(t_0)}{\alpha_S(t)}\right)^{-C_F \ln j/\pi b} = j^{-a(t_0) - C_F \ln(\alpha_S(t_0)/\alpha_S(t))/\pi b}\,. \tag{4.136}$$

The solution of the evolution equation in the $x \to 1$ limit is therefore

$$V(x,t) \sim (1-x)^{a_0 + C_F \ln(\alpha_S(t_0)/\alpha_S(t))/\pi b}\,, \tag{4.137}$$

where a_0 is the exponent at the starting scale t_0. As t increases, the exponent grows linearly with $\ln\ln t$, confirming that the distribution decreases at large x as the scale increases.

We now turn to the flavour singlet combination of quark distributions. At leading order we have

$$\begin{aligned} t\frac{\partial \Sigma}{\partial t} &= \frac{\alpha_S(t)}{2\pi}\left[P_{qq}^{(0)} \otimes \Sigma + 2n_f P_{qg}^{(0)} \otimes g\right] + O\left(\alpha_S^2(t)\right) \\ t\frac{\partial g}{\partial t} &= \frac{\alpha_S(t)}{2\pi}\left[P_{gq}^{(0} \otimes \Sigma + P_{gg}^{(0)} \otimes g\right] + O\left(\alpha_S^2(t)\right)\,. \end{aligned} \tag{4.138}$$

These equations are most easily solved by direct numerical integration in x space starting with input distributions obtained from data. The analytic solution in moment space, which requires finding the eigenvectors

Downloaded from https://www.cambridge.org/core. UNIVERSIDAD AUTONOMA METROPOLITANA, on 15 Nov 2026 at 15:53:11, subject to the Cambridge Core terms of use, available at https://www.cambridge.org/core/terms. https://doi.org/10.1017/CBO9780511628788.005

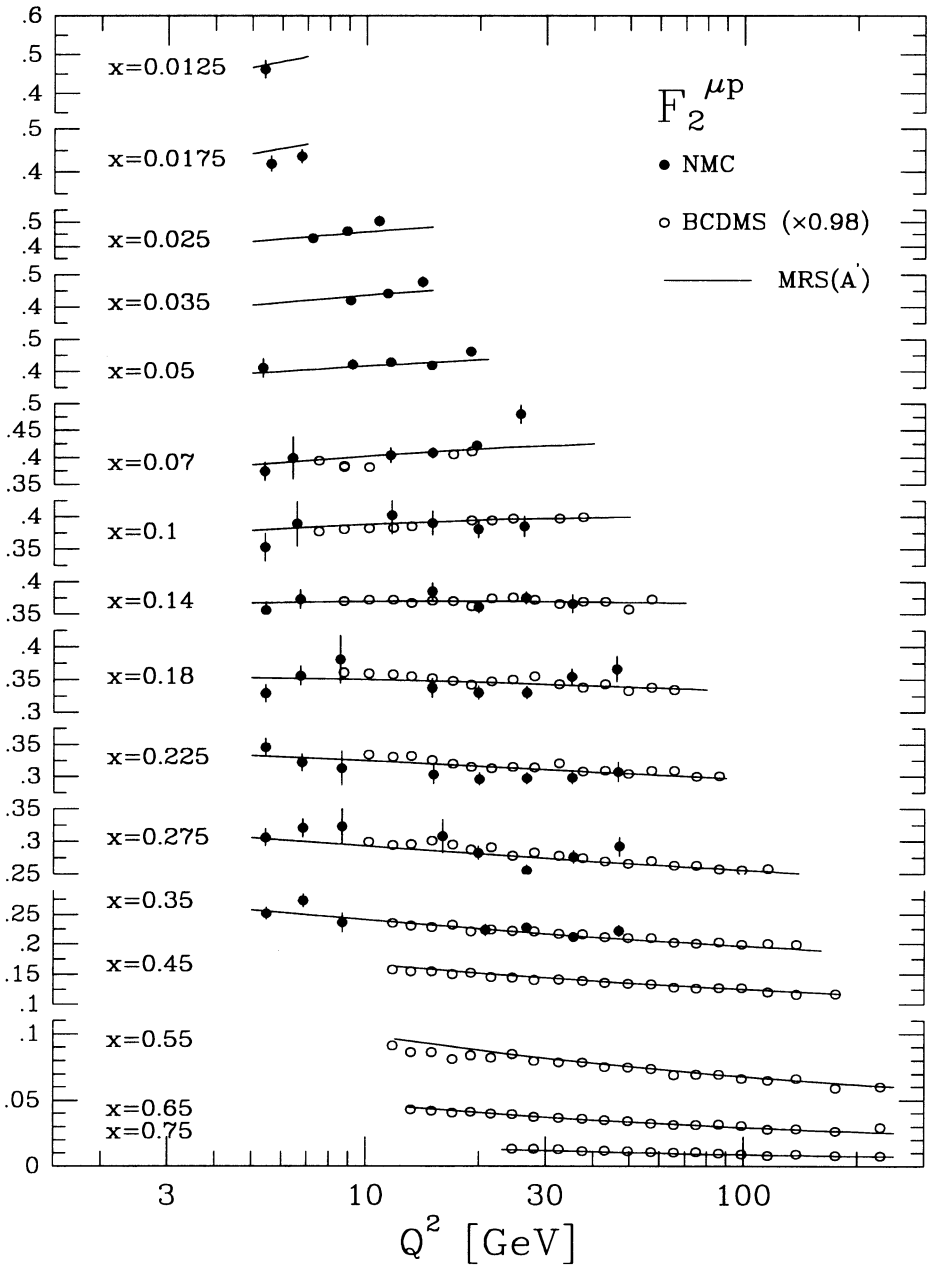


Fig. 4.10. Data on the structure function F_2 in muon-proton deep inelastic scattering, from BCDMS [4] and NMC [18]. The curves are QCD fits [7] as described in the text.

Downloaded from https://www.cambridge.org/core. UNIVERSIDAD AUTONOMA METROPOLITANA, on 15 Nov 2026 at 15:53:11, subject to the Cambridge Core terms of use, available at https://www.cambridge.org/core/terms. https://doi.org/10.1017/CBO9780511628788.005

and eigenvalues of the 2×2 matrix of anomalous dimensions, is rather cumbersome. The eigenvalues $\gamma_\pm$ are the solutions of the quadratic equation given by

$$\begin{vmatrix} \gamma_{qq} - \gamma & 2n_f\gamma_{qg} \\ \gamma_{gq} & \gamma_{gg} - \gamma \end{vmatrix} , \tag{4.139}$$

i.e.

$$\gamma_\pm = \frac{1}{2}\left[\gamma_{gg} + \gamma_{qq} \pm \sqrt{(\gamma_{gg} - \gamma_{qq})^2 + 8n_f\gamma_{gq}\gamma_{qg}}\right] . \tag{4.140}$$

The moment method can be used to illustrate some simple analytic properties of the solutions. For the second ($j = 2$) moment we have

$$t\frac{\partial}{\partial t}\begin{pmatrix} \Sigma(2,t) \\ g(2,t) \end{pmatrix} = \frac{\alpha_S(t)}{2\pi}\begin{pmatrix} -\frac{4}{3}C_F & \frac{1}{3}n_f \\ \frac{4}{3}C_F & -\frac{1}{3}n_f \end{pmatrix}\begin{pmatrix} \Sigma(2,t) \\ g(2,t) \end{pmatrix} . \tag{4.141}$$

The eigenvectors and associated eigenvalues of this system of equations are

$$\begin{aligned} O^+(2,t) &= \Sigma(2,t) + g(2,t) \quad \text{with eigenvalue } 0 , \\ O^-(2,t) &= \Sigma(2,t) - \frac{n_f}{4C_F}g(2,t) \quad \text{with eigenvalue } -\left(\frac{4}{3}C_F + \frac{n_f}{3}\right) . \end{aligned} \tag{4.142}$$

Note that the combination O^+, which corresponds to the total momentum carried by the quarks and gluons, is independent of t. The eigenvector O^- vanishes in the limit $t \to \infty$:

$$O^-(2,t) = \left(\frac{\alpha_S(t_0)}{\alpha_S(t)}\right)^{d^-(2)} \to 0, \quad \text{with } d^-(2) = \frac{\gamma_-(2)}{2\pi b} = -\frac{(\frac{4}{3}C_F + \frac{1}{3}n_f)}{2\pi b} , \tag{4.143}$$

so that asymptotically we have

$$\frac{\Sigma(2,t)}{g(2,t)} \to \frac{n_f}{4C_F} = \frac{3}{16}n_f . \tag{4.144}$$

The momentum fractions f_q and f_g carried by the quarks and gluons in the $\mu^2 = t \to \infty$ limit are therefore

$$f_q = \frac{3n_f}{16 + 3n_f} , \quad f_g = \frac{16}{16 + 3n_f} . \tag{4.145}$$

Note, however, that the approach to this asymptotic limit is controlled by $\ln t$ and is therefore quite slow. Expressions for the eigenvectors and eigenvalues of the moments of Eq. (4.138) can be found in ref. [19].

From the solution of the evolution equations for the moments of non-singlet and singlet combinations of quark distributions, the evolution of

Downloaded from https://www.cambridge.org/core. UNIVERSIDAD AUTONOMA METROPOLITANA, on 15 Nov 2026 at 15:53:11, subject to the Cambridge Core terms of use, available at https://www.cambridge.org/core/terms. https://doi.org/10.1017/CBO9780511628788.005

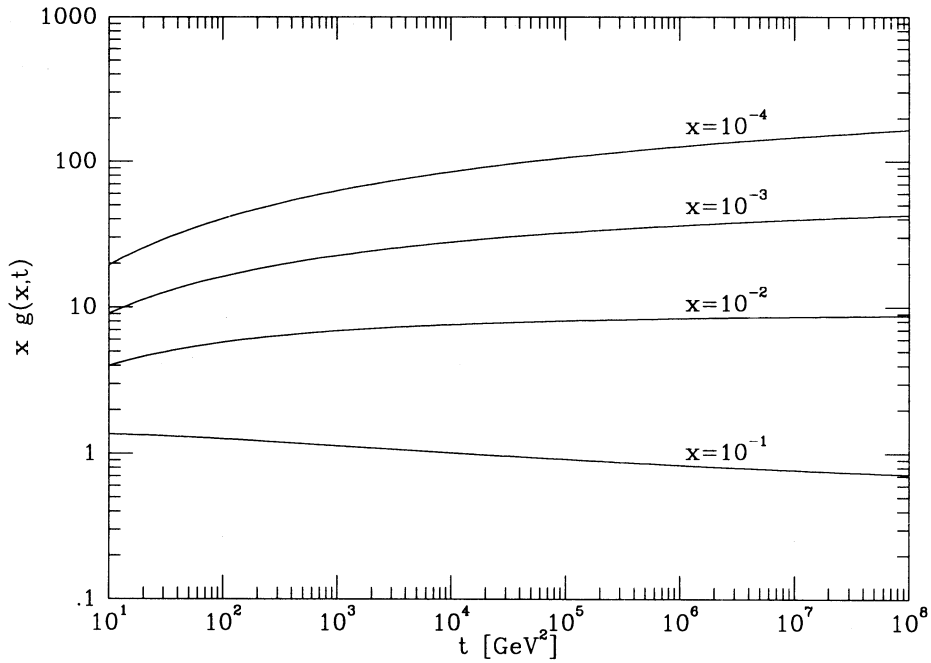


Fig. 4.11. The scale dependence of the gluon distribution.

the moments of any individual flavour of quark distribution can be determined. The x distributions themselves are then obtained by an inverse Mellin transformation, *cf.* Eq. (4.134),

$$f_a(x,\mu^2) = \frac{1}{2\pi i}\int_C dj\; x^{-j}\; f_a(j,\mu^2)\;, \quad a = q_i, g\;. \tag{4.146}$$

An alternative method of solution, which avoids a numerical integration in the complex plane, is to solve the integro-differential evolution equations directly in x space by a numerical procedure. This is particularly convenient if a simultaneous solution for all $(2n_f+1)$ parton distributions is required, given a set of starting distributions $f_a(x,\mu_0^2)$ at some reference scale μ_0. In either the moment or direct integration method, the inclusion of higher-order contributions to the splitting function, Eq. (4.91), is relatively straightforward.

Figs. 4.11, 4.12 and 4.13 illustrate the scale dependence of the gluon, valence up-quark and up-antiquark distributions [7] respectively. In each case, the distributions decrease with increasing scale at large x, and increase at small x. Fig. 4.14 shows the momentum fractions carried by the individual quarks and gluons as functions of the scale.

Downloaded from https://www.cambridge.org/core. UNIVERSIDAD AUTONOMA METROPOLITANA, on 15 Nov 2026 at 15:53:11, subject to the Cambridge Core terms of use, available at https://www.cambridge.org/core/terms. https://doi.org/10.1017/CBO9780511628788.005

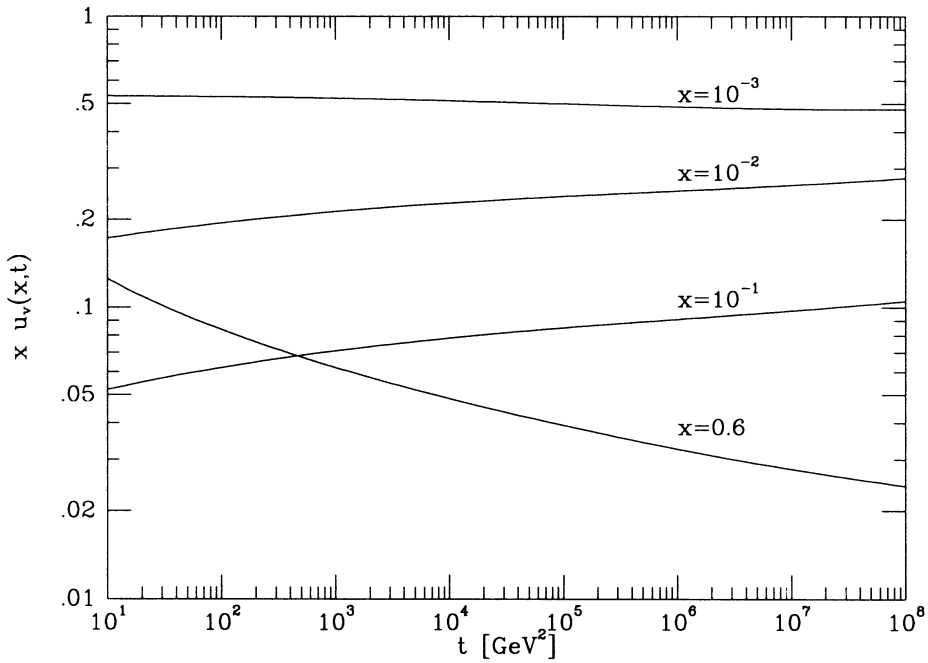


Fig. 4.12. The scale dependence of the valence up-quark distribution.

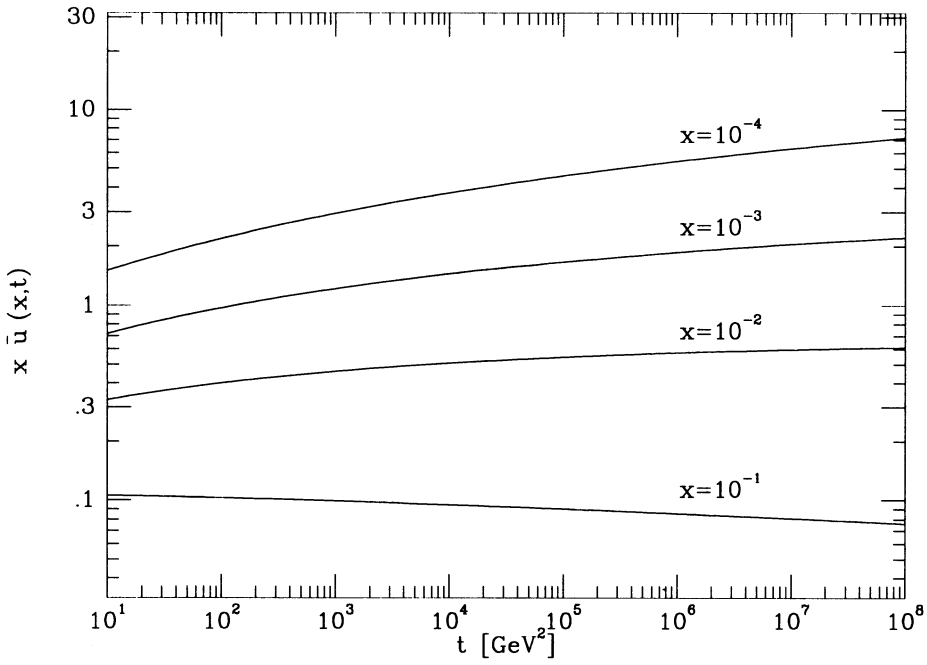


Fig. 4.13. The scale dependence of the up-antiquark distribution.

Downloaded from https://www.cambridge.org/core. UNIVERSIDAD AUTONOMA METROPOLITANA, on 15 Nov 2026 at 15:53:11, subject to the Cambridge Core terms of use, available at https://www.cambridge.org/core/terms. https://doi.org/10.1017/CBO9780511628788.005

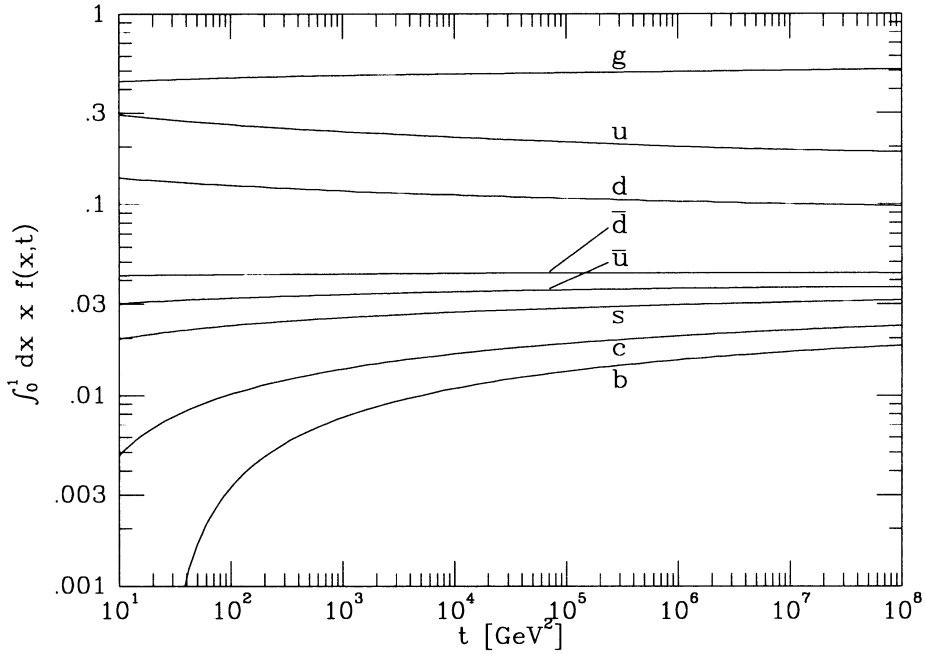


Fig. 4.14. Momentum fractions carried by the quarks and gluons as functions of the scale.

4.4 QCD fits to deep inelastic data

In the previous section we saw that perturbative QCD predicts the Q^2 *evolution* of the structure functions, rather than the size and shape of the functions themselves. In particular, for non-singlet structure functions ($F_2^{\mu p} - F_2^{\mu n}$ and $xF_3^{\nu N}$ are examples in practice — see Eq. (4.17)) the variation with Q^2 is comparatively simple,

$$Q^2 \frac{\partial}{\partial Q^2} F_{\rm NS}(x,Q^2) = \frac{\alpha_S(Q^2)}{2\pi} \int_x^1 \frac{d\xi}{\xi}\, F_{\rm NS}(\xi,Q^2)\, \frac{x}{\xi} P\left(\frac{x}{\xi}\right) . \qquad (4.147)$$

For structure functions like $F_2^{\mu p}$, which is a linear combination of singlet and non-singlet pieces, the differential equation has an additional term on the right-hand side proportional to the gluon distribution. Quantitatively, the strength of the scaling violation is controlled by $\alpha_S(Q^2)$ and hence by the QCD scale parameter Λ. Deep inelastic scattering data of the type shown in Fig. 4.10, therefore, provide one of the precision tests of QCD and one of the most accurate determinations of α_S.

Although the theoretical predictions appear simplest when expressed in terms of structure function moments, it is difficult to extract such moments from the data. This is because the measurements do not extend

Downloaded from https://www.cambridge.org/core. UNIVERSIDAD AUTONOMA METROPOLITANA, on 15 Nov 2026 at 15:53:11, subject to the Cambridge Core terms of use, available at https://www.cambridge.org/core/terms. https://doi.org/10.1017/CBO9780511628788.005

to very large and very small x, and some form of *ad hoc* extrapolation is required to construct the moment integrals. A more practical and accurate method is to choose a reference value Q_0 and parametrize the parton distributions at that value, *e.g.* $q(x,Q_0^2) = Ax^a(1+c\sqrt{x}+dx)(1-x)^b$. These distributions are then evolved numerically, using the GLAP equations, to obtain values for the $F_i(x,Q^2)$ in the kinematic regions where they are measured. Note that in this approach the rate of change with Q^2 of the structure function at a given x manifestly depends only on the structure function evaluated at $\xi > x$. Finally, a global numerical fit is performed to determine the 'best' values for the parameters, including Λ. The extent to which the measured value of Λ depends on the other parameters can also be quantified and used to derive a systematic error.

The above procedure is not, however, without problems. In QCD, the structure functions have 'higher-twist' power corrections, which are much more difficult to estimate quantitatively:

$$F(x,Q^2) = F^{(2)}(x,Q^2) + \frac{F^{(4)}(x,Q^2)}{Q^2} + \ldots , \tag{4.148}$$

where the superscripts on the right-hand side refer to the 'twist' = (dimension − spin) of the contributing operators. Such power corrections are indeed visible in the structure function data — a phenomenological fit to both low- and high-Q^2 F_2^{lp} data [20] of the form $F^{(4)} = C(x)F^{(2)}$ yields

$$C(x) \approx 0.5 \text{ GeV}^2 \, \Theta(x - \tfrac{1}{3}) \left(\frac{1}{1-x} - \frac{3}{2} \right) , \tag{4.149}$$

where $\Theta(z) = 1$ for $z > 0$ and 0 for $z < 0$. The term proportional to $(1-x)^{-1}$ is expected on general theoretical grounds — there are j times more operators which contribute to the jth moment of $F^{(4)}$ than to $F^{(2)}$. Therefore at large j the moments are expected to differ by a factor of j, corresponding to a factor $(1-x)^{-1}$ difference in the contributions to the structure function. To avoid complications from higher-twist contributions in extracting parton distributions and a value of Λ, the analysis must be performed at large $(1-x)Q^2$ where such contributions are expected to be negligible.

A second problem is that the most precise data are for F_2 measured in fixed-target electron, muon and neutrino scattering on nucleon and nuclear targets. Except at large x, the Q^2 variation of these is sensitive to the *a priori* unknown gluon distribution and there is potentially a strong Λ-gluon correlation. Although the evolution of *non-singlet* structure functions does not suffer from this problem, see Eq. (4.147), these are only measurable experimentally by constructing differences between cross sections, *e.g.* $\sigma^{\mu p} - \sigma^{\mu n}$. This inevitably introduces additional systematic

Downloaded from https://www.cambridge.org/core. UNIVERSIDAD AUTONOMA METROPOLITANA, on 15 Nov 2026 at 15:53:11, subject to the Cambridge Core terms of use, available at https://www.cambridge.org/core/terms. https://doi.org/10.1017/CBO9780511628788.005

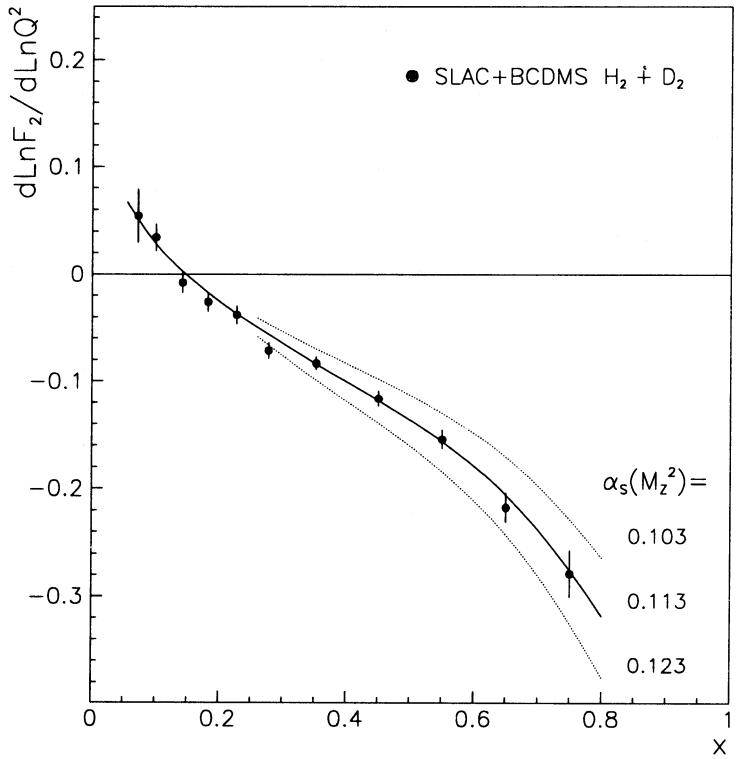


Fig. 4.15. Logarithmic Q^2 derivative of the F_2 structure function measured on hydrogen and deuterium together with QCD fits. Figure from ref. [20].

and statistical uncertainties.

The most recent generation of fixed-target deep inelastic experiments partially solve these problems by collecting high statistics data at large x and Q^2. In fact the precision of contemporary data demands that the next-to-leading-order QCD corrections are incorporated in the fits. Beyond leading order a specific renormalization scheme must be chosen, in addition to the factorization scheme discussed in the previous section, and in practice this is usually the $\overline{\text{MS}}$ scheme. For this reason the results quoted in the literature almost always refer to $\Lambda_{\overline{\text{MS}}}$.

Some of the most precise data come from the BCDMS collaboration [4,21]. As an example, Fig. 4.10 shows the structure function F_2 measured by BCDMS in deep inelastic muon-hydrogen scattering, together with similar data from the NMC collaboration [18]. The measurements extend up to x values of 0.75 and Q^2 values of several hundred GeV^2. Fig. 4.15 shows the $\ln Q^2$ derivative of $\ln F_2$ as a function of x, obtained from a combined analysis [20] of BCDMS [4,21] and SLAC [22] data. Note that the derivatives in the high-x (low-x) region are negative (positive),

Downloaded from https://www.cambridge.org/core. UNIVERSIDAD AUTONOMA METROPOLITANA, on 15 Nov 2026 at 15:53:11, subject to the Cambridge Core terms of use, available at https://www.cambridge.org/core/terms. https://doi.org/10.1017/CBO9780511628788.005

consistent with a structure function which decreases (increases) with increasing Q^2. The solid line in Fig. 4.15 is a next-to-leading-order QCD fit, which gives [20]

$$\Lambda^{(4)}_{\overline{\rm MS}} \;=\; 263 \;\pm\; 42 \;\text{MeV}\,. \tag{4.150}$$

Using the formulae given in Section 2.5, it is straightforward to convert this to a value of $\alpha_S(M_Z^2)$:

$$\alpha_S(M_Z^2) \;=\; 0.113 \;\pm\; 0.003\,. \tag{4.151}$$

Note that four light quark flavours are generally appropriate for the range of Q^2 probed by fixed-target deep inelastic scattering experiments. In ref. [20] an additional theoretical uncertainty in $\alpha_S(M_Z^2)$ is estimated by varying the values of the renormalization and factorization scales in the fit about the nominal choice $\mu_R^2 = \mu_F^2 = Q^2$. This gives $\Delta\alpha_S(M_Z^2)(\text{theory}) = \pm 0.004$, which when combined with the experimental error in (4.151) gives

$$\alpha_S(M_Z^2) \;=\; 0.113 \;\pm\; 0.005\,, \tag{4.152}$$

one of the most precise measurements of the strong coupling constant. This value is compared with determinations from other processes in Chapter 12. Note that the broken lines in Fig. 4.15 correspond to $\Delta\alpha_S(M_Z^2) = \pm 0.010$.

Fixed-target experiments measure quark distributions very accurately over a broad range in x ($\sim 0.01 - 0.8$) up to scales of order $\mu^2 \sim 200\,\text{GeV}^2$. (The HERA high-energy ep collider is able to extend the x range down to very small values — see below.) Knowing $\Lambda_{\overline{\rm MS}}$, one can then evolve these to higher μ^2 and use them for hadron collider phenomenology. Instead of laboriously integrating the GLAP equations each time a parton distribution is required, it is useful to have an analytic approximation, valid to a sufficient accuracy over a prescribed (x, μ^2) range. Such parametrizations are widely available. An analytic form which is commonly used is

$$\begin{aligned} q(x,\mu^2) &= Ax^a(1 + c\sqrt{x} + dx)(1-x)^b \\ A &= A_0 + A_1 s + A_2 s^2 \\ a &= a_0 + a_1 s + a_2 s^2 \qquad \text{etc.} \\ s &= \ln\left(\frac{\ln(\mu^2/\Lambda^2)}{\ln(\mu_0^2/\Lambda^2)}\right) \;>\; 0\,, \end{aligned} \tag{4.153}$$

with the parameters $A_0, A_1, \ldots$ fitted to an exact numerical solution of the leading-order or next-to-leading-order evolution equations, to an accuracy at the per cent level. Because deep inelastic scattering data do not significantly constrain the gluon distribution, it is necessary to include in the parton distribution fit data from other processes where the gluon distribution plays a more leading role. An example of such a process is the

Downloaded from https://www.cambridge.org/core. UNIVERSIDAD AUTONOMA METROPOLITANA, on 15 Nov 2026 at 15:53:11, subject to the Cambridge Core terms of use, available at https://www.cambridge.org/core/terms. https://doi.org/10.1017/CBO9780511628788.005

production of large transverse momentum photons in hadron-hadron collisions, where the leading-order $qg \to \gamma q$ scattering process is important. In this way data from high precision fixed-target direct photon experiments are able to constrain the gluon distribution, particularly in the medium x ($\sim 0.2 - 0.4$) range. This is will be discussed in more detail in Chapter 7.

A recent set of parton distributions [7] resulting from a global next-to-leading-order QCD fit to deep-inelastic scattering, prompt photon and other data is shown in Fig. 4.3, at scale $\mu^2 = 10$ GeV^2. Distributions like these cover a wide range in x and μ^2, and are invaluable for making quantitative predictions for present and future hadron-hadron and lepton-hadron colliders.

4.5 Sum rules

In Section 4.1 we saw how the integrals over certain combinations of parton distributions had particular values in the parton model. Several examples were given in Eq. (4.24). Such integrals are called sum rules. In QCD these sum rules remain valid, up to perturbative corrections, because of the vanishing of the first moment of the non-singlet anomalous dimensions to all orders in perturbation theory. At lowest order in α_S this property is evident in Eqs. (4.129,4.133). In practice the sum rules provide a variety of information, from constraints on parton distributions and tests of conservation laws to precision measurements of α_S. In this section we shall describe some of the more important sum rules.

4.5.1 Gross–Llewellyn Smith sum rule

The Gross–Llewellyn Smith sum rule [23] applies to the F_3 structure function measured in neutrino– and antineutrino–proton scattering:

$$I_{GLLS} = \tfrac{1}{2} \int_0^1 dx \ (F_3^{\nu p} + F_3^{\bar{\nu} p}) \ . \tag{4.154}$$

In the parton model, we can substitute for the structure functions using (4.17) to obtain

$$\begin{aligned} I_{GLLS} &= \int_0^1 dx \ (d - \bar{u} + u - \bar{d}) \\ &= \int_0^1 dx \ (u_V + d_V) \\ &= 3 \, . \end{aligned} \tag{4.155}$$

Downloaded from https://www.cambridge.org/core. UNIVERSIDAD AUTONOMA METROPOLITANA, on 15 Nov 2026 at 15:53:11, subject to the Cambridge Core terms of use, available at https://www.cambridge.org/core/terms. https://doi.org/10.1017/CBO9780511628788.005

In perturbative QCD there are finite $O(\alpha_S)$ corrections, so that the parton model value is only attained in the $Q^2 \to \infty$ limit:

$$I_{GLLS}(Q^2) = 3\left[1 + d_1\frac{\alpha_S}{\pi} + d_2\left(\frac{\alpha_S}{\pi}\right)^2 + d_3\left(\frac{\alpha_S}{\pi}\right)^3 + \ldots\right] \qquad (4.156)$$

where $\alpha_S \equiv \alpha_S(\mu^2)$ and the coefficients are functions of Q^2/μ^2. In the $\overline{\text{MS}}$ renormalization scheme with $\mu^2 = Q^2$,

$$\begin{aligned} d_1 &= -1 \qquad [9,10] \\ d_2 &= -\frac{55}{12} + n_f\frac{1}{3} \qquad [24] \\ d_3 &= -\frac{13841}{216} - \frac{44}{9}\zeta(3) + \frac{55}{2}\zeta(5) \\ &\quad + n_f\left(\frac{10009}{1296} + \frac{91}{54}\zeta(3) - \frac{5}{3}\zeta(5)\right) - n_f^2\frac{115}{648} \qquad [25] \end{aligned} \qquad (4.157)$$

where $C_F = 4/3$ and $C_A = 3$ have been substituted. The values of the Riemann zeta functions are given in Eq. (3.19). The CCFR collaboration [26] have measured the Gross–Llewellyn Smith sum in (anti)neutrino–nucleon scattering at $\langle Q^2\rangle \sim 3$ GeV^2. This has been used to measure α_S, as will be discussed in Chapter 12.

4.5.2 Adler sum rule

The Adler sum rule [27] applies to the F_2 structure function measured in neutrino– and antineutrino–proton scattering:

$$\begin{aligned} I_A &= \int_0^1 \frac{dx}{x}(F_2^{\bar{\nu}p} - F_2^{\nu p}) \\ &= 4\langle I_3\rangle = 2 \end{aligned} \qquad (4.158)$$

where I_3 is the third component of the isospin of the target, which for a proton is equal to one half. The value of I_A is exact and follows from the conservation of the charged weak current. Unlike the Gross–Llewellyn Smith sum rule there are no higher-order perturbative or higher-twist power corrections. Unfortunately the sum rule is not straightforward to measure, since all of the high precision neutrino scattering data is taken on heavy (approximately isoscalar) nuclear targets. (Note that for an isoscalar target $F_2^{\nu N} = F_2^{\bar{\nu}N}$, and so the integral corresponding to Eq. (4.158) vanishes.) The only measurement in the literature is from the BEBC collaboration [28]:

$$I_A = 2.02 \pm 0.40\,, \qquad (4.159)$$

in agreement with the theoretical prediction (4.158).

Downloaded from https://www.cambridge.org/core. UNIVERSIDAD AUTONOMA METROPOLITANA, on 15 Nov 2026 at 15:53:11, subject to the Cambridge Core terms of use, available at https://www.cambridge.org/core/terms. https://doi.org/10.1017/CBO9780511628788.005

4.5.3 Gottfried sum rule

Important information on the sea quark distributions is provided by the Gottfried sum [29],

$$I_G = \int_0^1 \frac{dx}{x}(F_2^{\mu p} - F_2^{\mu n}) \,. \tag{4.160}$$

Again using the parton model expressions given in Section 4.1, together with isospin symmetry to relate the distributions in protons and neutrons, we find

$$\begin{aligned} I_G &= \tfrac{1}{3}\int_0^1 dx\ (u_V - d_V + \bar{u} - \bar{d}) \\ &= \tfrac{1}{3} + \int_0^1 dx\ (\bar{u} - \bar{d}) \,. \end{aligned} \tag{4.161}$$

In particular, if the quark sea is symmetric under the interchange of u and d, then one obtains the Gottfried sum rule $I_G = 1/3$. However, the measurement from the NMC collaboration is [30]

$$I_G(0.004 < x < 0.8) = 0.236 \pm 0.008 \,. \tag{4.162}$$

Note that the measurement, and hence the integral, does not extend either to $x = 0$ or to $x = 1$. This is a problem with all such sum rule measurements. However, with a reasonable extrapolation outside the measured range one finds [30] that the sum rule $I_G = 1/3$ is badly violated, indicating a strong light quark flavour asymmetry in the sea,

$$\int_0^1 dx\ (\bar{u} - \bar{d}) \approx -0.1 \,. \tag{4.163}$$

The constraint from the Gottfried sum is incorporated in the most recent global parton distribution fits. For example, Fig. 4.3 shows a clear difference between the $\bar{u}$ and $\bar{d}$ distributions in the MRS(A) partons [7].

4.6 Deep inelastic scattering at small x

The form of the parton distributions in the small-x region is of considerable theoretical interest. In the parton model, one can show that the x dependence in the limit $x \to 0$ is related by Regge theory to the behaviour of hadronic scattering cross sections at high energy. As these arguments are based on non-perturbative dynamics, they presumably relate to the distributions at a typical hadronic scale, $\mu^2 \sim 1$ GeV^2. We have already seen that perturbative GLAP evolution causes the distributions to rise with increasing μ^2 at small x. In fact, in certain circumstances the behaviour in the double asymptotic limit $x \to 0$, $\mu^2 \to \infty$ can be determined analytically.

Downloaded from https://www.cambridge.org/core. UNIVERSIDAD AUTONOMA METROPOLITANA, on 15 Nov 2026 at 15:53:11, subject to the Cambridge Core terms of use, available at https://www.cambridge.org/core/terms. https://doi.org/10.1017/CBO9780511628788.005

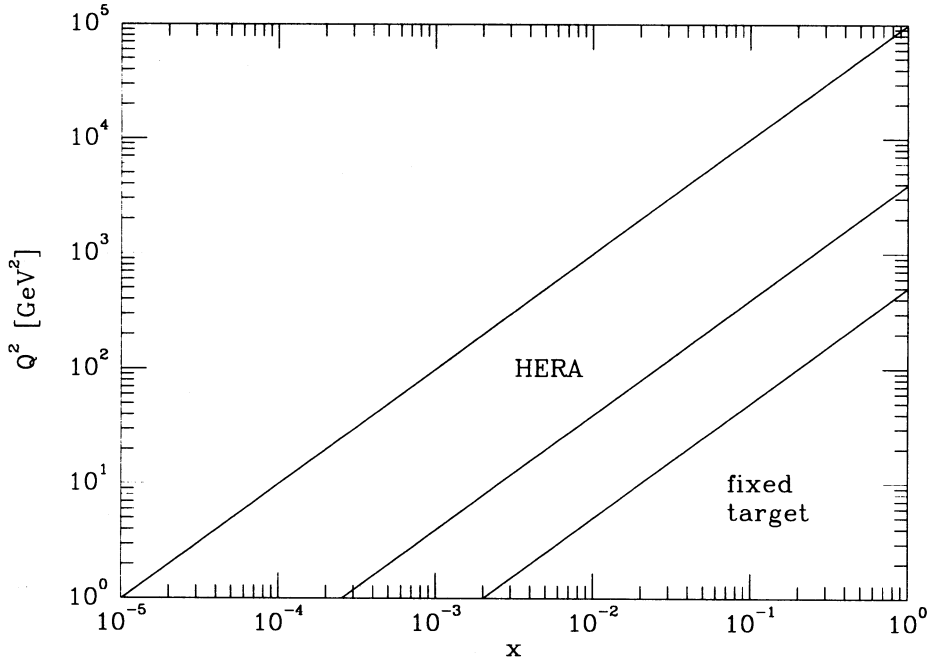


Fig. 4.16. Kinematic region for HERA and fixed-target deep inelastic scattering experiments.

To test these theoretical ideas requires precise structure function measurements at very small x, and in a range of Q^2 which spans both the perturbative and non-perturbative regimes. The HERA high-energy electron-proton collider ($\sqrt{s_{ep}} \sim 300$ GeV) provides the ideal kinematic conditions for such measurements. In practice, the range in x and Q^2 is approximately determined by the limits on the variable y defined in Eq. (4.1):

$$y_{min} < y = \frac{Q^2}{x s_{ep}} < 1 \,. \tag{4.164}$$

Taking the typical values $\sqrt{s_{ep}} = 314$ GeV and $y_{min} = 0.04$ gives the region in the two-dimensional x and Q^2 plane shown in Fig. 4.16. Also shown is the region corresponding to fixed-target experiments. We see immediately that the HERA kinematics allow (i) tests of GLAP evolution at medium and large x to very high Q^2 values (but recall from Eq. (4.5) that the cross section at fixed x decreases rapidly, as $1/Q^4$), and (ii) a test of the small-x behaviour down to $x \sim 10^{-5}$ in the deep inelastic regime. The crucial point here is that at such small-x values $\ln(1/x)$ can be regarded as a 'large logarithm', and a perturbative treatment which resums these large logarithms to all orders may be applicable. In the sections which follow we will describe several approximations to the small-

Downloaded from https://www.cambridge.org/core. UNIVERSIDAD AUTONOMA METROPOLITANA, on 15 Nov 2026 at 15:53:11, subject to the Cambridge Core terms of use, available at https://www.cambridge.org/core/terms. https://doi.org/10.1017/CBO9780511628788.005

x behaviour based on perturbation theory. First, however, we discuss the original non-perturbative Regge arguments for structure functions in the $x \to 0$ limit.

4.6.1 Regge theory

In Section 4.2 we saw how in the parton model the deep inelastic structure functions can be extracted from the hadronic tensor $W^{\alpha\beta}(p,q)$, which in turn is obtained from the handbag diagram, Fig. 4.4. The invariant mass of the system left behind when the quark is removed from the proton is $s_0 = (p-k)^2$. Using the decomposition of the quark four-momentum given in Eq. (4.37), we have (setting the proton mass to zero)

$$s_0 = k^2 - 2p\cdot k = \frac{-k^2(1-x) - k_T^2}{x}\,, \tag{4.165}$$

and so $s_0 \to \infty$ as $x \to 0$. Now according to Regge theory, the high-energy behaviour of an elastic hadron scattering amplitude is controlled by a sequence of Regge trajectories corresponding to the exchange of families of particles with different spin, see for example ref. [31]. Applying this to the quark-proton amplitude B in the $s_0 \to \infty$ limit gives

$$B \sim \beta_{\mathcal{P}} s_0^{\alpha_{\mathcal{P}}-1} + \beta_{\mathcal{R}} s_0^{\alpha_{\mathcal{R}}-1} + \dots\,, \tag{4.166}$$

where the leading trajectories are

$$\begin{aligned} \alpha_{\mathcal{P}} &\simeq 1 && \text{pomeron } \mathcal{P} \\ \alpha_{\mathcal{R}} &\simeq \tfrac{1}{2} && \rho, \omega, a_2, f_2, \dots\,. \end{aligned} \tag{4.167}$$

Inserting this behaviour into the parton-model calculation of the F_2 structure function, Eq. (4.39), gives the leading small-x behaviour

$$F_2(x) \sim \beta_{\mathcal{P}} x^{1-\alpha_{\mathcal{P}}} + \beta_{\mathcal{R}} x^{1-\alpha_{\mathcal{R}}}\,. \tag{4.168}$$

We may interpret the two terms in (4.168) as the contributions to the structure function from the flavour-singlet quark sea, with behaviour determined by the leading 'pomeron' trajectory $\alpha_{\mathcal{P}}$, and from the flavour-non-singlet valence quarks, with behaviour controlled by the 'reggeon' trajectory $\alpha_{\mathcal{R}}$. We would likewise expect that the behaviour of the gluon distribution at small x would also be determined by the pomeron trajectory, yielding the predictions

$$S, g \sim x^{-1}, \qquad q_V \sim x^{-\frac{1}{2}} \tag{4.169}$$

in the $x \to 0$ limit, or equivalently

$$F_2^p \sim x^0, \qquad F_2^p - F_2^n \sim x^{\frac{1}{2}}\,. \tag{4.170}$$

A detailed analysis of small-x structure function measurements at fixed-target energies [32] shows that they are indeed approximately consis-

Downloaded from https://www.cambridge.org/core. UNIVERSIDAD AUTONOMA METROPOLITANA, on 15 Nov 2026 at 15:53:11, subject to the Cambridge Core terms of use, available at https://www.cambridge.org/core/terms. https://doi.org/10.1017/CBO9780511628788.005

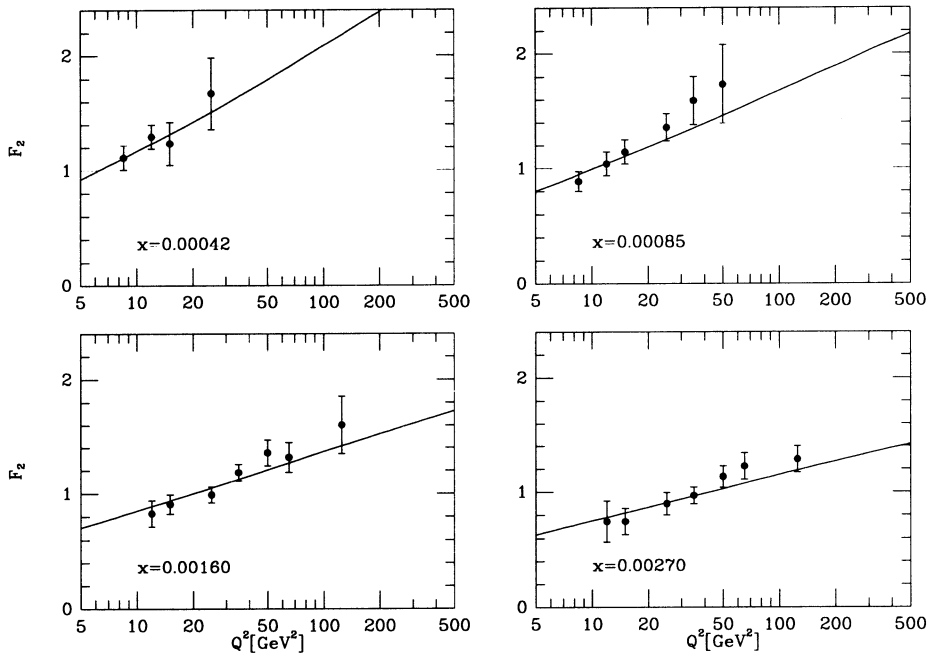


Fig. 4.17. The description of F_2 data from the ZEUS collaboration [6] at HERA by a NLO QCD fit from ref. [33].

tent with the predictions of Regge theory. For example, the behaviour $F_2 \sim$ constant at small x is evident in the fixed-target data shown in Fig. 4.2. However this figure also shows an apparent steepening of the behaviour at small x as Q^2 increases. An attractive interpretation of this rise is that it is caused by the onset of the perturbative GLAP evolution described in Section 4.3, with the non-perturbative Regge theory describing the form of the starting distributions for the evolution, at a typical hadronic scale of order 1 GeV^2. Indeed the HERA small-x F_2 data are very well described by NLO GLAP-based fits. As an example, Fig. 4.17 shows the description of data from the ZEUS collaboration [6] by a NLO QCD fit from ref. [33]. Note that F_2 grows approximately linearly with $\ln Q^2$ at small x, consistent with the theoretical prediction. The starting distributions in this fit have

$$S, g \sim x^{-1.17} \quad \text{at } \mu_0^2 = 4 \text{ GeV}^2 , \tag{4.171}$$

in line with Regge theory expectations.

Downloaded from https://www.cambridge.org/core. UNIVERSIDAD AUTONOMA METROPOLITANA, on 15 Nov 2026 at 15:53:11, subject to the Cambridge Core terms of use, available at https://www.cambridge.org/core/terms. https://doi.org/10.1017/CBO9780511628788.005

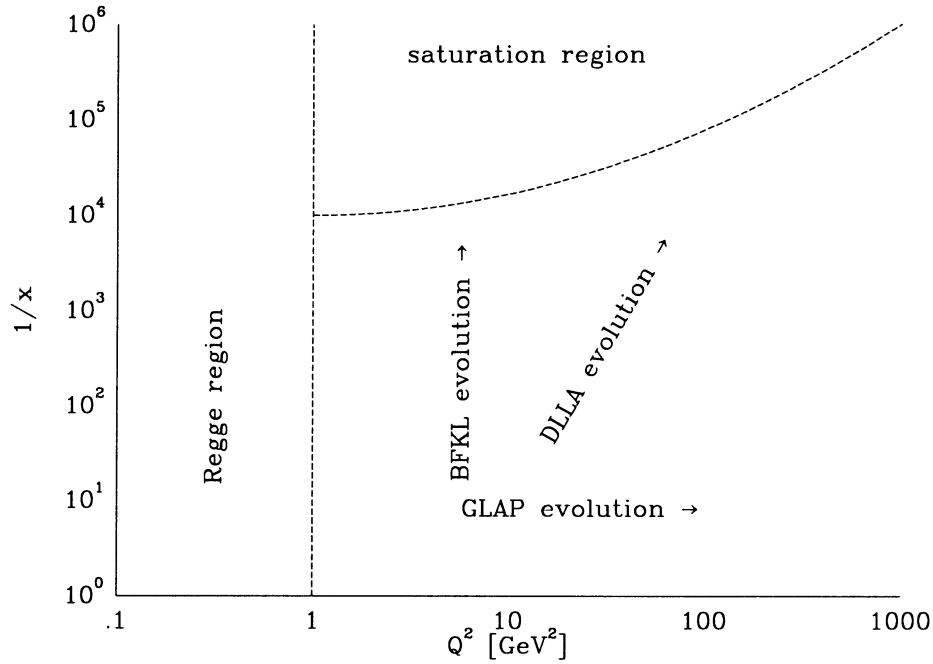


Fig. 4.18. The various regions of the $1/x$ vs Q^2 plane discussed in the text.

4.6.2 The double asymptotic limit $Q^2 \to \infty$, $x \to 0$

If the parton distributions at the starting scale t_0 $(= \mu_0^2)$ are indeed specified by Regge theory, *i.e.* $q(x,t_0), g(x,t_0) \sim x^{-1}$ for $x \ll 1$, then we see from Figs. 4.11 and 4.17 that the evolution causes the distributions to grow rapidly at small x with increasing t. In the asymptotic limit where $x \to 0$ and $t \to \infty$ it is possible to determine the behaviour of the distributions directly from the GLAP equations [34]. In effect, the leading $\ln Q^2$ resummation of the GLAP equations is supplemented by an additional approximation in which only the most singular (leading $\ln(1/x)$) x-dependent contributions are retained. This is then called the double-leading-logarithm approximation (DLLA). Fig. 4.18 shows the region in the x, Q^2 plane which corresponds to this limit.

The $x \to 0$ limit of the parton distributions is controlled by the behaviour of the anomalous dimensions $\gamma(j)$ near $j = 1$. At leading order, the anomalous dimensions $\gamma_{gq}^{(0)}$ and $\gamma_{gg}^{(0)}$ are singular at $j = 1$ (Eq. (4.129), Fig. 4.9) and it is these that dominate the evolution of the distributions at small x. To avoid complications due to the mixing under evolution of the quark singlet and gluon distributions, we begin by considering the

Downloaded from https://www.cambridge.org/core. UNIVERSIDAD AUTONOMA METROPOLITANA, on 15 Nov 2026 at 15:53:11, subject to the Cambridge Core terms of use, available at https://www.cambridge.org/core/terms. https://doi.org/10.1017/CBO9780511628788.005

evolution in a theory with gluons only:

$$t\frac{\partial}{\partial t}g(j,t) = \frac{\alpha(t)}{2\pi}\gamma_{gg}^{(0)}(j)g(j,t) \tag{4.172}$$

where from Eq. (4.129) (see also Fig. 4.9),

$$\gamma_{gg}^{(0)}(j) \approx \frac{2N}{j-1}\,. \tag{4.173}$$

In this limit the solution for the moments of the gluon distribution is

$$g(j,t) = g(j,t_0)\exp\left(\frac{\xi}{j-1}\right), \tag{4.174}$$

where ξ is defined by

$$\xi = \frac{N}{\pi}\int_{t_0}^{t}\frac{dt'}{t'}\alpha_S(t') = \frac{N}{\pi b}\ln\left(\frac{\ln t/\Lambda^2}{\ln t_0/\Lambda^2}\right)\,. \tag{4.175}$$

To return to x space we perform the inverse Mellin transform as given by Eq. (4.146):

$$\begin{aligned} xg(x,t) &= \frac{1}{2\pi i}\int dj\; x^{-(j-1)}g(j,t) \\ &\equiv \frac{1}{2\pi i}\int dj\; g(j,t_0)\exp\Big[f(j)\Big]\,, \end{aligned} \tag{4.176}$$

where the exponent f is

$$f(j) = (j-1)Y + \frac{\xi}{j-1}\,, \tag{4.177}$$

with $Y \equiv \ln(1/x)$. In the limit in which both Y and ξ become asymptotically large, we can estimate this integral by expanding about the saddle point of the exponential,

$$f(j) = 2\sqrt{\xi Y} + O(j-j_0)^2, \qquad j_0 = 1+\sqrt{\frac{\xi}{Y}}\,, \tag{4.178}$$

which gives, for the asymptotic solution,

$$xg(x,t) = g(j_0,t_0)\exp(2\sqrt{\xi Y})\,. \tag{4.179}$$

When expressed in terms of the original variables, this becomes [34]

$$g(x,\mu^2) \sim \frac{1}{x}\exp\sqrt{\frac{4N}{\pi b}\ln\frac{\ln\mu^2/\Lambda^2}{\ln\mu_0^2/\Lambda^2}\ln\frac{1}{x}}, \quad N=3, \quad b=\frac{(33-2n_f)}{12\pi}\,. \tag{4.180}$$

Notice that the dependence on the starting distribution enters via the j_0th moment of g. Therefore at fixed ξ/Y the initial information enters only as an overall factor. An important point to note is that the above derivation breaks down if the starting distribution is too singular as $x \to 0$.

Downloaded from https://www.cambridge.org/core. UNIVERSIDAD AUTONOMA METROPOLITANA, on 15 Nov 2026 at 15:53:11, subject to the Cambridge Core terms of use, available at https://www.cambridge.org/core/terms. https://doi.org/10.1017/CBO9780511628788.005

The contour in the complex j-plane must be located to the right of all the singularities of $g(j,t_0)$. If $xg(x,t_0) \sim x^{-\lambda}$ as $x \to 0$, then $g(j,t_0)$ has a pole at $j = 1+\lambda$. If the saddle point j_0, Eq. (4.178), is to the left of this, *i.e.* $\lambda > j_0 - 1$, then the asymptotic behaviour is more complicated than that given in Eq. (4.179) and, in particular, depends on λ. Physically, if the starting gluon distribution is too steep then there are not enough faster moving gluons to emit the slower gluons which build up the perturbative rise at small x.

It is straightforward to compute various sub-leading corrections to the asymptotic behaviour given in (4.179). For example, the residual Gaussian saddle-point integral gives an additional overall factor of $\xi^{1/4}Y^{-3/4}$. Keeping the next-to-leading (constant) term in the expansion of the anomalous dimension around $j = 1$, *i.e.*

$$\gamma_{gg}^{(0)}(j) = N\left[\frac{2}{j-1} + \kappa + O(j-1)\right], \tag{4.181}$$

where $\kappa = -11/6 - n_f/(3N)$, gives an overall factor of $\exp(\xi\kappa/2)$.

Since the evolution of the gluon and quark-singlet distributions is coupled (see Eq. (4.138)), the above asymptotic behaviour also applies to the *quark* distributions at small x and large t and therefore to the structure function F_2. In this case we must replace γ_{gg} by γ_+, defined in Eq. (4.140), the leading eigenvalue of the anomalous dimension matrix as $j \to 1$. This substitution does not change the leading term in Eq. (4.181) but changes κ to $-11/6 - n_f/(3N^3)$. It is interesting to investigate whether the asymptotic behaviour predicted by perturbative QCD is already visible in the HERA F_2 data. In this context, it is convenient to introduce [35] two new variables:

$$\begin{aligned} \sigma &= \left[\ln(x_0/x)\ln\left(\ln(Q^2/\Lambda^2)/\ln(Q_0^2/\Lambda^2)\right)\right]^{1/2} = \gamma^{-1}\sqrt{(Y-Y_0)\xi}\,, \\ \rho &= \left[\frac{\ln(x_0/x)}{\ln\left(\ln(Q^2/\Lambda^2)/\ln(Q_0^2/\Lambda^2)\right)}\right]^{1/2} = \gamma\sqrt{(Y-Y_0)/\xi}\,, \end{aligned} \tag{4.182}$$

with $Y_0 = \ln(1/x_0)$ and $\gamma = \sqrt{N/(\pi b)} = 6(33-2n_f)^{-1/2}$, so that the double asymptotic limit is $\sigma \to \infty$, $\rho = O(1)$. Note that an additional parameter x_0 has been introduced to define the 'small-x' region, $x < x_0$, in the same way that $Q^2 > Q_0^2$ defines the large-Q^2 region. In terms of these new variables, the asymptotic result (4.179) for the gluon distribution is simply $xg \sim \exp(2\gamma\sigma)$, *i.e.* the quantity $\ln(xg)/(2\gamma\sigma)$ becomes independent of σ and ρ in the $\sigma \to \infty$ limit. This behaviour is known as 'double asymptotic scaling'.

The corresponding result for F_2, including the sub-leading terms de-

Downloaded from https://www.cambridge.org/core. UNIVERSIDAD AUTONOMA METROPOLITANA, on 15 Nov 2026 at 15:53:11, subject to the Cambridge Core terms of use, available at https://www.cambridge.org/core/terms. https://doi.org/10.1017/CBO9780511628788.005

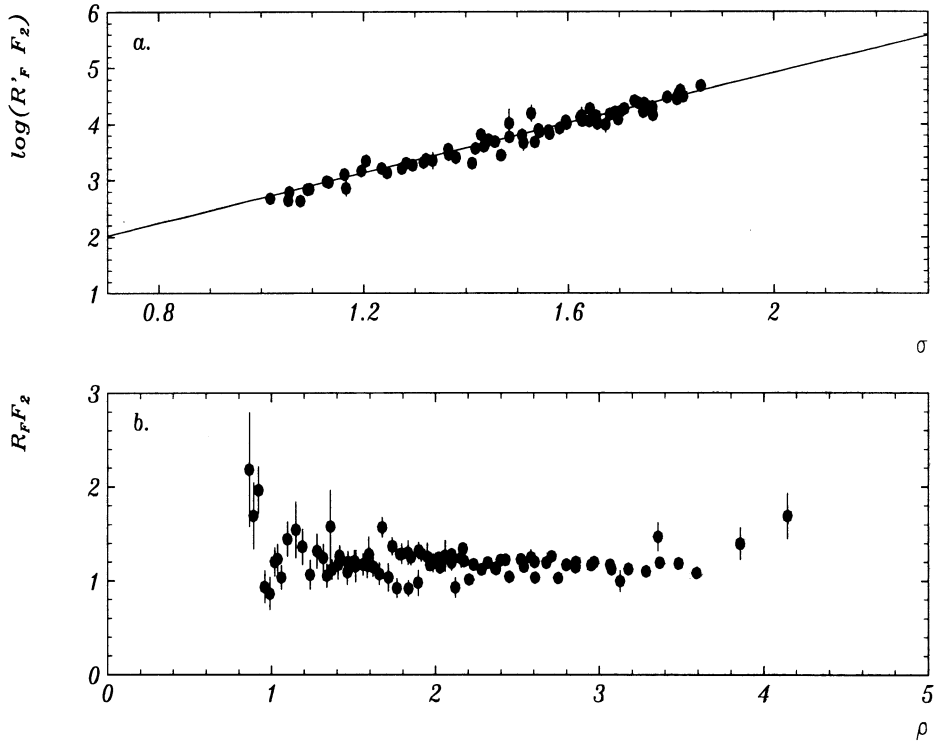


Fig. 4.19. F_2 from the H1 collaboration at HERA, showing evidence for double asymptotic scaling. Figure from ref. [36].

scribed above, is [35]

$$F_2(\sigma,\rho) \approx A_0(\gamma/\rho)\sqrt{\frac{\gamma}{\sigma\rho^2}}\exp(2\gamma\sigma-\delta\sigma/\rho)\left[1+O\left(\frac{1}{\sigma}\right)\right], \quad (4.183)$$

with $\delta = 61/45$. For non-singular starting distributions, the overall normalization A_0 becomes constant for large ρ.

Parameters x_0, Q_0 and Λ can be found such that the HERA F_2 data show clear evidence for the asymptotic scaling behaviour predicted by Eq. (4.183). As an illustration, Fig. 4.19(a) shows H1 data [36] for the quantity $\log(R'_F F_2)$, where

$$R'_F(\sigma,\rho) = 8.1\sqrt{\sigma}\,\frac{\rho}{\gamma}\exp(\delta\sigma/\rho)\,, \quad (4.184)$$

which according to (4.183) is predicted to rise linearly with σ, as a function of σ for different (fixed) values of ρ. The parameters are $x_0 = 0.1$, $Q_0 = 1$ GeV, and $\Lambda^{(4)}_{LO} = 185$ MeV. A clear linear rise is seen, and the measured slope value $2.22 \pm 0.04(\text{stat.}) \pm 0.10(\text{sys.})$ is consistent with the prediction $2\gamma = 2.4$. Fig. 4.19(b) shows F_2 scaled by $\exp(-2\gamma\sigma)R'_F$,

Downloaded from https://www.cambridge.org/core. UNIVERSIDAD AUTONOMA METROPOLITANA, on 15 Nov 2026 at 15:53:11, subject to the Cambridge Core terms of use, available at https://www.cambridge.org/core/terms. https://doi.org/10.1017/CBO9780511628788.005

which removes all the model-independent leading behaviour of the asymptotic result (4.183). The observed approximate scaling in ρ for large ρ is consistent with a 'soft' small-x starting distribution at Q_0 [35].

4.6.3 Higher-order corrections to the GLAP equation at small x

The splitting functions which appear on the right-hand side of the GLAP equation have a perturbative expansion in powers of α_S, Eq. (4.91):

$$P(x,\alpha_S) = P^{(0)}(x) + \frac{\alpha_S}{2\pi}P^{(1)}(x) + \ldots, \tag{4.185}$$

for $P = P_{q_i q_j}$, $P_{q_i g}, \ldots$. In the next-to-leading-order (NLO) global parton analyses described in Section 4.4, only the first two terms in the perturbation series (4.185) are retained, together with the next-to-leading contributions to the coefficient functions which relate the parton distributions to the measured structure functions. Away from $x = 0$ and $x = 1$ this is a good approximation, in that the NLO correction to the leading-order (LO) evolution is quite small.

However care must be taken at small x, where large logarithms $Y = \ln(1/x)$ can appear in the higher-order contributions to the splitting functions (and coefficient functions) and spoil the convergence. The trend can already be seen in the behaviour of the anomalous dimensions as $j \to 1$, equivalent to $x \to 0$, in Fig. 4.9. For γ_{qg}, for example, the NLO contribution exceeds the LO contribution for $j - 1 \lesssim 0.3$.

In general one can show that

$$xP^{(n)}(x) = A_n^{(n)}Y^n + A_{n-1}^{(n)}Y^{n-1} + \ldots + A_0^{(n)} + x\overline{P}^{(n)}(x)\,, \tag{4.186}$$

where $\overline{P}^{(n)}$ is finite in the limit $x \to 0$. The full splitting function is then

$$xP(x,\alpha_S) = \sum_{n=0}^{\infty}\left(\frac{\alpha_S}{2\pi}\right)^n\left[\sum_{m=0}^{n}A_m^{(n)}Y^m + x\overline{P}^{(n)}(x)\right]. \tag{4.187}$$

This expression holds for all four splitting functions, P_{gg}, P_{qg}, P_{gq} and P_{qq}. Explicit calculation of the leading P_{gg} coefficients gives, for example,

$$A_0^{(0)} = 6, \quad A_1^{(1)} = A_2^{(2)} = 0, \quad A_3^{(3)} = 518.4, \quad \ldots\,. \tag{4.188}$$

The general expansion (4.187) can be used to define various approximations to GLAP evolution:

- $(n = 0;\ m = 0) + \overline{P}^{(1)}$: LO.
- $(n = 0;\ m = 0)$: DLLA (Sec. 4.6.2).
- $(n = 0, 1;\ m = 0, 1) + \overline{P}^{(0,1)}$: NLO.
- $(n \geq 0;\ m = n)$: leading-log in $1/x$ (LL_x).

Downloaded from https://www.cambridge.org/core. UNIVERSIDAD AUTONOMA METROPOLITANA, on 15 Nov 2026 at 15:53:11, subject to the Cambridge Core terms of use, available at https://www.cambridge.org/core/terms. https://doi.org/10.1017/CBO9780511628788.005

- $(n \geq 0;\ m = n, n-1)$: next-to-leading-log in $1/x$ (NL_x).

Only the P_{gg} and P_{gq} splitting functions have non-zero LL_x coefficients in general. These leading contributions can be resummed using the BFKL equation [37] (see Section 4.6.5), and eventually give rise to the characteristic behaviour at very small x

$$xg \sim x^{-\lambda}, \quad \lambda = 12 \ln 2 \, \frac{\alpha_S}{\pi} \approx 0.5 \,, \tag{4.189}$$

i.e. more singular than the double-asymptotic scaling behaviour of the DLLA (Section 4.6.2). The NL_x contributions to P_{qg} and P_{qq} are also known [38], while those for P_{gg} and P_{gq} remain unknown at present.

There are a number of important questions raised by the above observations. Clearly the fixed-order approximation to the evolution equations will break down when x is sufficiently small that $\alpha_S \ln(1/x) \sim 1$. Where and how LO or NLO GLAP evolution breaks down, and whether an 'improved' prediction can be obtained by incorporating the known resummed LL_x and NL_x contributions, are open questions at present. From recent numerical studies [39] it appears that (i) the importance of the higher-order $\ln(1/x)$ corrections is very dependent on the form of the starting distributions at μ_0^2 — steep starting distributions are evidently less affected than flat distributions, and (ii) the dominant influence on the evolution of F_2 in the HERA kinematic region comes not from the leading P_{gg} or P_{gq} LL_x contributions, but rather from the formally subleading P_{qg} NL_x contribution. The reason for this is that the gluon distribution is much larger than the quark distributions at small x and so the evolution of the structure function is dominated by the term proportional to g, *i.e.* $\delta F_2 \sim P_{qg} \otimes g$.

There are, however, several important issues still to be clarified. At any order in perturbation theory, the full splitting functions satisfy momentum conservation sum rule constraints:

$$\int_0^1 dx\, x \left[\sum_i P_{q_i g}^{(n)} + P_{gg}^{(n)} \right] = 0 \,, \tag{4.190}$$

$$\int_0^1 dx\, x \left[\sum_j P_{q_j q_i}^{(n)} + P_{g q_i}^{(n)} \right] = 0 \,. \tag{4.191}$$

This is *not* satisfied by the LL_x or NL_x contributions, and it is not clear to what extent momentum conservation is important for small-x GLAP evolution. Another issue concerns the factorization scheme dependence at small x — changing schemes can move large L_x contributions from the splitting functions into the coefficient functions, and therefore corrections to the evolution at small x can be less important in some schemes than in others.

Downloaded from https://www.cambridge.org/core. UNIVERSIDAD AUTONOMA METROPOLITANA, on 15 Nov 2026 at 15:53:11, subject to the Cambridge Core terms of use, available at https://www.cambridge.org/core/terms. https://doi.org/10.1017/CBO9780511628788.005

4.6.4 The BFKL description of F_2

Traditionally, simple parton model and Regge arguments were used to justify using gluon and sea quark 'starting distributions' which behave at small x as $x^{-1-\lambda}$ with $\lambda \approx 0$. In the previous sections we have seen how perturbative QCD evolution in Q^2 causes the distributions to rapidly develop a steeper shape at small x. The GLAP equation effectively sums leading powers of $[\alpha_S \ln Q^2]^n$ generated by multigluon emission in a region of phase space where the gluons have strongly-ordered transverse momenta, $Q^2 \gg k_{nT}^2 \gg \ldots \gg k_{1T}^2$:

$$\int^{Q^2} \frac{dk_{nT}^2}{k_{nT}^2} \cdots \int^{k_{3T}^2} \frac{dk_{2T}^2}{k_{2T}^2} \int^{k_{2T}^2} \frac{dk_{1T}^2}{k_{1T}^2} \sim \frac{[\ln Q^2]^n}{n!} . \tag{4.192}$$

Such a resummation is appropriate for $\ln Q^2$ much larger than $\ln(1/x)$. When the two logarithms are large and of the same order, the DLLA sums leading powers of $[\alpha_S \ln(1/x) \ln Q^2]^n$ and the corresponding distributions increase faster than any power of $\ln(1/x)$ as $x \to 0$.

However, at HERA Q^2 is not so large at very small x (Fig. 4.16), and so it may be more appropriate to consider the case when $\ln Q^2 \ll \ln(1/x)$. GLAP evolution does *not* include all the leading terms in this limit: it neglects those terms which contain the leading power of $\ln(1/x)$ but which are not accompanied by the leading power of $\ln Q^2$. The resummation of terms proportional to $\alpha_S \ln(1/x)$ to all orders, retaining the full Q^2 dependence and not just the leading $\ln Q^2$ terms, is accomplished by the Balitsky–Fadin–Kuraev–Lipatov (BFKL) equation [37]. Here the integration is taken over the full k_T phase space of the gluons, not just the strongly-ordered part as in (4.192).

In the following section the BFKL equation will be derived from first principles. In terms of the small-x behaviour of parton distributions, the result is most conveniently established for the gluon distribution unintegrated over k_T,

$$xg(x, Q^2) = \int^{Q^2} dk_T^2 \, \mathcal{G}(x, k_T^2), \tag{4.193}$$

and is

$$\mathcal{G}(x, k_T^2) \sim h(k_T^2) x^{-\lambda}, \tag{4.194}$$

where $h \sim (k_T^2)^{-\frac{1}{2}}$ at large k_T^2 and λ is the the maximum eigenvalue of the kernel K of the BFKL equation

$$\frac{\partial \mathcal{G}}{\partial \ln(1/x)} = \int d^2 k_T' \, K(\vec{k}_T, \vec{k}_T') \, \mathcal{G}(x, k_T'^2) . \tag{4.195}$$

For fixed α_S, λ has the value given in Eq. (4.189). The prediction for F_2

Downloaded from https://www.cambridge.org/core. UNIVERSIDAD AUTONOMA METROPOLITANA, on 15 Nov 2026 at 15:53:11, subject to the Cambridge Core terms of use, available at https://www.cambridge.org/core/terms. https://doi.org/10.1017/CBO9780511628788.005

is obtained by using the k_T-factorization theorem [40]

$$F_2(x,Q^2) = \int_x^1 \frac{dx'}{x'} \int \frac{dk_T^2}{k_T^4} \mathcal{G}\left(\frac{x}{x'}, k_T^2\right) \overline{F}_2(x', k_T^2, Q^2), \qquad (4.196)$$

where $\overline{F}_2$ denotes the quark-box contribution $\gamma g \to q\bar{q}$ for the scattering of a photon of virtuality Q^2 off a gluon with longitudinal momentum fraction x' and transverse momentum k_T.

The BFKL predictions for F_2, based on the above results, can be obtained by numerical methods, see for example ref. [41]. The result can be summarized as

$$F_2(x,Q^2) = C(Q^2)x^{-\lambda} + F_2^{NP}, \qquad (4.197)$$

where $\lambda \approx 0.5$ and F_2^{NP} is a non-perturbative background contribution which is constant at small x. A good description of the HERA data is obtained. However the BFKL–based analysis is not entirely satisfactory: (i) there are infra-red problems associated with integrating $\int dk_T^2 \alpha_S(k_T^2)$ down to $k_T^2 = 0$,[7] which in practice means that the predictions depend to some extent on an undetermined infra-red cut-off parameter, and (ii) the next-to-leading (in $\ln(1/x)$) corrections to the BFKL equation are as yet unknown. Kinematic constraints such as momentum conservation and the upper limit on transverse momenta, although formally sub-leading, may also be important in the HERA kinematic regime.

Ultimately one would like to achieve a 'unified' treatment of the x and Q^2 dependence of parton distributions and structure functions which incorporates both the GLAP and BFKL dynamics. Progress in this direction has been reported in ref. [42], where a modified evolution equation based on gluon emission with angular ordering (see Chapter 5) has been derived. This reproduces the results of GLAP evolution at large x and BFKL behaviour at small x [43].

4.6.5 The BFKL equation

Although the most important phenomenological application of BFKL physics is to the small-x behaviour of deep inelastic structure functions, it is more convenient to derive the equation for the small-x behaviour of the *wave function* of a bound state of a heavy quark–antiquark pair (quarkonium), for which complications from non-perturbative contributions are absent. We shall follow the 'colour dipole' formulation of the problem used by Mueller [44]. The wave function can in principle be used to compute the structure functions, and its small-x behaviour is similar.

[7] We expect the argument of α_S to be the transverse momentum-squared k_T^2 (see the discussion in Chapter 5), because of the breakdown of strong ordering of k_T at small x. This leads to values of k_T^2 much lower than Q^2 and hence to larger α_S values.

Downloaded from https://www.cambridge.org/core. UNIVERSIDAD AUTONOMA METROPOLITANA, on 15 Nov 2026 at 15:53:11, subject to the Cambridge Core terms of use, available at https://www.cambridge.org/core/terms. https://doi.org/10.1017/CBO9780511628788.005

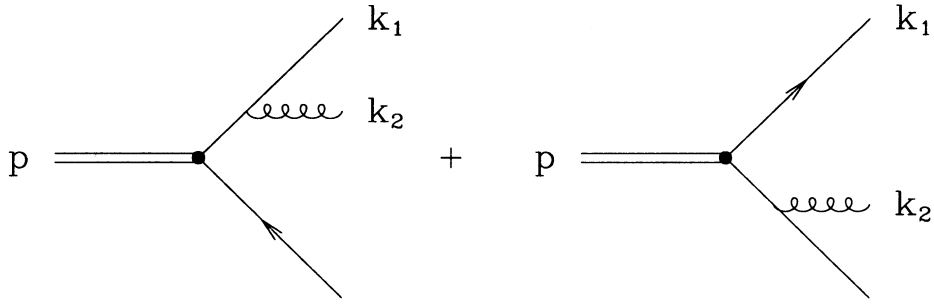


Fig. 4.20. Feynman diagrams for the $Q\overline{Q}g$ light-cone wave function.

Consider the wave function $\psi^{(n)}$ of a quarkonium state of momentum p, consisting of a quark of momentum k_1, n gluons of momenta $k_2, \ldots, k_{n+1}$ and an antiquark of momentum $k_0 = p - k_1 - \ldots$. Ignoring the spin of the quarks, which is irrelevant when the gluons are soft, the 1-gluon and 0-gluon wave functions are related by the diagrams in Fig. 4.20, which give

$$\psi^{(1)}(k_1, k_2) \sim gt^A \left[\psi^{(0)}(k_1 + k_2)\frac{k_1 \cdot \epsilon_2}{k_1 \cdot k_2} - \psi^{(0)}(k_1)\frac{k_0 \cdot \epsilon_2}{k_0 \cdot k_2}\right] \tag{4.198}$$

for a gluon with colour index A.

We use a light-cone representation in which

$$k_i = x_i p + y_i n + k_{Ti} \,, \quad \epsilon_i = \omega_i n + \epsilon_{Ti} \tag{4.199}$$

with $p = (P, 0, 0, P)$, $n = (1/(2P), 0, 0, -1/(2P))$, and $k_T = (0, k_x, k_y, 0)$. Note that we choose P so large that the quarkonium mass is negligible. Writing transverse vectors as $\boldsymbol{k} = (k_x, k_y)$ etc., we find from the mass-shell and transversality $(k_i \cdot \epsilon_i = 0)$ conditions that

$$y_i = \boldsymbol{k}_i^2/x_i \,, \quad \omega_i = \boldsymbol{k}_i \cdot \boldsymbol{\epsilon}_i/x_i \,. \tag{4.200}$$

Then for $x_2 \ll x_1, (1 - x_1)$ Eq. (4.198) becomes

$$\psi^{(1)}(x_1, \boldsymbol{k}_1, x_2, \boldsymbol{k}_2) \sim 2gt^A[\psi^{(0)}(x_1, \boldsymbol{k}_1 + \boldsymbol{k}_2) - \psi^{(0)}(x_1, \boldsymbol{k}_1)]\frac{\boldsymbol{k}_2 \cdot \boldsymbol{\epsilon}_2}{\boldsymbol{k}_2^2} \,. \tag{4.201}$$

A standard trick for simplifying this type of equation is to perform a two-dimensional Fourier transformation from transverse momenta $\boldsymbol{k}_i$ to transverse coordinates (*impact parameters*) $\boldsymbol{b}_i$:

$$\tilde{\psi}^{(n-1)}(x_1, \boldsymbol{b}_1 \ldots x_n, \boldsymbol{b}_n) = \int \prod_{i=1}^{n} \frac{d^2\boldsymbol{k}_i}{(2\pi)^2} e^{i\boldsymbol{k}_i \cdot \boldsymbol{b}_i} \psi^{(n-1)}(x_1, \boldsymbol{k}_1 \ldots x_n, \boldsymbol{k}_n) \,. \tag{4.202}$$

Downloaded from https://www.cambridge.org/core. UNIVERSIDAD AUTONOMA METROPOLITANA, on 15 Nov 2026 at 15:53:11, subject to the Cambridge Core terms of use, available at https://www.cambridge.org/core/terms. https://doi.org/10.1017/CBO9780511628788.005

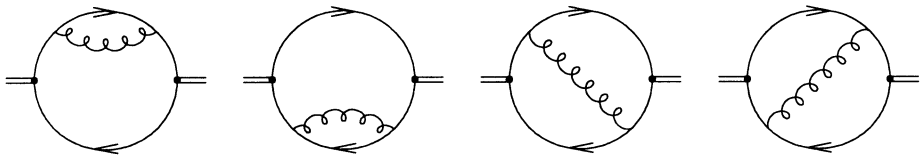


Fig. 4.21. Loop diagrams corresponding to the terms of Eq. (4.205).

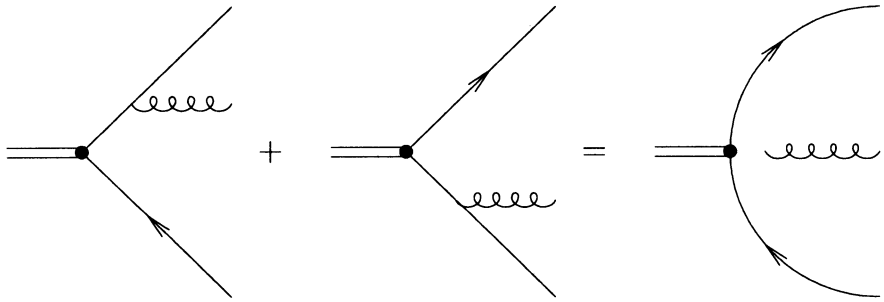


Fig. 4.22. Representation of gluon emission from a dipole.

Then we find that Eq. (4.201) becomes simply

$$\tilde{\psi}^{(1)}(x_1, \boldsymbol{b}_1, x_2, \boldsymbol{b}_2) = \frac{ig}{\pi} t^A \tilde{\psi}^{(0)}(x_1, \boldsymbol{b}_1) \left(\frac{\boldsymbol{b}_{21}}{b_{21}^2} - \frac{\boldsymbol{b}_{20}}{b_{20}^2} \right) \cdot \boldsymbol{\epsilon}_2 \tag{4.203}$$

where $\boldsymbol{b}_{ij} = \boldsymbol{b}_i - \boldsymbol{b}_j$ ($\boldsymbol{b}_0 = 0$). Taking the square modulus and performing the polarization and colour sums gives

$$|\tilde{\psi}^{(1)}|^2 = 4C_F \frac{\alpha_S}{\pi} |\tilde{\psi}^{(0)}|^2 \frac{b_{10}^2}{b_{20}^2 b_{21}^2} \,. \tag{4.204}$$

In writing Eq. (4.204) we have used the fact that

$$\frac{1}{b_{21}^2} + \frac{1}{b_{20}^2} - 2\frac{\boldsymbol{b}_{21} \cdot \boldsymbol{b}_{20}}{b_{21}^2 b_{20}^2} = \frac{b_{10}^2}{b_{20}^2 b_{21}^2} \,. \tag{4.205}$$

The terms on the left-hand side correspond to the four contributions to $|\tilde{\psi}^{(1)}|^2$ depicted in Fig. 4.21. We represent the whole dipole expression (4.204) symbolically by the diagram on the right-hand side of Fig. 4.22, which is not a Feynman graph but simply a representation of the fact that the gluon is radiated coherently by the quark and antiquark.

Next we compute the 2-gluon contribution to the wave function when one of the gluons is much softer, $x_3 \ll x_2 \ll x_1, (1 - x_1)$. This is the relevant configuration because it gives rise to the largest number of factors of $\ln x$ in the inclusive gluon distribution. There will be contributions corresponding to adding a gluon line to the loops in Fig. 4.21 in all possible ways. At this order it is not difficult to compute all the contributions,

Downloaded from https://www.cambridge.org/core. UNIVERSIDAD AUTONOMA METROPOLITANA, on 15 Nov 2026 at 15:53:11, subject to the Cambridge Core terms of use, available at https://www.cambridge.org/core/terms. https://doi.org/10.1017/CBO9780511628788.005

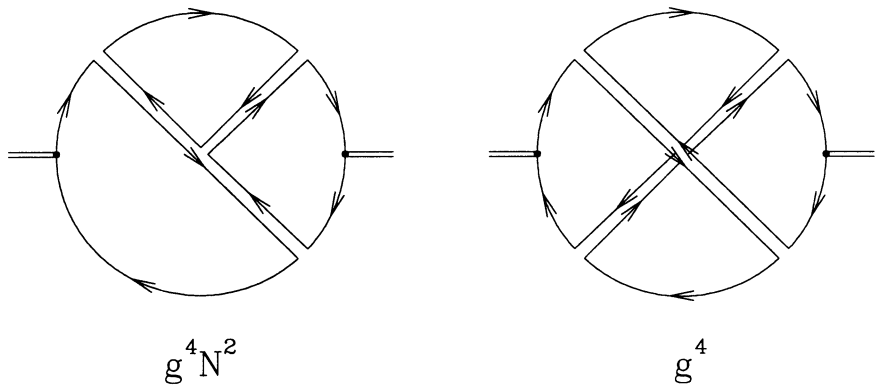


Fig. 4.23. Planar and non-planar diagrams.

but the full calculation becomes too complicated in higher orders, so we shall simplify things by making the *planar approximation.*

All contributions in which additional gluon lines are added to Fig. 4.21 can be classified as *planar* (possible to draw with all gluons inside the quark loop and not overlapping) or *non-planar.* The non-planar graphs are suppressed relative to the planar ones by powers of $1/N$ where N is the number of colours [45]. Examples of the two types of contributions are shown in Fig. 4.23, where the gluons are represented by double lines indicating the flow of colour and anticolour. This representation corresponds to the approximation that there are N^2 gluons instead of $N^2 - 1$ and $C_A = 2C_F = N$, so it is valid at large N.

The two graphs in Fig. 4.23 are of the same order in the coupling g, but the planar one has three closed colour loops while the non-planar graph has only one. The quarkonium vertices each introduce a normalization factor of $1/\sqrt{N}$, since the state must be a colour singlet. Thus the planar graph is $\mathcal{O}(g^4N^2)$ while the other is $\mathcal{O}(g^4)$ with no factors of N. The planar limit corresponds to taking $g \to 0$, $N \to \infty$ while keeping g^2N fixed. In this limit the non-planar graph vanishes like $1/N^2$. In fact $1/N^2 = 1/9$ so the planar approximation is expected to be reasonable at the 10% level.

The two-gluon wave-function-squared in the planar approximation is found to be

$$|\tilde{\psi}^{(2)}|^2 = 2N\frac{\alpha_S}{\pi}|\tilde{\psi}^{(1)}|^2\left(\frac{b_{21}^2}{b_{31}^2 b_{32}^2} + \frac{b_{20}^2}{b_{30}^2 b_{32}^2}\right) . \qquad (4.206)$$

This result has a simple interpretation in terms of the dipole picture, represented by Fig. 4.24. In a planar graph, the extra gluon has to be inserted either between the quark and the first gluon (as in Fig. 4.23) or between the gluon and the antiquark. Thus it is either radiated by

Downloaded from https://www.cambridge.org/core. UNIVERSIDAD AUTONOMA METROPOLITANA, on 15 Nov 2026 at 15:53:11, subject to the Cambridge Core terms of use, available at https://www.cambridge.org/core/terms. https://doi.org/10.1017/CBO9780511628788.005

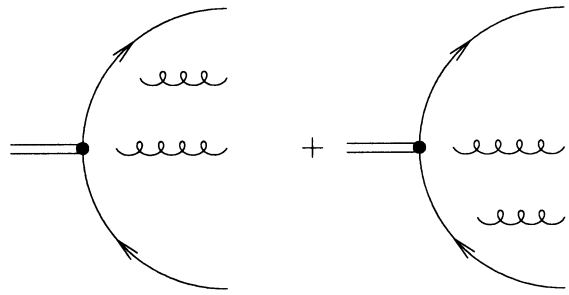


Fig. 4.24. Emission of a second gluon in dipole representation.

the (21) dipole (the first term) or by the (20) dipole (the second term). Similarly in higher orders an additional gluon can be emitted by any of the dipoles corresponding to pairs of partons that are adjacent when the diagram is drawn on a plane. The neglected non-planar graphs correspond to interference between different dipoles.

We next compute the *inclusive* gluon $\ln x$ distribution $\tilde{\mathcal{G}}(x, b_{10}^2; x_1)$ in the wave function of a quarkonium state of transverse size b_{10} with quark momentum fraction x_1. 'Inclusive' means that we sum over all contributions with any number of gluons. We construct a differential equation for this function in a way similar to that used for the (GLAP) Q^2 evolution of parton distributions. The difference is that here we study the evolution in x rather than Q^2.

Consider first the change $\delta\tilde{\mathcal{G}}$ in $\tilde{\mathcal{G}}$ when the quark momentum fraction is increased by a small amount δx_1. This opens up a new region of phase space for the emission of the hardest gluon (remember that $x < x_1$ in a leading $\ln x$ treatment). If a gluon 2 is emitted in the interval δx_1, this creates two dipoles (21) and (20) in place of the original one (10). Thus we have

$$\begin{aligned}\delta\tilde{\mathcal{G}}(x, b_{10}^2; x_1) &= 2N\frac{\alpha_S}{\pi}\frac{\delta x_1}{2x_1}\int\frac{d^2\boldsymbol{b}_2}{2\pi}\frac{b_{10}^2}{b_{20}^2 b_{21}^2} \\ &\quad\times[\tilde{\mathcal{G}}(x, b_{21}^2; x_1) + \tilde{\mathcal{G}}(x, b_{20}^2; x_1) - \tilde{\mathcal{G}}(x, b_{10}^2; x_1)]\,.\end{aligned} \tag{4.207}$$

From invariance under longitudinal boosts, $\tilde{\mathcal{G}}$ can only be a function of x/x_1. Hence

$$x\frac{\partial\tilde{\mathcal{G}}}{\partial x} = -x_1\frac{\partial\tilde{\mathcal{G}}}{\partial x_1}\,, \tag{4.208}$$

Downloaded from https://www.cambridge.org/core. UNIVERSIDAD AUTONOMA METROPOLITANA, on 15 Nov 2026 at 15:53:11, subject to the Cambridge Core terms of use, available at https://www.cambridge.org/core/terms. https://doi.org/10.1017/CBO9780511628788.005

which gives (dropping the argument x_1 from now on)

$$x\frac{\partial}{\partial x}\tilde{\mathcal{G}}(x,b_{10}^2) = -\frac{N\alpha_S}{2\pi^2}\int d^2\boldsymbol{b}_2 \frac{b_{10}^2}{b_{20}^2 b_{21}^2}[\tilde{\mathcal{G}}(x,b_{21}^2)+\tilde{\mathcal{G}}(x,b_{20}^2)-\tilde{\mathcal{G}}(x,b_{10}^2)]\,. \tag{4.209}$$

This is essentially Mueller's form of the BFKL equation, Eq. (4.195).

The quantity $\tilde{\mathcal{G}}$ is the inclusive gluon distribution in the quarkonium wave function, but this does not tell us directly the distribution of gluons relevant to the deep inelastic scattering structure functions. However, the small-x behaviour should be the same. As a check of this, we can calculate the small-x solution in the approximation that transverse momenta $k_{T_i}^2 \sim t_i$ are strongly ordered, which should reproduce the DLLA GLAP form (4.180).

Strong ordering of transverse momenta implies strong ordering of impact parameters, *i.e.* gluon 2 is either very close to the quark ($b_{21}^2 \ll b_{10}^2$ and $b_{20}^2 \simeq b_{10}^2$) or to the antiquark ($b_{20}^2 \ll b_{10}^2$ and $b_{21}^2 \simeq b_{10}^2$). These regions of the impact parameter integration give

$$x\frac{\partial}{\partial x}\tilde{\mathcal{G}}(x,b_{10}^2) \sim -\frac{N\alpha_S}{2\pi}\left[\int^{b_{10}^2}\frac{db_{21}^2}{b_{21}^2}\tilde{\mathcal{G}}(x,b_{21}^2)+\int^{b_{10}^2}\frac{db_{20}^2}{b_{20}^2}\tilde{\mathcal{G}}(x,b_{20}^2)\right] \tag{4.210}$$

and hence

$$b^2\frac{\partial}{\partial b^2}x\frac{\partial}{\partial x}\tilde{\mathcal{G}}(x,b^2) \sim -\frac{N\alpha_S}{\pi}\tilde{\mathcal{G}}(x,b^2)\,. \tag{4.211}$$

The solution of this equation has the asymptotic form

$$\tilde{\mathcal{G}}(x,b^2) \sim \tilde{\mathcal{G}}(x_0,b_0^2)\exp\sqrt{\frac{4N\alpha_S}{\pi}\ln\frac{x_0}{x}\ln\frac{b_0^2}{b^2}}\,, \tag{4.212}$$

where x_0 and b_0 here represent arbitrary boundary values. Eq. (4.212) is essentially the fixed-α_S version of Eq. (4.180) in impact-parameter space, obtained by putting $\xi = (N\alpha_S/\pi)\ln(b_0^2/b^2)$ in Eq. (4.179), and it exhibits the same $\exp\sqrt{\ln 1/x}$ behaviour at small x.

In fact there is *no* strong ordering in k_T^2 or b^2 at small x: the region in which gluon 2 is not close to either the quark or the antiquark gives a significant contribution, which causes the inclusive gluon distribution to rise faster than $\exp\sqrt{\ln 1/x}$. To see this we note that after azimuthal integration we have, schematically,

$$\int\frac{d^2\boldsymbol{b}_2}{b_{21}^2} = \int\frac{b_{20}db_{20}d\phi}{b_{20}^2+b_{10}^2-2b_{20}b_{10}\cos\phi} = \pi\int_0^\infty\frac{db_{20}^2}{|b_{20}^2-b_{10}^2|}\,. \tag{4.213}$$

The combination of integrals in Eq. (4.209) is regular, but the part in (4.213) is divergent, so one must be careful about regularization. Writing $b_{10}^2 = b^2$ and defining $b_{20}^2 = ub^2$ when $b_{20}^2 < b^2$ and $b_{20}^2 = b^2/u$ when

Downloaded from https://www.cambridge.org/core. UNIVERSIDAD AUTONOMA METROPOLITANA, on 15 Nov 2026 at 15:53:11, subject to the Cambridge Core terms of use, available at https://www.cambridge.org/core/terms. https://doi.org/10.1017/CBO9780511628788.005

$b_{20}^2 > b^2$, we find that Eq. (4.209) becomes

$$x\frac{\partial}{\partial x}\tilde{\mathcal{G}}(x,b^2) = -\frac{N\alpha_S}{\pi}\int_0^1 \frac{du}{1-u}[\tilde{\mathcal{G}}(x,ub^2)/u + \tilde{\mathcal{G}}(x,b^2/u) - 2\tilde{\mathcal{G}}(x,b^2)]\,. \tag{4.214}$$

Eq. (4.214) seems to be the simplest form in which the BFKL equation can be written. We can diagonalize it (*i.e.* remove the coupling between different values of b^2) by using a Mellin representation

$$\tilde{\mathcal{G}}(x,b^2) = \int_{\frac{1}{2}-i\infty}^{\frac{1}{2}+i\infty}\frac{d\gamma}{2\pi i}(b^2)^\gamma\hat{\mathcal{G}}(x,\gamma)\,, \tag{4.215}$$

which gives

$$x\frac{\partial\hat{\mathcal{G}}}{\partial x} = -\bar{\alpha}_S\,\hat{\mathcal{G}}\int_0^1\frac{u}{1-u}(u^{\gamma-1}+u^{-\gamma}-2) \equiv -\bar{\alpha}_S\,\hat{\mathcal{G}}\,\chi(\gamma) \tag{4.216}$$

and hence

$$\hat{\mathcal{G}}(x,\gamma) = \hat{\mathcal{G}}(x_0,\gamma)\left(\frac{x_0}{x}\right)^{\bar{\alpha}_S\chi(\gamma)} \tag{4.217}$$

where $\bar{\alpha}_S = N\alpha_S/\pi$ and χ is the *Lipatov characteristic function*

$$\chi(\gamma) = \int_0^1\frac{u}{1-u}(u^{\gamma-1}+u^{-\gamma}-2) = 2\psi(1) - \psi(\gamma) - \psi(1-\gamma)\,. \tag{4.218}$$

Here ψ is the digamma function,

$$\psi(z) = \Gamma'(z)/\Gamma(z)\,, \tag{4.219}$$

with the Euler gamma function Γ defined in Eq. (2.57). Inserting the solution (4.217) into Eq. (4.215) then gives

$$\tilde{\mathcal{G}}(x,b^2) = \int\frac{d\gamma}{2\pi i}\hat{\mathcal{G}}(x_0,\gamma)\exp[\gamma\ln b^2 + \bar{\alpha}_S\chi(\gamma)\ln(x_0/x)]\,. \tag{4.220}$$

Given the assumed form of $\tilde{\mathcal{G}}(x_0,b^2)$ at some starting value x_0, one can Mellin transform to obtain $\hat{\mathcal{G}}(x_0,\gamma)$ using the inverse of Eq. (4.215),

$$\hat{\mathcal{G}}(x,\gamma) = \int_0^\infty db^2(b^2)^{-\gamma-1}\tilde{\mathcal{G}}(x,b^2)\,, \tag{4.221}$$

and then deduce $\tilde{\mathcal{G}}(x,b^2)$ at any $x < x_0$. For large values of $\ln(x_0/x)$ the integral will be dominated by the saddle point of the integrand, *i.e.* the point $\gamma = \gamma_s$ at which the derivative of the exponent vanishes. Denoting the exponent by

$$\phi(\gamma) = \gamma\ln b^2 + \bar{\alpha}_S\chi(\gamma)\ln(x_0/x)\,, \tag{4.222}$$

we have

$$\tilde{\mathcal{G}}(x,b^2) \;\sim\; \int\frac{d\gamma}{2\pi i}\hat{\mathcal{G}}(x_0,\gamma_s)\exp[\phi(\gamma_s) + \tfrac{1}{2}\phi''(\gamma_s)(\gamma-\gamma_s)^2]$$

Downloaded from https://www.cambridge.org/core. UNIVERSIDAD AUTONOMA METROPOLITANA, on 15 Nov 2026 at 15:53:11, subject to the Cambridge Core terms of use, available at https://www.cambridge.org/core/terms. https://doi.org/10.1017/CBO9780511628788.005

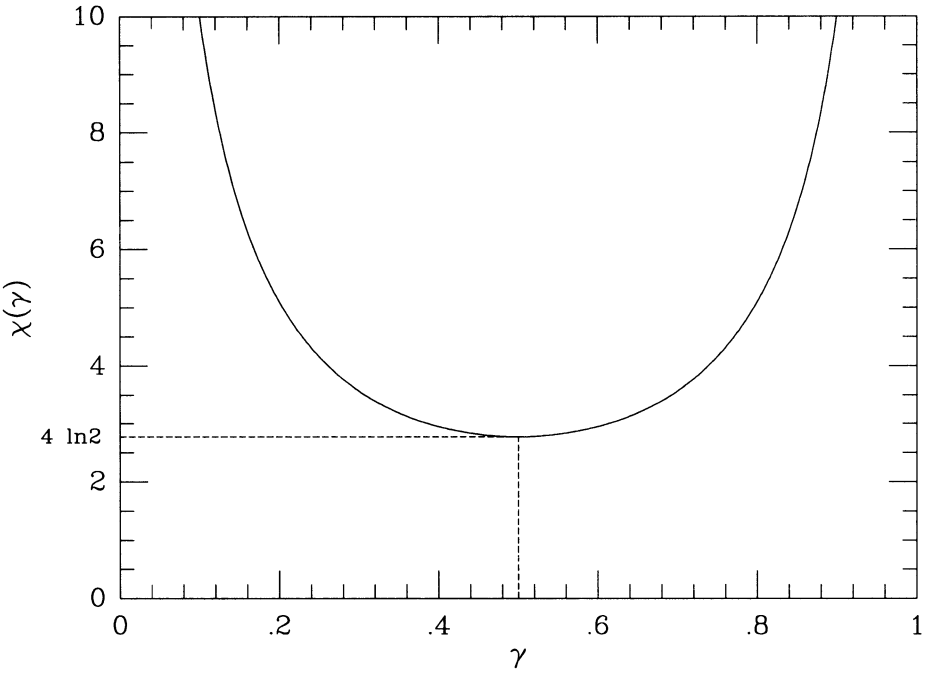


Fig. 4.25. The Lipatov characteristic function.

$$= \frac{1}{\sqrt{2\pi\phi''(\gamma_s)}}\hat{\mathcal{G}}(x_0,\gamma_s)\exp\phi(\gamma_s) \tag{4.223}$$

where

$$\phi'(\gamma_s) = \ln b^2 + \bar{\alpha}_S\chi'(\gamma_s)\ln(x_0/x) = 0\,. \tag{4.224}$$

The form of the Lipatov characteristic function χ is shown in Fig. 4.25. For any fixed value of b^2, we have $\gamma_s \to \frac{1}{2}$ as $x \to 0$, since $\chi'(\frac{1}{2}) = 0$. Thus $\tilde{\mathcal{G}}(x,b^2)$ at small x is power behaved:

$$\tilde{\mathcal{G}}(x,b^2) \sim \frac{1}{\sqrt{2\pi\phi''(\frac{1}{2})}}\hat{\mathcal{G}}(x_0,\tfrac{1}{2})\exp[\phi(\tfrac{1}{2})] \propto bx^{-\lambda} \tag{4.225}$$

where

$$\lambda = \bar{\alpha}_S\chi(\tfrac{1}{2}) = 4N\ln 2\,\frac{\alpha_S}{\pi}\,, \tag{4.226}$$

as in Eq. (4.189). Finally, we may take the inverse two-dimensional Fourier transformation to obtain the inclusive gluon distribution as a function of x and k_T:

$$\mathcal{G}(x,k_T^2) = \int d^2\boldsymbol{b}_i\, e^{-i\boldsymbol{k}_i\cdot\boldsymbol{b}_i}\tilde{\mathcal{G}}(x,b^2) \propto \frac{1}{\sqrt{k_T^2}}x^{-\lambda}\,, \tag{4.227}$$

Downloaded from https://www.cambridge.org/core. UNIVERSIDAD AUTONOMA METROPOLITANA, on 15 Nov 2026 at 15:53:11, subject to the Cambridge Core terms of use, available at https://www.cambridge.org/core/terms. https://doi.org/10.1017/CBO9780511628788.005

which is the result for the gluon distribution function quoted in Eq. (4.194). The parameter λ is about 0.5 for $\alpha_S \simeq 0.2$, leading to an approximate $x^{-3/2}$ divergence in the gluon distribution at small x.

4.6.6 Parton saturation

In the previous sections we have seen how perturbative QCD predicts a rapid increase of the parton distributions at small x. However this increase cannot go on indefinitely. If the number density of partons becomes too large inside the proton then they can no longer be treated as free. The effect is evidently most important for gluons, whose distribution at small x exceeds that of the sea quarks by more than an order of magnitude.

When the number density becomes so large that the gluons 'saturate' the proton, we would expect that gluon recombination effects would limit any further growth of the distribution [46]. A simple geometric argument gives an indication as to where in x and μ^2 space this saturation may be expected to occur. In the infinite momentum frame the gluon momentum distribution $xg(x,\mu^2)$ gives the number of gluons per unit of longitudinal phase space dx/x, with a transverse size greater than $1/\mu$, when probed at a deep inelastic scale $Q^2 = \mu^2$. Therefore the gluons occupy a transverse area $\sim xg(x,\mu^2)/\mu^2$ of the disc shown in Fig. 4.5. As x decreases this area becomes large, and we would expect saturation effects to become important when

$$\frac{\alpha_S(\mu^2)}{\mu^2}\, xg(x,\mu^2) \gtrsim \pi R^2 \,, \tag{4.228}$$

where $R \sim 5$ GeV^{-1} is the proton radius. Note the additional factor of $\alpha_S(\mu^2)$ which enters because the effective gluon-gluon cross section is $\sigma_{gg} \sim \alpha_S(\mu^2)/\mu^2$. For a typical gluon distribution, the x, μ^2 region where the inequality (4.228) is satisfied is shown in Fig. 4.18. From Fig. 4.16, we see that parton saturation is unlikely to play a major role in the HERA kinematic region. Detailed analytic and numerical studies, which go beyond the crude estimate of Eq. (4.228), support this conclusion, see for example refs. [47,48].

4.7 Polarized scattering

All the deep inelastic structure functions discussed so far in this chapter correspond to *spin-averaged* scattering. In this section we generalize the discussion to the situation where the lepton beam and nucleon target are polarized in the longitudinal direction. Such scattering processes yield information on the spin content of the nucleon, in particular how the spin of a fast-moving nucleon is distributed among its parton constituents. For

Downloaded from https://www.cambridge.org/core. UNIVERSIDAD AUTONOMA METROPOLITANA, on 15 Nov 2026 at 15:53:11, subject to the Cambridge Core terms of use, available at https://www.cambridge.org/core/terms. https://doi.org/10.1017/CBO9780511628788.005

simplicity we shall consider only the electromagnetic (photon exchange) contribution to the cross section.

In deep inelastic scattering experiments where both the beam and target can be longitudinally polarized one can measure the spin asymmetry

$$A(x,Q^2) = \frac{d\sigma^{\uparrow\downarrow}(x,Q^2) - d\sigma^{\uparrow\uparrow}(x,Q^2)}{d\sigma^{\uparrow\downarrow}(x,Q^2) + d\sigma^{\uparrow\uparrow}(x,Q^2)} \tag{4.229}$$

where the cross section $d\sigma^{\uparrow\uparrow}$ ($d\sigma^{\uparrow\downarrow}$) corresponds to the incoming lepton and nucleon being polarized parallel (anti-parallel) to one another. The denominator in (4.229) is simply twice the spin-averaged cross section discussed in Section 4.1. The numerator can be written in terms of two new structure functions g_1 and g_2 (*cf.* Eq. (4.2))

$$\begin{aligned}\frac{d^2\sigma^{\uparrow\downarrow}}{dxdy} - \frac{d^2\sigma^{\uparrow\uparrow}}{dxdy} &= \frac{8\pi\alpha^2 ME}{Q^4}\left[\left(2y - y^2 - \frac{Mxy^2}{E}\right)2xg_1(x,Q^2)\right. \\ &\quad \left. -\frac{4M}{E}x^2 y g_2(x,Q^2)\right]. \end{aligned} \tag{4.230}$$

The structure functions g_1, g_2 are the polarized analogues of F_1, F_2. They represent the two independent contributions to the *antisymmetric* part of the hadronic tensor $W_{\alpha\beta}(p,q)$ (4.28) allowed by P and T invariance. In the kinematic region characteristic of fixed-target experiments, the numerator and denominator in Eq. (4.229) are dominated by the terms proportional to g_1 and F_1 respectively, and

$$A(x,Q^2) \approx \frac{g_1(x,Q^2)}{F_1(x,Q^2)}\,. \tag{4.231}$$

Thus the polarized structure function can be extracted from a measurement of the longitudinal asymmetry combined with a measurement of the unpolarized structure function. In the current range of x and Q^2 probed by (fixed-target) experiments the asymmetry is observed to be essentially Q^2 independent, from which we deduce that g_1 also satisfies approximate Bjorken scaling.

4.7.1 Parton model interpretation

To establish the parton model description of the polarized structure functions we may proceed exactly as in Section 4.1. We consider scattering off a pointlike, massless quark constituent of a longitudinally polarized proton in the infinite momentum frame. There are now two probability distributions, $q^{\uparrow}(\xi)$ and $q^{\downarrow}(\xi)$, representing the probabilities that the quark spin is respectively parallel and antiparallel to the spin of the parent proton. A straightforward calculation of the spin-dependent $eq \to eq$

Downloaded from https://www.cambridge.org/core. UNIVERSIDAD AUTONOMA METROPOLITANA, on 15 Nov 2026 at 15:53:11, subject to the Cambridge Core terms of use, available at https://www.cambridge.org/core/terms. https://doi.org/10.1017/CBO9780511628788.005

scattering cross section then gives

$$\begin{aligned} F_1(x) &= \tfrac{1}{2}\sum_q e_q^2\,[q(x)+\bar{q}(x)]\,, \\ g_1(x) &= \tfrac{1}{2}\sum_q e_q^2\,[\Delta q(x)+\Delta\bar{q}(x)]\,, \end{aligned} \tag{4.232}$$

where

$$q = q^{\uparrow} + q^{\downarrow}\,, \qquad \Delta q = q^{\uparrow} - q^{\downarrow}\,. \tag{4.233}$$

Note that $g_2 = 0$ in this simple model. However this is misleading. A more realistic parton model calculation, in which the quark can be both off-shell and have non-zero transverse momentum with respect to the parent proton direction of motion, gives a non-zero g_2 of similar magnitude to g_1. A more complete discussion can be found, for example, in ref. [49].

In a model with three quark flavours, the structure function g_1 for proton and neutron targets can be written as

$$\begin{aligned} g_1^p(x) &= \frac{2}{9}\,[\Delta u(x)+\Delta\bar{u}(x)] + \frac{1}{18}\,[\Delta d(x)+\Delta\bar{d}(x)) + \Delta s(x) + \Delta\bar{s}(x)]\,, \\ g_1^n(x) &= \frac{2}{9}\,[\Delta d(x)+\Delta\bar{d}(x)] + \frac{1}{18}\,[\Delta u(x)+\Delta\bar{u}(x)) + \Delta s(x) + \Delta\bar{s}(x)]\,. \end{aligned} \tag{4.234}$$

Several important sum rules can be derived for the first moment of g_1, $\Gamma_1 = \int_0^1 dx\; g_1(x)$. From Eq. (4.234) it follows that

$$\Gamma_1^{p,n} = \frac{1}{9}a_0 \pm \frac{1}{12}a_3 + \frac{1}{36}a_8 \tag{4.235}$$

where a_0, a_3 and a_8 are respectively the SU(3) flavour singlet, octet isotriplet and octet isosinglet combinations of the first moments of the quark distributions:

$$\begin{aligned} a_0 &= \eta_u + \eta_d + \eta_s \\ a_3 &= \eta_u - \eta_d \\ a_8 &= \eta_u + \eta_d - 2\eta_s\,, \end{aligned} \tag{4.236}$$

with $\eta_u = \int_0^1 dx\;[\Delta u(x) + \Delta\bar{u}(x)]$ denoting the net spin carried by the different quark flavours. The triplet combination a_3 is particularly interesting since it corresponds to the matrix element of a current which is directly measured in neutron β-decay. Taking the difference between Γ_1^p and Γ_1^n gives the *Bjorken sum rule* [50]

$$\Gamma_1^p - \Gamma_1^n = \int_0^1 dx\;(g_1^p - g_1^n) = \frac{1}{6}\left|\frac{g_A}{g_V}\right| = 0.209 \pm 0.001\,. \tag{4.237}$$

This sum rule, based on current algebra and SU(2) isospin symmetry, provides a fundamental test of the theory. In practice, perturbative QCD

Downloaded from https://www.cambridge.org/core. UNIVERSIDAD AUTONOMA METROPOLITANA, on 15 Nov 2026 at 15:53:11, subject to the Cambridge Core terms of use, available at https://www.cambridge.org/core/terms. https://doi.org/10.1017/CBO9780511628788.005

corrections to the right-hand side of (4.237) (see below) must also be taken into account.

More generally, the axial-vector couplings measured in hyperon (Λ, Σ, Ξ) decays give information on other combinations of η_u, η_d and η_s, assuming SU(3) flavour symmetry. There are two independent parameters, F and D, which can be determined for example from $n \to p$ and $\Sigma^- \to n$ decays and in terms of which

$$\begin{aligned} a_3 &= F + D = 1.257 \pm 0.003 , \\ a_8 &= 3F - D = 0.58 \pm 0.02 , \end{aligned} \tag{4.238}$$

where the numerical values are taken from ref. [51].

The above information is, by itself, insufficient to determine the individual Γ_1^p and Γ_1^n. However with the further assumption that the strange quark sea in the proton is unpolarized ($\eta_s = 0$), we obtain the *Ellis-Jaffe* [52] sum rule:

$$\Gamma_1^p = \int_0^1 dx\, g^p = \frac{1}{12}\left|\frac{g_A}{g_V}\right| \left[1 + \frac{5}{3}\,\frac{3F - D}{F + D}\right] = 0.185 \pm 0.003 . \tag{4.239}$$

Similarly, for the neutron we have

$$\Gamma_1^n = \int_0^1 dx\, g_1^n = \frac{1}{12}\left|\frac{g_A}{g_V}\right| \left[-1 + \frac{5}{3}\,\frac{3F - D}{F + D}\right] = -0.024 \pm 0.003 . \tag{4.240}$$

A recent experimental measurement of Γ_1^p, which includes all available data, gives [53]

$$\Gamma_1^p = 0.142 \pm 0.008(\text{stat.}) \pm 0.011(\text{sys.}) \qquad (Q^2 = 10\ \text{GeV}^2) . \tag{4.241}$$

Even allowing for the perturbative QCD correction $1 - O(\alpha_S(Q^2)/\pi)$ to the right-hand side of (4.239), the measured value is significantly below the theoretical prediction. A possible explanation for this discrepancy is that the strange quarks do carry some of the proton's spin. In fact by combining the results from hyperon decays and the measured values of $\Gamma_1^{p,n}$, and including perturbative QCD corrections, one can deduce that, at $Q^2 = 10\ \text{GeV}^2$, [54]

$$\eta_u = +0.83 \pm 0.03,\ \eta_d = -0.43 \pm 0.03,\ \eta_s = -0.10 \pm 0.03 , \tag{4.242}$$

and therefore

$$\eta_\Sigma = \eta_u + \eta_d + \eta_s = 0.31 \pm 0.07 . \tag{4.243}$$

These can be compared with the SU(6) constituent quark model predictions [55]

$$\eta_u = \frac{4}{3},\ \eta_d = -\frac{1}{3},\ \eta_s = 0\ , \eta_\Sigma = 1 . \tag{4.244}$$

Downloaded from https://www.cambridge.org/core. UNIVERSIDAD AUTONOMA METROPOLITANA, on 15 Nov 2026 at 15:53:11, subject to the Cambridge Core terms of use, available at https://www.cambridge.org/core/terms. https://doi.org/10.1017/CBO9780511628788.005

4.7.2 Perturbative QCD corrections

The relatively large strange quark polarization and small total spin carried by the quarks, compared to the naive expectations of Eq. (4.244), has been the subject of much theoretical discussion in recent years. Although there is no reason why η_Σ should equal 1, since orbital angular momentum also contributes to the total spin of the nucleon, it seems somehow unnatural that the quarks should carry so little of the net spin. One of the more compelling explanations for this result is that a substantial amount of the nucleon's spin is carried by gluons. If we denote the net polarized gluon contribution by $\eta_g = \int_0^1 dx\, \Delta g(x)$, where $\Delta g = g^\uparrow - g^\downarrow$, then conservation of angular momentum implies

$$\frac{1}{2} = \frac{1}{2}\eta_\Sigma + \eta_g + \langle L_z \rangle \,. \tag{4.245}$$

The polarized gluon contributes to g_1 at $O(\alpha_S)$, just as in the unpolarized case. In perturbative QCD the parton model result of Eq. (4.232) is replaced by (*cf.* Eq. (4.84) for F_2)

$$\begin{aligned} g_1(x,Q^2) &= \tfrac{1}{2}\sum_q e_q^2 \int_x^1 \frac{d\xi}{\xi}\, [\Delta q(x/\xi,Q^2) + \Delta\bar{q}(x/\xi,Q^2)] \\ &\quad \times \left\{ \delta(1-\xi) + \frac{\alpha_S(Q^2)}{2\pi}\Delta C_q(\xi) + \ldots \right\} \\ &\quad + \left(\sum_q e_q^2 \right) \int_x^1 \frac{d\xi}{\xi}\, \Delta g(x/\xi,Q^2) \left\{ \frac{\alpha_S(Q^2)}{2\pi}\Delta C_g(\xi) + \ldots \right\} . \end{aligned} \tag{4.246}$$

The leading-order GLAP equations for the evolution of the polarized quark and gluon distributions are

$$\begin{aligned} t\frac{\partial}{\partial t}\begin{pmatrix} \Delta q_i(x,t) \\ \Delta g(x,t) \end{pmatrix} &= \frac{\alpha_S(t)}{2\pi}\sum_j \int_x^1 \frac{d\xi}{\xi} \\ &\quad \times \begin{pmatrix} \Delta P_{q_i q_j}\left(\frac{x}{\xi}\right) & \Delta P_{qg}\left(\frac{x}{\xi}\right) \\ \Delta P_{gq}\left(\frac{x}{\xi}\right) & \Delta P_{gg}\left(\frac{x}{\xi}\right) \end{pmatrix} \begin{pmatrix} \Delta q_j(\xi,t) \\ \Delta g(\xi,t) \end{pmatrix} . \end{aligned} \tag{4.247}$$

The splitting functions are [8]

$$\begin{aligned} \Delta P_{qq}^{(0)}(x) &= C_F \left[\frac{1+x^2}{(1-x)_+} + \frac{3}{2}\delta(1-x) \right] , \\ \Delta P_{qg}^{(0)}(x) &= T_R\,[2x-1], \quad T_R = \frac{1}{2} , \\ \Delta P_{gq}^{(0)}(x) &= C_F\,[2-x] , \end{aligned}$$

Downloaded from https://www.cambridge.org/core. UNIVERSIDAD AUTONOMA METROPOLITANA, on 15 Nov 2026 at 15:53:11, subject to the Cambridge Core terms of use, available at https://www.cambridge.org/core/terms. https://doi.org/10.1017/CBO9780511628788.005

$$\Delta P_{gg}^{(0)}(x) = C_A \left[\frac{2}{(1-x)_+} - 4x + 2 \right] + \delta(1-x) \frac{11C_A - 4n_f T_R}{6} , \quad (4.248)$$

where the 'plus prescription' on the singular parts of the splitting functions has been defined in Eq. (4.72). The next-to-leading ($O(\alpha_S^2)$) contributions to the polarized splitting functions have also been calculated [56].

The evolution of the first ($j = 1$) moments of the quark flavour singlet and gluon distributions can be obtained from Eqs. (4.247) and (4.248):

$$t\frac{\partial}{\partial t} \begin{pmatrix} \Delta\Sigma(1,t) \\ \Delta g(1,t) \end{pmatrix} = \frac{\alpha_S(t)}{2\pi} \begin{pmatrix} 0 & 0 \\ \frac{3}{2}C_F & 2\pi b \end{pmatrix} \begin{pmatrix} \Delta\Sigma(1,t) \\ \Delta g(1,t) \end{pmatrix} . \quad (4.249)$$

Hence

$$t\frac{\partial}{\partial t} \eta_\Sigma(t) = 0 + O(\alpha_S^2) , \quad (4.250)$$

$$t\frac{\partial}{\partial t} \alpha_S(t)\eta_g(t) = 0 + O(\alpha_S^2) . \quad (4.251)$$

which implies that the gluon contribution to g_1 ($\sim \alpha_S \Delta g$) is formally of the same order as the quark contribution. The polarized structure function has been separated into two conserved (at leading order) quantities associated with quark and gluon contributions, the former to be identified with the SU(6) 'constituent' quarks. If we attribute the difference between the Ellis-Jaffe sum rule prediction (*i.e.* assuming no strange quark polarization at low Q^2) and the measured value to the gluon contribution, then we find $\eta_g(Q_0^2 = 4\ \mathrm{GeV}^2) \approx 2$ [57]. The importance of the polarized gluon contribution to the structure function was first pointed out in refs. [58,59].

In the Bjorken sum (4.237) the gluon contribution cancels, and perturbative QCD corrections simply modify the leading-order result. In fact the corrections are closely related to those for the Gross–Llewellyn Smith sum rule (4.156), and are known to $O(\alpha_S^3)$ [25]. In the $\overline{\mathrm{MS}}$ renormalization scheme

$$\Gamma_1^p(Q^2) - \Gamma_1^n(Q^2) = \frac{1}{6}\left|\frac{g_A}{g_V}\right| \left[1 - \frac{\alpha_S(Q^2)}{\pi} + \left(\frac{\alpha_S(Q^2)}{\pi}\right)^2 \left(-\frac{55}{12} + n_f \frac{1}{3}\right) + \left(\frac{\alpha_S(Q^2)}{\pi}\right)^3 \left(-\frac{13841}{216} - \frac{44}{9}\zeta(3) + \frac{55}{2}\zeta(5) + n_f\left(\frac{10339}{1296} + \frac{61}{54}\zeta(3) - \frac{5}{3}\zeta(5)\right) - n_f^2 \frac{115}{648}\right)\right] . \quad (4.252)$$

Comparison of the theoretical prediction with the measured value gives a measurement of the strong coupling, see Chapter 12.

Downloaded from https://www.cambridge.org/core. UNIVERSIDAD AUTONOMA METROPOLITANA, on 15 Nov 2026 at 15:53:11, subject to the Cambridge Core terms of use, available at https://www.cambridge.org/core/terms. https://doi.org/10.1017/CBO9780511628788.005

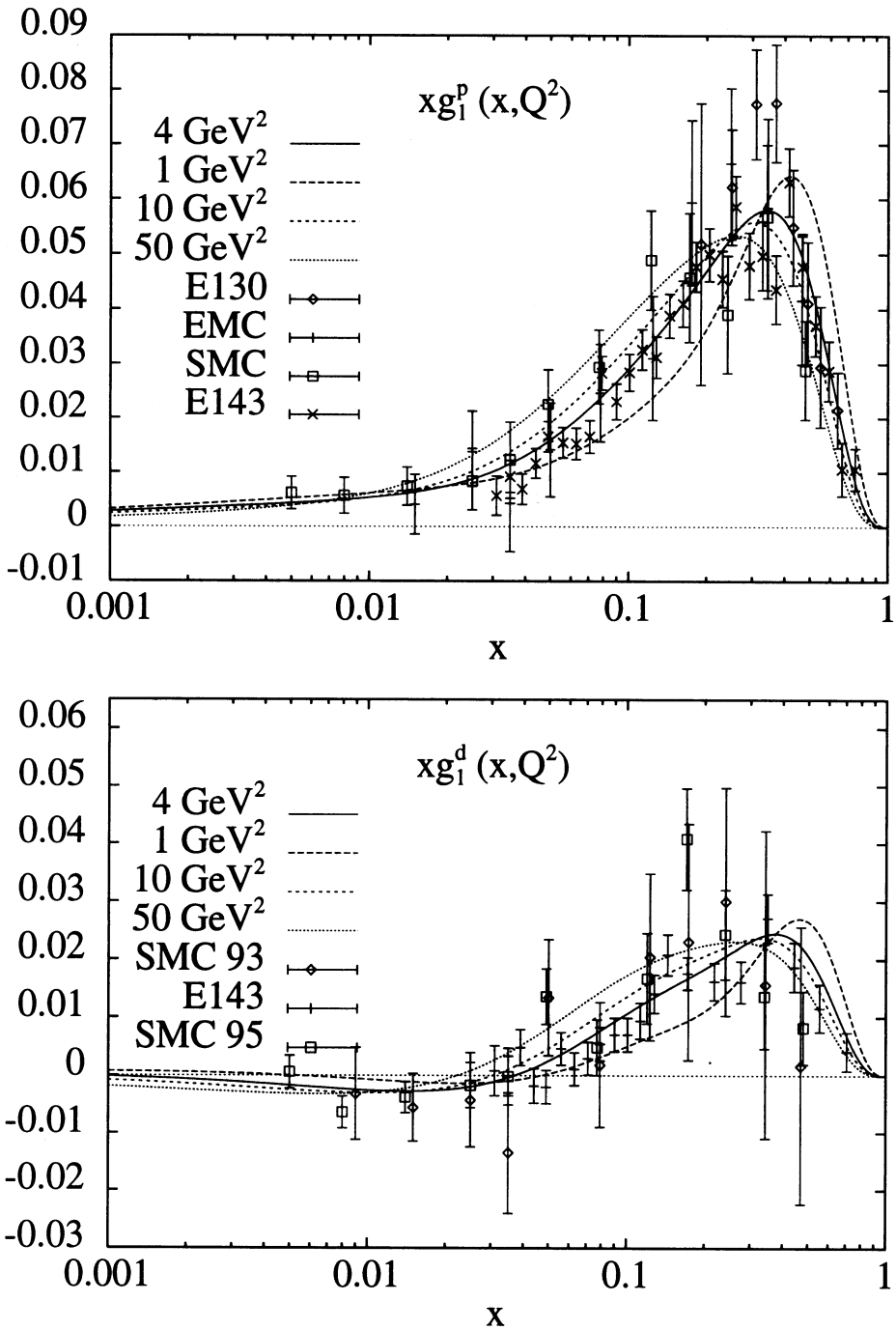


Fig. 4.26. Data on the structure function g_1 for proton and deuteron targets. The curves are NLO QCD fits. Figure from ref. [57].

Downloaded from https://www.cambridge.org/core. UNIVERSIDAD AUTONOMA METROPOLITANA, on 15 Nov 2026 at 15:53:11, subject to the Cambridge Core terms of use, available at https://www.cambridge.org/core/terms. https://doi.org/10.1017/CBO9780511628788.005

Concerning the *shape* in x of the polarized parton distributions, the situation is very different from the unpolarized case, where a combination of structure function measurements with charged lepton and neutrino beams and measurements of gluon-induced processes, such as direct photon and heavy quark production, pin down quite accurately the shape of the individual distributions. Here, the only useful information at present comes from $g_1(x, Q^2)$ measured with proton, neutron and deuteron targets. These data essentially only determine the shape of the valence u and d quark distributions, and the sea and gluon distributions are largely unconstrained. Parton distribution fits, similar to those described in Section 4.4, must therefore be supplemented by model assumptions about the behaviours at large and small x, the flavour decomposition of the sea, the shape of the gluon distribution etc. Nevertheless, the high-Q^2 g_1 structure function data *can* be very well described in either leading- or next-to-leading-order fits based on the perturbative QCD evolution equations. This is illustrated in Fig. 4.26, which shows the NLO description [57] of various g_1 measurements [60] using a particular ansatz for the shape of the gluon distribution. The curves correspond to $Q^2 = 1, 4, 10, 50\ \mathrm{GeV}^2$, reflecting the spread in Q^2 values of the different data sets. There is a systematic decrease in the Q^2 values of the data points from large x to small x.

References

1) J.D. Bjorken, *Phys. Rev.* **179** (1969) 1547.
2) R.P. Feynman, *Photon Hadron Interactions*, W.A. Benjamin, New York (1972).
3) SLAC-MIT collaboration, G. Miller *et al.*, *Phys. Rev.* **D5** (1972) 528.
4) BCDMS collaboration, A.C. Benvenuti *et al.*, *Phys. Lett.* **B223** (1989) 485.
5) H1 collaboration, T. Ahmed *et al.*, *Nucl. Phys.* **B439** (1995) 471.
6) ZEUS collaboration, M. Derrick *et al.*, *Zeit. Phys.* **C65** (1995) 379.
7) A.D. Martin, R.G. Roberts and W.J. Stirling, *Phys. Rev.* **D50** (1994) 6734.
8) G. Altarelli and G. Parisi, *Nucl. Phys.* **B126** (1977) 298.
9) G. Altarelli, R.K. Ellis and G. Martinelli, *Nucl. Phys.* **B143** (1978) 521; *ibid.* **B146** (1978) 544(erratum).
10) W.A. Bardeen, A.J. Buras, D.W. Duke and T. Muta, *Phys. Rev.* **D18** (1978) 3998.
11) M. Göckeler *et al.*, *Phys. Rev.* **D53** (1996) 2317.
12) L.N. Lipatov, *Sov. J. Nucl. Phys.* **20** (1975) 95;
V.N. Gribov and L.N. Lipatov, *Sov. J. Nucl. Phys.* **15** (1972) 438;
G. Altarelli and G. Parisi, ref. [8];
Yu.L. Dokshitzer *Sov. Phys. JETP* **46** (1977) 641.
13) H. Georgi and H.D. Politzer, *Phys. Rev.* **D9** (1974) 416.
14) D. Gross and F. Wilczek, *Phys. Rev.* **D9** (1974) 980.
15) G. Curci, W. Furmanski and R. Petronzio, *Nucl. Phys.* **B175** (1980) 27.
16) W. Furmanski and R. Petronzio, *Phys. Lett.* **B97** (1980) 437.

Downloaded from https://www.cambridge.org/core. UNIVERSIDAD AUTONOMA METROPOLITANA, on 15 Nov 2026 at 15:53:11, subject to the Cambridge Core terms of use, available at https://www.cambridge.org/core/terms. https://doi.org/10.1017/CBO9780511628788.005

17) E.G. Floratos, D.A. Ross and C.T. Sachrajda, *Nucl. Phys.* **B129** (1977) 66; *ibid.* **B139** (1978) 545(erratum); *ibid.* **B152** (1979) 493;
A. Gonzalez-Arroyo, C. Lopez and F.J. Yndurain, *Nucl. Phys.* **B153** (1979) 161;
E.G. Floratos, R. Lacaze and C. Kounnas, *Nucl. Phys.* **B192** (1981) 417.

18) NMC collaboration, P. Amaudruz *et al.*, *Phys. Lett.* **B295** (1992) 159.

19) G. Altarelli, *Phys. Rep.* **81** (1982) 1.

20) A. Milsztajn and M. Virchaux, *Phys. Lett.* **B274** (1992) 221.

21) BCDMS collaboration, A.C. Benvenuti *et al.*, *Phys. Lett.* **B237** (1990) 592.

22) L.W. Whitlow, Ph.D. thesis, SLAC-Report -357 (1990).

23) D.J. Gross and C.H. Llewellyn Smith, *Nucl. Phys.* **B14** (1969) 337.

24) S.G. Gorishny and S.A. Larin, *Phys. Lett.* **B172** (1986) 109.

25) S.A. Larin and J.A.M. Vermaseren, *Phys. Lett.* **B259** (1991) 345.

26) CCFR–NUTEV collaboration, M.H. Shaevitz *et al.*, *Nucl. Phys.* **B** (*Proc. Suppl.*) **38** (1995) 188.

27) S.L. Adler, *Phys. Rev.* **143** (1963) 1144.

28) BEBC collaboration, D. Allasia *et al.*, *Phys. Lett.* **B135** (1984) 231; *Zeit. Phys.* **C28** (1985) 321.

29) K. Gottfried, *Phys. Rev. Lett.* **18** (1967) 1154

30) NMC collaboration, P. Amaudruz *et al.*, *Phys. Rev. Lett.* **66** (1991) 2712.

31) P.D.B. Collins, *Introduction to Regge Theory*, Cambridge University Press (1977).

32) A. Donnachie and P.V. Landshoff, *Zeit. Phys.* **C61** (1994) 139.

33) A.D. Martin, R.G. Roberts and W.J. Stirling, *Phys. Lett.* **B354** (1995) 155.

34) A. De Rujula, S.L. Glashow, H.D. Politzer, S.B. Treiman, F. Wilczek and A. Zee, *Phys. Rev.* **10** (1974) 1649.

35) R.D. Ball and S. Forte, *Phys. Lett.* **B335** (1994) 77; *ibid.* **B336** (1994) 77.

36) H1 collaboration, S. Aid *et al.*, *Phys. Lett.* **B354** (1995) 494.

37) E.A. Kuraev, L.N. Lipatov and V.S. Fadin, *Phys. Lett.* **B60** (1975) 50; *Sov. Phys. JETP* **44** (1976) 433; *ibid.* **45** (1977) 199;
Ya.Ya. Balitsky and L.N. Lipatov, *Sov. J. Nucl. Phys.* **28** (1978) 822.

38) S. Catani and F. Hautmann, *Nucl. Phys.* **B427** (1994) 475.

39) See for example:
R.K. Ellis, Z. Kunszt and E. Levin, *Nucl. Phys.* **B420** (1994) 517; *ibid.* **B433** (1995) 498(erratum);
R.K. Ellis, F. Hautmann and B.R. Webber, *Phys. Lett.* **B348** (1995) 582;
R.D. Ball and S. Forte, *Phys. Lett.* **B351** (1995) 513;
J.R. Forshaw, R.G. Roberts and R.S. Thorne, *Phys. Lett.* **B356** (1995) 79.

40) S. Catani, M. Ciafaloni and F. Hautmann, *Phys. Lett.* **B242** (1990) 97; *Nucl. Phys.* **B366** (1991) 657.

41) A.J. Askew, J. Kwiecinski, A.D. Martin and P.J. Sutton, *Phys. Rev.* **D47** (1993) 3775; *ibid.* **D49** (1994) 4402; *Mod. Phys. Lett.* **A8** (1993) 3813.

42) M. Ciafaloni, *Nucl. Phys.* **B296** (1988) 49;
S. Catani, F. Fiorani and G. Marchesini, *Phys. Lett.* **B234** (1990) 339; *Nucl. Phys.* **B336** (1990) 18.

43) J. Kwiecinski, A.D. Martin and P.J. Sutton, *Phys. Rev.* **D52** (1995) 1445.

44) A.H. Mueller, *Nucl. Phys.* **B415** (1994) 373;
A.H. Mueller and B. Patel, *Nucl. Phys.* **B425** (1994) 471;
See also: N.N. Nikolaev, B.G. Zakharov and V.R. Zoller, *Phys. Lett.* **B328** (1994) 486.

45) G. 't Hooft, *Nucl. Phys.* **B72** (1974) 461.

46) L.V. Gribov, E.M. Levin and M.G. Ryskin, *Phys. Rep.* **100** (1983) 1.

Downloaded from https://www.cambridge.org/core. UNIVERSIDAD AUTONOMA METROPOLITANA, on 15 Nov 2026 at 15:53:11, subject to the Cambridge Core terms of use, available at https://www.cambridge.org/core/terms. https://doi.org/10.1017/CBO9780511628788.005

47) A.H. Mueller and J. Qiu, *Nucl. Phys.* **B268** (1986) 427

48) J. Kwiecinski, A.D. Martin, R.G. Roberts and W.J. Stirling, *Phys. Rev.* **D42** (1990) 3645.

49) R.G. Roberts, *The Structure of the Proton*, Cambridge University Press (1990).

50) J.D. Bjorken, *Phys. Rev.* **148** (1966) 1467; *Phys. Rev.* **D1** (1970) 1376.

51) F.E. Close and R.G. Roberts, *Phys. Lett.* **B316** (1993) 165.

52) J. Ellis and R.L. Jaffe, *Phys. Rev.* **D9** (1974) 1444; *ibid.* **D10** (1974) 1669.

53) SMC collaboration, D. Adams *et al.*, *Phys. Lett.* **B329** (1994) 399.

54) J. Ellis and M. Karliner, *Phys. Lett.* **B341** (1995) 397.

55) M. Gourdin, *Nucl. Phys.* **B38** (1972) 418.

56) R. Mertig and W.L. van Neerven, *Zeit. Phys.* **C70** (1996) 637;
W. Vogelsang, *Phys. Rev.* **D54** (1996) 2023.

57) T. Gehrmann and W.J. Stirling, *Phys. Rev.* **D53** (1996) 6100.

58) G. Altarelli and G.G. Ross, *Phys. Lett.* **B212** (1988) 391.

59) A.V. Efremov and O.V. Teryaev, Proc. *Int. Hadron Symposium*, Bechnye, Czechoslovakia, 1988, eds. X. Fischer *et al.*, Czech Academy of Sciences, 1989, p. 302.

60) SLAC-E130 collaboration, M.J. Alguard *et al.*, *Phys. Rev. Lett.* **37** (1976) 1261; G. Baum *et al.*, *Phys. Rev. Lett.* **45** (1980) 2000; *ibid.* **51** (1983) 1135;
SLAC-E143 collaboration, K. Abe *et al.*, *Phys. Rev. Lett.* **74** (1995) 346; *ibid.* **75** (1995) 25;
EMC collaboration, J. Ashman *et al.*, *Nucl. Phys.* **B328** (1989) 1;
SMC collaboration, B. Adeva *et al.*, *Phys. Lett.* **B302** (1993) 533; D. Adams *et al.*, *Phys. Lett.* **B329** (1994) 399; *ibid.* **B357** (1995) 248.

Downloaded from https://www.cambridge.org/core. UNIVERSIDAD AUTONOMA METROPOLITANA, on 15 Nov 2026 at 15:53:11, subject to the Cambridge Core terms of use, available at https://www.cambridge.org/core/terms. https://doi.org/10.1017/CBO9780511628788.005